2014-10-24

Neural Orchestration of the C. elegans Escape Response: A Dissertation

Christopher M. Clark
University of Massachusetts Medical School

NEURAL ORCHESTRATION OF THE *C.ELEGANS* ESCAPE RESPONSE

A Dissertation Presented

By

CHRISTOPHER MICHAEL CLARK

Submitted to the Faculty of the
University of Massachusetts Graduate School of Biomedical Sciences, Worcester
in partial fulfilment of the requirements for the degree of

DOCTOR OF PHILOSOPHY

OCTOBER 24, 2014

BIOMEDICAL SCIENCE

PROGRAM IN NEUROSCIENCE

NEURAL ORCHESTRATION OF THE *C.ELEGANS* ESCAPE RESPONSE

A Dissertation Presented By

CHRISTOPHER MICHAEL CLARK

The signatures of the Dissertation Defense Committee signify completion and approval as to style and content of the Dissertation

_____
Mark Alkema, Ph.D., Thesis Advisor

_____
Claire Bénard, Ph.D., Member of Committee

_____
Michael Francis, Ph.D., Member of Committee

_____
Carlos Lois, Ph.D., Member of Committee

_____
Jagan Srinivasan, Ph.D., Member of Committee

The signature of the Chair of the Committee signifies that the written dissertation meets the requirements of the Dissertation Committee

_____
Marc Freeman, Ph.D., Chair of Committee

The signature of the Dean of the Graduate School of Biomedical Sciences signifies that the student has met all graduation requirements of the school.

_____
Anthony Carruthers, Ph.D.,
Dean of the Graduate School of Biomedical Sciences

Program in Neuroscience
October 24, 2014

Dedicated to my wife Andrea and my daughter Samantha.

ACKNOWLEDGEMENTS

I was born and raised in the high desert city of Reno, Nevada. So, moving across the country to New England was quite a change of scenery. My wife and I moved here together and built a support system from scratch. I am extremely grateful for the friends and mentors I've met along the way during my graduate career at UMass and my time in Massachusetts; in addition to the long distance love sent from family supporting this adventure.

I want to thank Graduate School of Biomedical Sciences, the Neurobiology Department, the two neighboring worm labs of Mike Francis and Claire Bénard and all the friends I've made. I am so glad that I took the risk of trying a neuroscience rotation having no experience in the field. I was coming from two stints in labs that studied hematopoetic processes when I went to the NeurOpen house for first year students. Mark Alkema basically convinced me when he said told everyone that cancer had been figured out and the unexplored frontiers of biology lay in hidden in neuroscience. I am very grateful for the mentorship that Mark Alkema has given me. In addition to invertebrate behavior, I've learned a lot about myself. I wouldn't trade my time in Mark's lab for anything. I'm sure he could have done with fewer Tolkien references in lab meetings, but I'm not ashamed. I also want to support my thesis advisory committee for guiding my research progess: Marc Freeman, Claire Bénard, Carlos Lois and Mike Francis of my TRAC committee, Jagan Srinivasan of WPI,

for agreeing to participate in my examination, and past TRAC and qualifier committee members Scott Waddell, Craig Coel, Sean Ryder, and Moto Yoshihara.

My project was unique in that it provided me an opportunity to foster a very fruitful collaboration with Andrew Leifer and Aravi Samuel. My entire thesis is inextricably linked to the support and intellectual wherewithal they provided. I am proud to present this thesis as an example of what can be accomplished at the interface of biology and engineering.

Chris Burke, Charles Nelson, Peter Trenh and I have maintained a healthy level of manitude over the years from the first Wood's Hole lobster dinner moustache-pact to man-camping and man-beers. While she can't grow a moustache, our cohort wouldn't be complete without Wendy Bennett. We started grad school together and I'm excited to see where our lives take us. The constant stream of undergrad interns and first year rotons in the lab made every day and every season a new and often amusing adventure. Previous lab members Sean Maguire and Jamie Donnelly provided great friendship and hilarity during my early days in the lab. The inviting lab atmosphere between Jaime, Sean and Jenn Pirri had the most influence on me joining the lab in the first place. Jenn the Cloner was really Jenn the Nurturer keeping sanity and perspective afloat in the lab. Yung-Chi Huang taught me to question all the English colloquialisms that I take for granted and Jeremy Florman saved my life by inheriting and dominating the oft neglected Alkema Lab worm tracker. Other

lab members that will leave a lasting impact on me are Jasmin Abraham, Diego Rayes, Laura Romanelli, Robbie Green, Ashleigh Stanton, and others I'm sure I've forgotten. I feel like I've made lifelong friends with these peers and colleagues and am so grateful to have had the chance to work with them every day.

My family back home in Reno and my extended family in Texas and California has been huge supporters of this process. My parents, Dan and Bunny, always allowed the biologist in me to take over the house when I was growing up. Though they probably don't know what impact they have on me, I have to thank my dog Sebastian and especially my baby daughter Samantha. These additions to our family provide a light and a perspective to the everyday goings-on of life, in grad school and otherwise. Coming home to a happy dog and a happy baby after work is truly priceless. Most of all, I want to thank my wife Andrea. She has supported me implicitly throughout this process. I could not have accomplished what I have without her. I could never express how much she means to me, so I'm dedicating this Dissertation to her

ABSTRACT

How does a nervous system orchestrate compound behaviors? Finding the neural basis of behavior requires knowing which neurons control the behavior and how they are connected. To accomplish this we measured and manipulated neural activity in a live, behaving animal with a completely define connectome. The *C. elegans* escape response is a compound behavior consisting of a sequence of behavioral motifs. Gentle touch induces a reversal and suppression of head movements, followed by a deep turn allowing the animal to navigate away from the stimulus. The connectome provides a framework for the neural circuit that controls this behavior. We used optical physiology to determine the activity patterns of individual neurons during the behavior. Calcium imaging of locomotion interneurons and motor neurons reveal unique activity profiles during different motifs of the escape response. Furthermore, we used optogenetics and laser ablations to determine the contribution of individual neurons to each motif. We show these that the suppression of head movements and turning motifs are distinct motor programs and can be uncoupled from the reversal. The molecular mechanisms that regulate these motifs involve from signaling with the neurotransmitter tyramine. Tyramine signaling and gap junctions between locomotion interneurons and motor neurons regulate the temporal orchestration of the turning motif with the reversal. Additionally, tyramine signaling through a GPCR in GABAergic neurons facilitates the asymmetric turning during forward

locomotion. The combination of optical tools and genetics allows us to dissect a how a neural circuit converts sensory information into a compound behavior.

TABLE OF CONTENTS

LIST OF FIGURES

LIST OF MOVIES

Chapter II

Chapter III

Appendix I

LIST OF ABBREVIATIONS

Nomenclature

ACh	acetylcholine
ATP	adenosine triphosphate
Arch	archaerhodopsin-3
BAPTA	1,2-Bis(2-aminophenoxy)ethane-N,N,N′,N′-tetraacetic acid
C.	*Caenorhabditis* genus
CaM	calmodulin
CC	ceolomocytes
ChR2	channelrhodopsin-2
CCD	charge-coupled device
CoLBeRT	Control of Locomotion and Behavior in Real Time
Cre	Cre recombinase
CFP	cyan fluorescent protein
cAMP	cyclic adenosine monophosphate
DNA	deoxyribonucleic acid
DAGθ	diacylglycerol kinase theta
D.	*Drechslerella* genus
FLP	flippase
FRT	flppase recognition target
FRET	Förster resonance energy transfer
Gα	G-protein alpha subunit
GPCR	G-protein coupled receptor
GABA	gamma-aminobutyric acid
GF	giant fiber
GFP	green fluorescent protein
GMP	guanosine monophosphate
GTP	guanosine triphosphate

HEPES	4-(2-Hydroxyethyl)-1-piperazineethanesulfonic acid
IR	infrared
ICF	intracellular fluid
IPSC	inhibitory post-synaptic current
kb	kilobase
L1- L4	*C. elegans* larval stages 1-4
LED	light-emitting diode
Lox	*LoxP* sequence
M-cell	Mauthner cell
MN	motor neurons
N2	*C. elegans* wild type strain N2 (Bristol)
NGM	nematode growth media
NMJ	neuromuscular junction
NpHr	halorhodopsin
OP50	*Escherischia coli* strain OP50
PBS	phosphate buffered saline
P	promoter
PROPS	proteorhodopsin optical proton sensor
QuasAr	quality superior to Arch
Q	quinic acid catabolism gene cluster of *Neurospora crassa*
RFP	red fluorescent protein
ROI	region of interest
RGS	regulator of G-protein signaling
ts	temperature sensitive
TA	tyramine
VIP	voltage indicating protein
wt	wild type
YFP	yellow fluorescent protein

Symbols and Units

A	anterior
B	background
C	Celsius
D	dorsal
fps	frames per second
g	gram
I	intensity
kHz	kilohertz
kV	kilovolt
l	liter
MΩ	mega ohm
m	meter
µl	microliter
µm	micrometer, micron
µM	micromolar
ml	milliliter
mm	millimeter
mM	millimolar
ms	millisecond
mV	millivolt
mW	milliwatt
min	minutes
M	molar
ng	nanogram
nm	nanometer
nmol	nanomole
ns	not significant
pA	picoampere

P	posterior
R	ratio of GCaMP (green) fluorescence to mCherry (red) fluorescence
rpm	revolutions per minute
s, sec	seconds
SEM	standard error of the mean
t	time
ti50	time to immobilize 50% of the animals
V	ventral
º	degrees
α	alpha
Δ	delta
θ	theta
σ	sigma
Ω	omega

COPYRIGHTED MATERIALS

The following figures and chapters were adapted or reproduced from copyrighted material:

Figure I-1:
von Uexküll J (1934) A Stroll Through the Worlds of Animals and Men. trans. Schiller CH. (1957) Instinctive Behavior: 5-80. (New York, NY: International Universities Press).

Figure I-2:
Camhi JM (1984) Neuroethology: Nerve Cells and the Natural Behavior of Animals. (Sunderland, MA: Sinauer Associates Inc. Publishers).

Figure 1-3:
Pirri JK, Alkema MJ (2012) The neuroethology of *C. elegans* escape. Curr Opin Neurobiol 22: 187-193.

Figure 1-4:
Pirri JK, McPherson AD, Donnelly JL, Francis MM, Alkema MJ (2009) A tyramine-gated chloride channel coordinates distinct motor programs of a *Caenorhabditis elegans* escape response. Neuron 62: 526-538.

Figure 1-5:
Shipley FB, Clark CM, Alkema MJ, Leifer AM (2014) Simultaneous optogenetic manipulation and calcium imaging in freely moving *C. elegans*. Front Neur Circuits 8(28).

Chapter III:

Donnelly JL, Clark CM, Leifer AM, Pirri JK, Haburcak M, Francis MM, Samuel AD, Alkema MJ (2013) Monoaminergic orchestration of motor programs in a complex *C. elegans* behavior. PLoS Biol 11: e1001529.

Appendix I:

Maguire SM, Clark CM, Nunnari J, Pirri JK, Alkema MJ (2011) The *C. elegans* touch response facilitates escape from predacious fungi. Curr Biol 21: 1326-1330.

CHAPTER I: INTRODUCTION

"All animals, from the simplest to
the most complex, are fitted into
their unique world with equal
completeness."

Jakob von Uexküll

A Stroll Through the Worlds of Animals and Men (1934)

Animal behavior

Behavior is the ultimate output of the nervous system's integration of external and internal stimuli. It is how animals interact with each other and with their environment. To survive in a complex environment, the nervous system must detect and interpret a wide range of sensory cues to produce appropriate behavioral outputs. The resulting behavioral repertoire allows an animal to interact with its peers and surroundings through feeding, reproduction, food and mate searching, escape and withdrawal, or navigation and migration. One of the most fundamental questions in neurobiology is how do nervous systems accomplish this task of converting sensory stimulation into behavior? Finding the neural basis of behavior, particularly those that are in response to environmental stimuli, must begin with an experimentally tractable behavior. Innate or reflexive responses to specific stimuli are often used to study the origins of behavior. Jakob von Uexküll (1934) defined an ethological principle in which animal behavior is a product of both how an animal perceives the world and the mechanics by which it can act. Behavior, therefore, becomes a product of both the perceptual and the effector space that an animal occupies. Throughout the animal kingdom, animals exhibit innate behaviors in response to cues from their environment. These innate responses can often be induced by experimental stimuli where the perception of the animal engages the effectors/motor programs to execute the innate behavior. A striking example of this principle is observed in jackdaw defensive behavior. The jackdaw, a relative of the crow, will assume an

attack posture if a fellow bird is preyed upon and carried away by a cat. The jackdaw will also assume this attack posture when presented with a limp piece of black clothing that resembles the black body of another jackdaw (Figure I-1). This posture is not seen in response to cats alone, cats carrying white birds, or limp fabric that is not black. The black object or limp bird body is the visual stimulus that initiates the attack posture behavior (von Uexküll, 1934). Nikolaas Tinbergen would later term this type of stimulus an innate releasing stimulus (1948). If the jackdaw perceives a threat, the effectors that drive defense behavior are released.

Innate behaviors induced by specific stimuli powerful tools in ethological studies. Examples of these behaviors are reflexes and fixed action patterns. Reflexes are involuntary behaviors characterized by a rapid motor response. Reflex behavior increases in magnitude as the intensity of a stimulus increases. In contrast, fixed action patterns are motor sequences that occur in response to specific stimuli. Once the stimulation is applied, the animal will execute a stereotyped behavioral pattern that meets the following four criteria. First, a specific sensory stimulus induces the response. Second, responses occur once a threshold of stimulation has been reached. Third, fixed action patterns are all-or-none behaviors. Once a response is initiated the behavioral pattern is executed to completion. Fourth, fixed action patterns can be evoked in all individuals of a species given the correct conditions (Camhi, 1984). A reflex is a single motor output to a specific stimulus while a fixed action pattern is a temporally

orchestrated sequence of motor outputs. Fixed action patterns lend themselves to the study of how nervous systems generate complex behaviors. In a pioneer study on innate behavior, Konrad Lorenz and Nikolaas Tinbergen described the fixed action pattern of egg retrieval by the greylag goose (1938). Greylag geese exhibit fixed action patterns when retrieving eggs that have rolled out of the nest. To move an egg back to the nest, the mother will extend her neck and pull the egg backwards with her bill while stabilizing the egg with lateral bill movements. Once this egg retrieval behavior is released by the visual stimulus of the lost egg, the mother goose will pull it backwards with her bill all the way to the nest, even if the egg is removed from her control (Figure I-2; Lorenz and Tinbergen, 1938). This innate behavior shows that her nervous system is tuned to execute the complete behavioral pattern once it is released. Greylag goose egg retrieval is an elegant example of a fixed action pattern; however, determining the neural correlates of behavior requires a more experimentally accessible nervous system.

Neural circuits of behavior

The nudibranch *Tritonia diomedea* exhibits a fixed action pattern in response to a touch stimulus. When touched, particularly by a predatory starfish, *Tritonia* will exhibit a rapid withdrawal response characterized by dorsal and ventral flexures that propel the animal vertically off the ocean floor and away from the stimulus (Figure I-3). The anatomy of the *Tritonia* nervous system is well

characterized and its large and accessible neurons are perfectly suited for measurement and manipulation through electrophysiology. The *Tritonia* withdrawal response can be divided into temporally discrete sub-behaviors. A touch stimulus induces a local contraction of the touched side of the body. This is followed by complete elongation of the entire body in preparation for swimming. Cycles of dorsal and ventral flexures follow as the animal swims away from the stimulus until the response is terminated by the resumption of a relaxed posture (Willows, et al., 1973) (Figure I-3). In this example of a fixed action pattern, the dorsal/ventral flexures will not occur unless the preceding local withdrawal and elongation motor programs occur. Stimulation and measurement of the activity patterns of individual neurons during the execution of behavior were used to define the neural circuit that controls the withdrawal response (Willows, et al., 1973; Katz, 1998).

The teleost fish startle response, the C-start, is another fixed action pattern controlled by a defined neural circuit. When presented with a noxious acoustic or visual stimulus a goldfish will rapidly turn and swim away (Figure I-3). As the fish bends into a C-shape, the muscles on one side of its body hypercontract while the contralateral side relaxes. Following the initial bend into the C-shape, the tail flips in the opposite direction of the C-bend to initiate propulsion away from the stimulus (Korn and Faber, 2005). This sequence of hypercontraction and relaxation is controlled by motor neurons that receive inputs from a large pair of interneurons called the Mauthner cells (M-cells)

(Furshpan and Furukawa, 1962; Eaton, 1984; Korn and Faber, 2005). The M-cells are a pair of cranial neurons that receive input from auditory sensory neurons, and they rapidly transduce sensory input to spinal relay interneurons and motor neurons along the length of the fish's body. These connections allow for the rapid coordination of distinct motor programs during the behavior. The M-cell circuit orchestrates these motor programs to occur in a fixed sequence to produce a coordinated behavioral response. The *Tritonia* touch response and the goldfish C-start highlight how the study of fixed action patterns in a system with defined neural anatomy can provide a deep understanding of how sensory information is translated into behavioral outputs.

Neural circuits of behavior are modeled to show the path of connectivity from sensory input to motor output. Sensory neuron connections converge onto a small number of large pre-motor interneurons and motor neurons that can be amenable to dissection and electrophysiology. Organizing circuits in this manner makes it easy to hypothesize how sensory information might move through a circuit over time. However, gathering this information over time requires measuring neural activity during behavior. Classic methods to measure neural activity involve electrophysiological recordings, electrical stimulations and cellular lesions of large axons or axon fibers. These powerful tools can define the connections between neurons and the synaptic nature of those connections, but the experiments have to be done on dissected preparations or on animals with surgical implants. In these cases, the behaviors being tested are often non-

existent, restricted, or reduced to fictive behaviors in motor neuron activity. For example, neural activity that controls leech swimming is measured in preparations where the peripheral nervous system containing the motor ganglia is dissected away from the body and muscle while remaining connected to the intact head and central nervous system. While great strides have been made to identify and understand the circuitry of cyclic activity patterns that generate swimming behavior, these immobilized and dissected preparations rely on motor neuron activity as a proxy for behavior. These approaches provide information on the connectivity and electrical properties of single neurons, but the nature of how these neurons function while the animal is naturally behaving remains a hypothesis (Friesen, et al., 1978; Iwasaki, et al., 2014).

Connectivity models of neural circuits detail how motor programs are connected to each other and to other neurons; but identifying the neural pathways through which sensory information is processed into motor outputs has proved difficult. Neural activity measurements that rely on immobilization and dissection are taken under conditions where any feedback communication between neurons and muscles during the execution of behavior is disrupted. Though the consistency of fixed action patterns has enabled neural circuits to be identified in many organisms, including vertebrates, the complexity in higher order organisms has limited the detailed knowledge of connectivity between individual neurons. This leaves us with a limited understanding of how sensory information is processed into dynamic neural activity.

Neural activity of a circuit that controls behavior should be measured during the uninterrupted execution of the behavior. This hurdle can be addressed with the advent of genetically encoded opto-physiological tools combined with the optical transparency and genetic amenability of the nematode *Caenorhabditis elegans.* With these tools and a structurally characterized nervous system, *C. elegans* is the ideal system to investigate the neural basis of behavior.

Caenorhabditis elegans

C. elegans has proven invaluable to the advance of biological sciences. This seemingly simple organism shares the same biological processes as higher organisms, and its husbandry lends itself to powerful genetic manipulations. With a generation time of only a few days, mutagenesis and rapid production of transgenic animals permit the study of neurobiology and behavior at a level unparalleled in other organisms. The strength of genetics combined with detailed neuroanatomy allow for neural circuits to be defined at both a cellular and molecular level.

Mammalian nervous systems can be comprised of billions of neurons, each potentially making thousands of synaptic connections with other neurons. Even arthropod nervous systems are made up of tens to hundreds of thousands of neurons. While nervous systems of these sizes magnify the complexity of their capabilities, teasing apart the cell to cell connections that make up neural circuits is quite difficult. The *C. elegans* adult nervous system is comprised of exactly 302

neurons, for which the connectivity is annotated (White, et al., 1986). Annotation of the synapses, both chemical and electrical (gap junctions), between all cells resulted in the first complete connectome; and this work, since supplemented by others, provides a foundation to identify the neural substrates of behavior with single cell resolution (Chen, et al., 2006; Varshney, et al., 2011; Xu, et al., 2013).

The C. elegans escape response

Similar to the *Tritonia* withdrawal response and the goldfish C-start, *C. elegans* also execute a fixed action pattern in response to a mechanical stimulation. Coupled with the connectome, the study of the *C. elegans* escape response provides an opportunity to study the cellular genesis of behavior. The *C. elegans* escape response is a complex behavior that requires the temporal coordination of individual motor programs, and can be divided into four phases (Figures I-3, II-1, III-13). During basal locomotion, *C. elegans* crawl forward in a sinusoidal pattern by propagating dorsal and ventral body flexures along the length of their body. Forward locomotion is accompanied by lateral exploratory head movements (Phase I). Gentle anterior touch or vibration induces backward locomotion away from the stimulus (Chalfie, et al., 1985; Wicks and Rankin, 1995) (Phase II). During backward locomotion, exploratory head movements cease due to the relaxation of head and neck muscles (Alkema, et al., 2005). Following a reversal, forward locomotion is reinitiated with a deep ventral turn of the head (Phase III). The worm turns ventrally until the nose touches the body,

and the worm slides along the length of its ventral side forming an omega shape, and reorients itself in the opposite direction (Phase IV) (Croll, 1975; Donnelly and Clark, et al., 2013). The speed of forward locomotion remains elevated for several minutes after the stimulation allowing the animal to make a successful escape (Figure I-3, II-1C; Chalfie, et al 1985; Pirri and Alkema, 2012).

The worm's robust response to mechanical stimulus may have evolved as a means to survive the harsh soil environment. Although our understanding of *C. elegans* natural history is limited, we know that *C. elegans* are soil dwelling nematodes that feed on bacteria, often in decaying organic material. This type of environment also supports many species of microbes and fungus, some of which prey on nematodes. Soil nematodes and nematophageous fungi have been found fossilized together suggesting that a long evolutionary arms-race between nematodes and fungus may have shaped nematode behavior (Schmidt et al., 2007; Drechsler, 1937; Duddington, 1951; Thorn and Barron, 1984). Nematophageous fungi employ a variety of mechanisms to capture nematodes. *Drechslerella doedycoides* uses constricting rings to capture nematodes around their necks. We have shown that effective execution of the escape response is critical for *C. elegans* survival in the presence of *D. doedycoides*. We identified genetic factors that impact escape behavior and fitness suggesting that the *C. elegans* escape response may have evolved through selective pressure from fungal encounters (Maguire, et al., 2011; Appendix I). Neuro-ethological studies such as this highlight how the evolutionary origins of behavior can provide insight

into how behavioral patterns occur, and in turn, how neural circuits are organized.

C. elegans escape response neural circuit

The neural circuit that governs the reversal response to touch has been described using laser ablations, electrophysiology and mutant analysis (Figure I-4). When a worm is touched on the neck, mechanosensory neurons in the anterior of the animal (ALM and AVM) transduce the mechanical stimulus to pre-motor interneurons (AVD, AVA, AVB and PVC). These interneurons send synaptic outputs to excitatory (VA, VB, DA and DB) and inhibitory (VD and DD) motor neurons that innervate the body wall muscles to stop forward locomotion and enable backward locomotion (Chalfie, et al., 1985; Kawano, et al., 2011). The AVA interneurons also activate the tyraminergic inter/motor neurons (RIM) through gap junctions (Chronis, et al., 2007; Guo, et al., 2009). Release of the neurotransmitter tyramine from the RIM regulates multiple aspects of the escape response (Alkema, et al., 2005). The AVB interneurons, SMD and RMD neck motor neurons and neck muscles express the tyramine gated chloride channel, LGC-55. These cells are post synaptic to the RIM. When the RIM releases tyramine during an escape response, tyramine activation of LCG-55 inhibits the AVB thus inhibiting forward movement and promoting backward movement. Also, tyramine activation of LCG-55 in the SMD, RMD and neck muscles inhibits muscle activation and promotes head and neck relaxation during the reversal

(Pirri, et al., 2009). The tyraminerigic coordination of backward locomotion and head movements is critical for facilitating an efficient escape response. Mutants defective for this coordination have lower survival rates from encounters with predacious fungi (Maguire, et al., 2011; Appendix I).

The wiring diagram in Figure I-4 presents a neural circuit that controls the initiation of the *C. elegans* escape response. Anterior mechanosensory neurons connect to interneurons that control the switch from forward locomotion (Phase I) to backward locomotion with a relaxed head and neck (Phase II). However, the ventral turning behavioral motifs that reorient the animal away from a threatening stimulus (Phases III and IV) are not described by this circuit.

Tyramine is a neurotransmitter that, when released from a pair of interneurons (RIM), coordinates the switch from Phase I to Phase II during an escape response. This role for tyramine is mediated by a tyramine gated chloride channel (LGC-55) post-synaptic to the tyraminergic interneurons (Pirri, et al., 2009). The *C. elegans* genome encodes three other tyramine receptors, SER-2, TYRA-2 and TYRA-3 (Rex and Komuniecki, 2002; Rex, et al., 2005; Wragg, et al., 2007). These receptors are widely expressed in the nervous system but their roles in modulating behavior are largely unknown. TYRA-3 has been shown to function in sensory neurons to modulate food behavioral choice, and TYRA-2 and SER-2 have been suggested to have roles in modulating feeding behaviors; however, their mechanisms of action remain unknown (Rex, et al., 2004; Rex, et al., 2005; Bendesky, et al., 2011). Only two sites of action for tyramine GPCRs

have been identified to play a role in modulating behavior. TYRA-3 functions in dopaminergic and octopaminergic interneurons to modulate responses to nociceptive aversive stimuli (Hapiak, et al., 2013); and SER-2 functions in GABAergic motor neurons to coordinate Phase IV of the escape response (Donnelly and Clark, et al., 2013; Chapter III). The sites of action for these GPCRs only accounts for a subset of the tissues in which they are expressed. Additionally, both of these behaviors are examples of extrasynaptic modulation. Presently, the limited understanding of how tyramine signaling regulates behavior underscores how little is known about neural activity dynamics during behavior. This highlights the strength of the *C. elegans* escape response in investigating neuromodulation and behavior. The escape response neural circuit lets one hypothesize how tyramine affects behavioral outputs during a compound motor sequence.

The neural circuit model for the *C. elegans* escape response is a connectivity map depicting how sensory information is signaled to the motor neurons that produce the behavioral output (Figure I-4). However, this static connectivity map does not provide any information about the dynamics of individual neuron activity and how individual neurons contribute to the temporal coordination of the different motor programs that comprise the escape response. For example, tyramine from the RIM coordinates multiple phases of the escape response (Alkema, et al., 2005; Pirri, et al., 2009; Donnelly and Clark, et al., 2013), but the activity and behavioral contribution of neurons in the circuit during

each phase of the behavior is unknown. Recent advances in optical physiology have provided a platform to study nervous systems in action. The advent of optogenetics and the development and optimization of genetically encoded optical probes permit the manipulation and measurement of neuronal function in intact nervous systems.

Optogenetics is the transgenic expression of optically activated proteins. Fungal and algal microbes use light sensitive rhodopsins for phototaxis in dark water environments (Bieszke, et al., 1996; Hegemann, et al., 2001). When transgenically expressed in cells, light sensitive rhodopsins can change the electrical properties of the cells in response to light. The most commonly used optogenetic protein is Channelrhodopsin-2 (ChR2). ChR2 is a seven-transmembrane cation channel cloned from the green alga, *Chlamydomonas reinhardtii*. ChR2 is bound with the chromophore retinal. When exposed to blue light, a conformational change in the retinal activates ChR2 allowing an influx of cations into the cell (Nagel, et al., 2003; Nagel, et al., 2005). When expressed in neurons, blue light activation of ChR2 depolarizes membranes and activates the neurons. Conversely, neurons can be inhibited with optogenetic proteins. The two most common rhodopsins used to inhibit neurons are Halorhodopsin (NpHR) and Archaerhodopsin-3 (Arch). NpHR is an inward chloride pump cloned from the archaebacterium, *Natronomas pharaonis. When exposed to yellow light, cells expressing NpHR become hyperpolarized through an influx of chloride (Han and Boyden, 2007).* Arch is an outward proton pump cloned from the halobacterium,

Halorubrum sodomense (Okazaki, et al., 2012). When exposed to green light, cells expressing Arch become hyperpolarized via the efflux of cations. Optogenetics allows for the conditional manipulation of neural activity without physically restraining or dissecting the animal. Additionally, the non-overlapping activation spectra of these rhodopsins allow for their combinatorial use in the same tissues to activate or silence neurons.

The development of optical probes that detect changes in intracellular calcium concentrations have allowed for the measurement of neural activity changes in single neurons. When a neuron becomes depolarized, the concentration of cytosolic calcium increases (Lev-Ram and Grindvald, 1987). Measuring this change in intracellular calcium is a proxy for measuring neural activity. The optical probe, GCaMP, is a GFP molecule bound to two peptides, a myosin light chain kinase (M13) peptide fragment and calmodulin. When calcium ions bind to calmodulin, calmodulin binds to the M13 peptide and changes the conformation of the GCaMP molecule. Conformational changes in GCaMP increase the green emission intensity of the GFP (Nakai, et al., 2001; Tian, et al., 2009). Previous versions of genetically encoded calcium indicators were chimeric proteins that utilized a similar mechanism of calcium induced conformational changes to bring two conjugated fluorophores into close proximity. Two color FRET based analysis was used to measure calcium activity (Miyawaki, et al., 1997; Palmer, et al., 2006; Mank, et al., 2008). Changes in GCaMP fluorescence, on the contrary, are measured through a single emission color allowing GCaMP

to be used in combination with other optically activated proteins or fluorophores with non-overlapping spectra (Oheim, et al., 2014). Genetically encoded rhodopsins and fluorescent calcium indicators are particularly well suited to study cellular function in a transparent organism like *C. elegans.*

Determining how neural circuits generate behavior requires the knowledge of how and when each neuron in the circuit contributes to the execution of a behavior. Genetically encoded optogenetic proteins and calcium indicators allow for the dissection of neural dynamics within a circuit; however, there is a tremendous technical challenge in measuring and stimulating neuron activity in a live, behaving animal. Recent advances in computer vision technology have automated the quantification of *C. elegans* behavior (Ramot, et al., 2008; Ben Arous, et al., 2010; Swierczek, et al., 2011; Leifer, et al., 2011; Husson, et al; 2012). This visual automation of behavior can be used to direct motorized stages to follow worm movement, particularly to allow worms to move while under a microscope. The need to immobilize worms under a slide to visualize the nervous system is unnecessary when they are allowed to freely behave while centered under a high objective magnification. The combination of worm tracking with fluorescent imaging has allowed for the simultaneous stimulation of rhodopsins and imaging of calcium indicators during unrestrained behavior.

Challenges with genetically encodes optical tools

One advantage of using *C. elegans* to study the dynamics of neural circuits during behavior is the well-defined neuroanatomy. While the identity, location and connectivity of every neuron is known, activating and measuring activity in single neurons is still a tremendous hurdle. There are many published *C. elegans* promoter sequences that drive gene expression in small subsets of the adult worm's 302 neurons, but few drive expression in single neurons. The challenge with using optogenetics is the stimulation of specific neurons. When bathing an animal in colored light to activate a genetically encoded rhodopsin, every cell expressing the rhodopsin is stimulated thus confounding the identity of the cells that drive a particular behavioral output. There are two ways to address this issue. One method to limit the number of neurons stimulated is to genetically refine the expression pattern of the rhodopsins. Promoter bashing or conditional expression techniques like FLP-FRT recombination, Cre-Lox recombination and the Q-binary expression system are used to limit expression to overlapping tissues of two different promoter regions (Davis, et al., 2008; Macosko, et al., 2009; Wei, et al., 2012). Another way to limit the number of neurons stimulated is to only illuminate a desired subset of the cells that express the rhodopsins. Leifer, et al. (2011) combined computer vision worm tracking with the control of a digital micro-mirror device to tightly control the light patterns that illuminate very small regions of the worm (approximately 30 μm). This system, CoLBeRT (Control of Locomotion and Behavior in Real Time), can illuminate small regions

of a worm to optically stimulate individual or small subsets of neurons that are spatially distinct.

The challenge with using genetically encoded calcium indicators is reliable cell identification during behavior. When tracking a moving animal to measure neural activity, there exists a trade-off between the number of neurons that can be identified and measured and the quality of the behavioral tracking. Computer vision tracking of behavior requires imaging the entire body of the worm. If the calcium indicator expression pattern is sparse, cell identification for calcium imaging can be done under low magnifications. Low magnification tracking allows for high throughput behavioral quantification (Swierczek, et al., 2011; Larsch, et al., 2103). If a high magnification is required to identify individual cells expressing calcium indicators, two imaging sources are needed to measure one animal at a time. One lower magnification image source measures and tracks worm behavior while a second higher magnification imaging source captures cellular fluorescence (Figure I-5; Piggott, et al., 2011; Kocabas, et al., 2012; Shipley, et al., 2014). Because the animal is moving, the higher magnification image stream can be quite susceptible to small direction changes that arise from the tracking software, motorized stage, uneven substrate or sudden movements of the animal. Technological improvements in the software and optics used for behavioral tracking, spatial illumination and cell identification are leading to a time when whole brain imaging will be used to study neural dynamics during behavior.

Thesis Outline

This thesis demonstrates how a neural circuit orchestrates a behavioral response by coordinating multiple motor programs. The model I used is the sensorimotor circuit of the nematode *C. elegans* escape response. The *C. elegans* escape response is a robust behavior that is thought to have been shaped through an evolutionary arms race. Animals defective in escape behavior have decreased fitness during encounters with nematophageous fungus. Our work demonstrating this predator-prey interaction is presented in Appendix I (Maguire, et al., 2011).

The wiring diagram for the *C. elegans* escape response is a structural model showing how sensory information is transduced through a circuit. In Chapter II, we utilize genetically encoded optical tools and computer vision technology to stimulate and measure neural activity in live, behaving animals. We use calcium imaging and optogenetics to measure the dynamics of neural activity during distinct phases of the escape response and the functional contribution of each neuron to the execution of each phase of the behavior. Optical activation and inhibition of specific neurons allowed us to uncouple phases of escape behavior demonstrating that the escape response is an orchestration of discrete motor programs. We use the temporal dynamics of neural activity to generate a functional map of the escape response neural circuit. Additionally, we define a sub-circuit that controls the initiation of the ventral turn that allows the animal to reorient its locomotion trajectory during an escape response. Two pairs of

locomotion interneurons (RIM and AIB) control the ventral head turn after a long reversal through two classes of neck motor neurons (SMDV and RIV). Tyramine signaling and gap junctions between these neurons may control the timing of the turn during escape behavior.

In Chapter III, we discover and describe an extrasynaptic role of the neurotransmitter tyramine. Tyramine coordinates the switch from forward to backward locomotion with the suppression of exploratory head movements during the *C. elegans* escape response (Alkema, et al., 2005; Pirri, et al., 2009). Our work presented in Chapter III demonstrates that tyramine also coordinates the final phase of the escape response where the animal makes a deep turn to navigate away from the stimulus. We show that tyramine's mechanism of action is through G-protein signaling in inhibitory motor neurons (VD) that are not post-synaptic to the tyraminergic RIM. Signaling mediated by a tyramine GPCR, SER-2, inhibits GABA release on the ventral side of the animal which facilitates ventral hypercontraction. This ventral turn occurs well after the escape response is initiated and is evidence of an extrasynaptic modulatory role of tyramine.

Wiring diagrams of neural circuits provide structural maps showing how information might flow from one neuron to another. In this thesis, I build upon the static representation of signaling within a circuit by providing a functional map of neural activity during behavior. I define the neural activity patterns and the behavioral roles of specific neurons during the sequential phases of a compound behavior. This thesis also provides further detail of the molecular signaling

mechanisms that orchestrate compound behavior. The *C. elegans* nervous system provides an amazing platform to study how a sensory cue is converted into a signal communicated between individual cells within a sensorimotor circuit, and ultimately, the molecular nature of behavior.

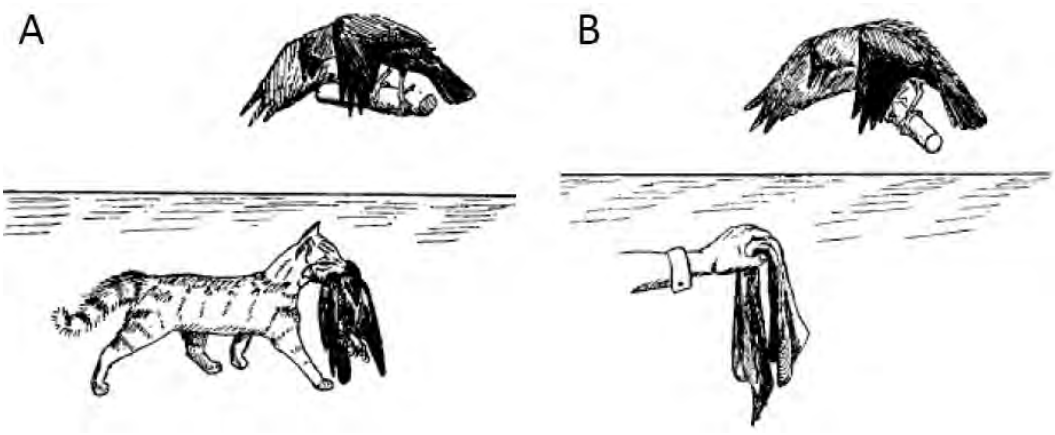

Figure I-1: Perception induced behavior of the jackdaw.

(A) Jackdaw exhibiting a defensive attack posture against a cat that preyed upon another jackdaw. (B) Jackdaw exhibiting a defensive attack posture against a piece of black clothing (adapted from von Uexküll, 1934).

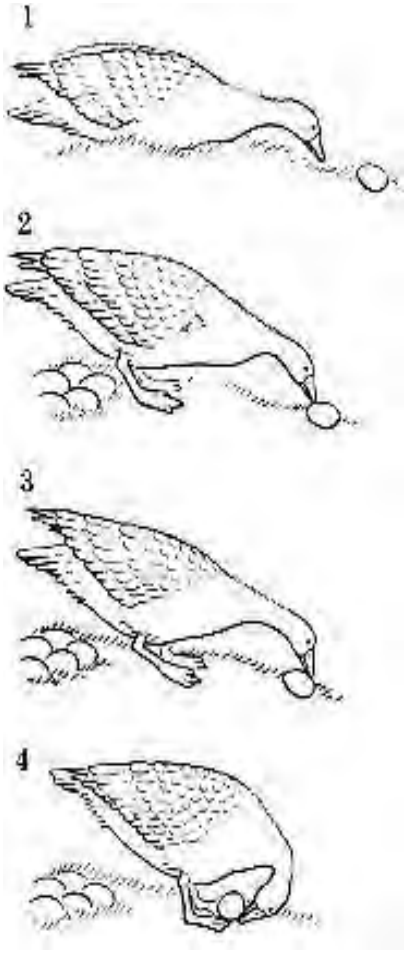

Figure I-2: Greylag goose exhibiting a fixed action pattern.

The mother greylag goose executes the egg retrieval fixed action pattern to recover an egg from outside of the nest. (1) Visual stimulus of the lost egg initiates the retrieval pattern. (2) The mother goose extends her neck to the egg. (3) She stabilizes the egg with her bill while (4) pulling the egg backwards back to the nest. Once the behavior is initiated, she will execute this complete pattern even if the egg stimulus is removed during the behavior (adapted from Camhi, 1984).

Figure I-3: Escape response behavioral patterns.

(A) The withdrawal response to touch of the nudibranch, *Tritonia diomedea.* (B) The C-start startle response of the teleost fish, goldfish (C) The nematode, *C. elegans,* escape response to gentle anterior touch (adapted from Pirri and Alkema, 2012).

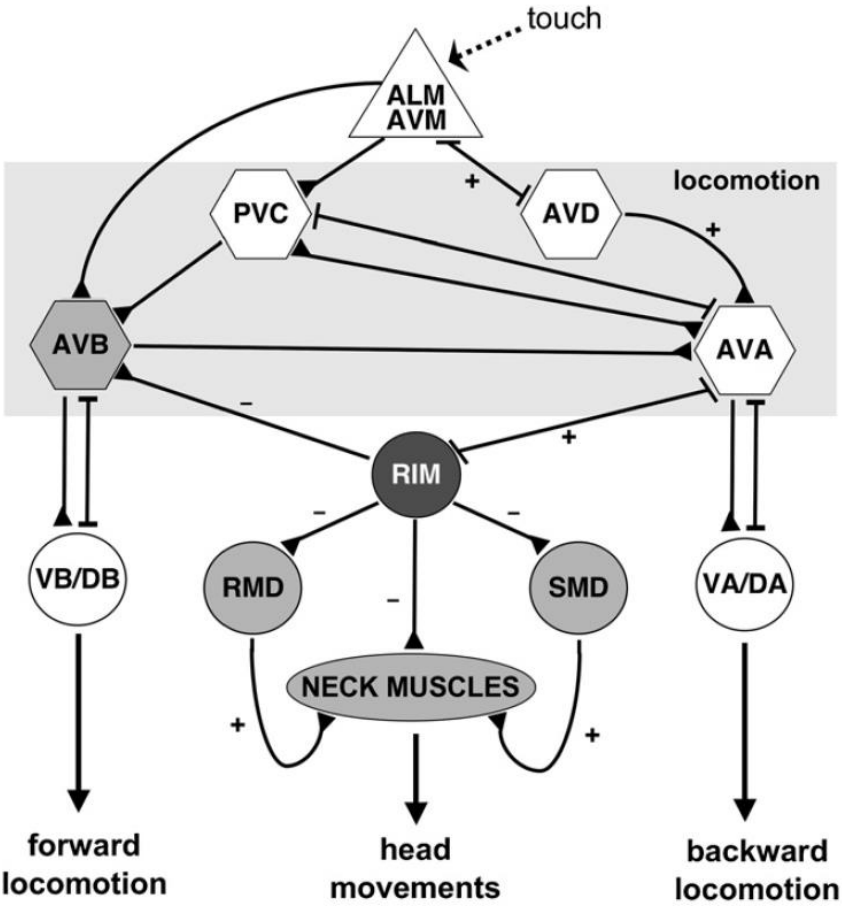

Figure I-4: Neural Circuit for the *C. elegans* escape response.

Gap junctions (indicated by bars) and synaptic connections (indicated by triangles) originally described by White, et al. (1986). Excitatory connections indicated by (+) and inhibitory connections indicated by (-). Touch activates mechanosensory neurons (triangle) that connect to locomotion pre-motor interneurons (hexagons) to drive backward locomotion. Tyramine release from the RIM (dark gray cell) inhibits forward locomotion through AVB inhibition, and head movements through RMD, SMD and neck muscle inhibition (gray cells). Motor neurons are shown as circles (Reproduced from Pirri, et al., 2009).

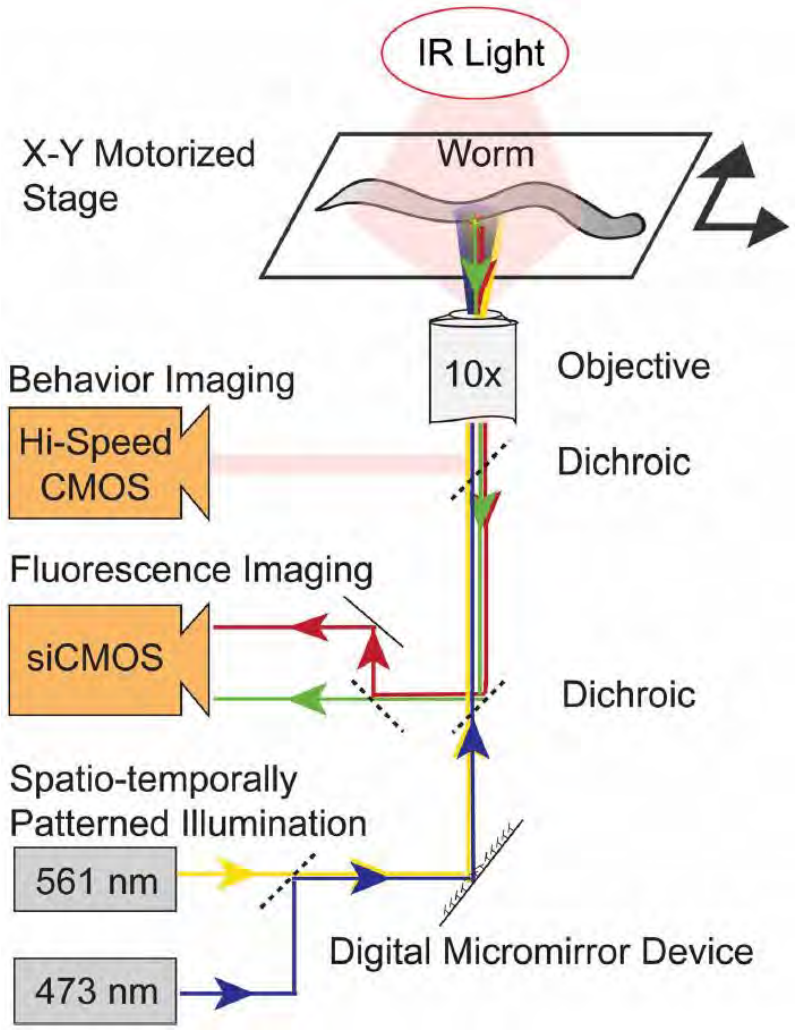

Figure I-5: Schematic of a worm tracking system to measure and manipulate neural activity in a live-behaving animal.

Computer vision software uses behavioral imaging under IR light to control a motorized stage that keeps the worm centered in the objective. Spatial illumination patterns are use controlled by a digital micro-mirror device to illuminate neurons expressing optogenetic rhodopsins and calcium indicators. Fluorescence imaging is used to measure neural activity in neurons expressing fluorescent calcium indicators (Reproduced from Shipley, et al., 2014).

PREFACE TO CHAPTER II

The work presented in this chapter demonstrates how a neural circuit orchestrates behavior. Neural circuit wiring diagrams present static models of connectivity between neurons. These models provide a platform to investigate the temporal activity patterns of neurons during behavior. With advent of genetically encoded tools that can be used to optically measure and manipulate neural activity, neural circuitry can be functionally tested in unrestrained behaving animals. In this chapter the sensorimotor circuit of the *C. elegans* escape response is dissected using optogenetics and calcium imaging to determine the roles of single neurons in the execution of a compound behavior. The *C. elegans* escape response is a complex behavior comprised of four phases: (I) forward locomotion accompanied by exploratory head movements, (II) touch induced backward locomotion accompanied by the suppression of head movements, (III) a deep ventral turn of the head with the reinitiation of forward locomotion, and (IV) the propagation of the deep turn where the nose slides along the ventral side of the body to reorient locomotion in the opposite direction. These phases are distinct motor programs that are orchestrated together. In this chapter, the activity profiles of individual neurons during each phase of the behavior were measured using calcium imaging and the phases were uncoupled from each other using optogenetics. Uncoupling of the ventral turn from the reversal revealed a signaling mechanism between four interneurons and four motor

neurons that regulated the timing of the turn. This chapter presents how a chain of synaptic connections in a neural circuit converts sensory information into coordinated behavioral outputs.

Christopher Clark and Jeremy Florman performed the behavioral experiments comparing spontaneous and escape behavior. Christopher Clark, Andrew Leifer and Ni Ji performed the calcium imaging experiments on behaving animals in the labs of Andrew Leifer and Aravinthan Samuel. Andrew Leifer and Ni Ji analyzed calcium imaging data. Christopher Clark, Andrew Leifer, Ni Ji, and Kevin Mizes performed the optogenetic experiments in labs of Mark Alkema, Andrea Leifer, and Aravinthan Samuel. Christopher Clark performed experiments involving fluorescent coexpression, laser ablations and ventral turn timing. Christopher Clark generated the transgenic strains used in the calcium imaging and optogenetics experiments. Andrew Leifer developed the software and designed the hardware that combined live worm tracking with optical stimulation and fluorescent recordings. Christopher Clark, Andrew Leifer, Aravinthan Samuel and Mark Alkema designed the experiments. Christopher Clark, Andrew Leifer, Aravinthan Samuel and Mark Alkema co-wrote the manuscript. All authors discussed the results and commented on the manuscript**.** This work was prepared for publication at the time of this thesis presentation

CHAPTER II: SYNAPTIC CHAIN MODEL FOR AN ESCAPE RESPONSE MOTOR SEQUENCE

Christopher M Clark[1†], Andrew M Leifer[2†], Ni Ji[3], Jeremy T Florman[1], Kevin Mizes[2], Aravinthan DT Samuel[3] and Mark J Alkema[1]

1. Department of Neurobiology, University of Massachusetts Medical School, 364 Plantation Street, Worcester, MA 01605, USA
2. Princeton University, Lewis Sigler Institute for Integrative Genomics, 170 Carl C. Icahn Laboratory, Princeton, NJ, 08544 USA
3. Department of Physics & Center for Brain Science, Harvard University, 17 Oxford Street, Cambridge, MA 02138, USA

† Authors contributed equally

Prepared for publication at the time of this thesis presentation.

Abstract

How does the nervous system orchestrate a compound motor sequence? The *C. elegans* escape response consists of a defined sequence of behavioral motifs allowing the animal to navigate away from a mechanical stimulus. The escape response consists of four phases: (I) forward locomotion accompanied by lateral head movements; (II) stimulus induced backward locomotion during which head movements are suppressed; (III) a deep ventral bend of the head; (IV) head sliding along the ventral side of the body (omega turn); (I) reorientation of forward locomotion in the opposite direction of the stimulus. Our previous work and that of others has provided a framework for the neural circuit that controls this behavior. We used calcium imaging to correlate activity patterns of individual neurons to the temporal sequence of the escape response phases. We used a combination of optogenetics and laser ablations to determine the contribution of individual neurons in the execution of each phase of the escape response. Optical physiology of the AVA, AVD and AVB locomotion command neurons, the RIM and AIB interneurons and the RIV motor neurons reveal unique activity profiles during reversals (II), ventral turns (III) and when the animal reinitiates forward movement (IV). Furthermore, individual activation of these neurons typically only elicits partial responses of the separate phases of escape behavior, while combinatorial activation and inhibition paradigms can attenuate the responses to mimic a touch stimulus. Using our system, we show that suppression of head movements and ventral bending can be uncoupled from the reversal indicating that these behavioral motifs are distinct motor programs. Moreover, we found a role for RIM and AIB interneurons in the deep ventral bend (III) uncovering a sub-circuit for ventral turning initiated by tyramine and gap junction signaling onto the SMD and RIV excitatory neck motorneurons. The combination of

optogenetics and calcium imaging allows us to dissect a complex behavior into its component motifs and understand how the omega turn is linked to a reversal in the escape response

Introduction

All animals rely on escape responses – robust motor programs triggered by threatening stimuli – to reliably avoid and orient away from danger. An effective escape response, even in animals with simple undulatory movement like *C. elegans*, can involve a set of stimulus-triggered reactions over time that cannot be explained by single reflexes. *C. elegans* moves forward or backward by propagating bending waves in the anterior or posterior direction along the muscle cells lining its ventral and dorsal sides. *C. elegans* explores its environment using small head movements and reorients itself using deep head bends. When subjected to a gentle anterior touch, the *C. elegans* escape response is a compound motor sequence involving all three movement types: anterior touch first elicits a reversal and suppression of head movement (Croll, 1975; Alkema, et al., 2005); followed by an omega turn that involves a deep ventral head bend and forward movement that drives the head along the ventral side of the body; ending in forward movement in a new direction of locomotion. Here, we used optogenetics, targeted cell killing, and functional imaging throughout the escape response circuit in behaving animals to elucidate how an elaborate progression of motor programs emanates from the dynamics and

structure of the connectome. We identify a chain of synapses from backward motor circuits to turning and forward motor circuits that drive and organize the full escape response motor sequence.

Fixed action patterns are compound behaviors in which a sequence of multiple motor programs are orchestrated and completed in response to an initiating stimulus. How sequential motor activities are encoded in synaptically connected neurons starting from sensory neurons remains poorly understood in any animal (Camhi, 1984). Synaptic chain models have long been proposed to encode temporal sequences, and are thought to exist, for example, in the forebrain motor structure of the zebra finch to encode song sequences (Long, et al., 2010). However, it has been difficult to demonstrate the existence or dynamics of such chains in birds or any other animal, or connect a synaptic chain to upstream sensory neurons or downstream motor neurons.

Results

Here, we study the *C. elegans* escape response to anterior touch, a concrete example of a stimulus-evoked fixed action pattern. Gentle touch to the anterior half of the nematode body evokes backward movement, whereas gentle touch to the posterior evokes accelerated forward movement (Croll, 1975). Closer observation of the escape response to anterior touch or mechanical vibration during forward movement reveals a more elaborate sequence of motor behaviors than the initial backward movement reflex, requiring the temporal

orchestration of independent motor programs. *C. elegans* moves forward at basal speed accompanied by exploratory lateral head movements. The mechanical stimulus induces rapid backward movement and suppression of head movements (Alkema, et al., 2005; Pirri, et al., 2009). The reversal is followed by a deep ventral bend of the head, and a subsequent slide of the head along the ventral side of the body, a maneuver called an omega turn. After the omega turn, the animal moves forward in the opposite direction (Figure II-1A; Donnelly and Clark, et al., 2013). A similar motor sequence – backward, turn, forward – can occur spontaneously in navigating worms, but with markedly different dynamics than the stimulus-evoked escape response (Figure II-1B, C). We found that reversals induced by anterior touch or mechanical vibration were longer (Figures II-1D, II-2C) and approximately twice as fast as spontaneous reversals (Figures II-1C, II-2A). Forward movement following a stimulus-evoked reversal was markedly increased whereas the locomotion rate following a spontaneous reversal resumed at the basal locomotion rate (Figures II-1C, II-2A). Omega turns almost exclusively occur after a reversal and thus constitute a context specific behavior (Ben Arous, et al., 2010; Donnelly and Clark, et al., 2013). The length of the reversal correlated with an increased probability of ending in a deep omega turn. However, omega turns occur more frequently following stimulus-evoked than spontaneous reversals independent of reversal length or duration (Figures II-1E, II-2B).

The relevance of the *C. elegans* neural wiring diagram was first demonstrated in the analysis of the initial backward or forward movement reflexes following touch stimulation. Laser ablation studies defined direct pathways from anterior mechanosensory neurons (ALM and AVM) to premotor interneurons (AVA and AVD) to motor circuits for backward movement; and from posterior mechanosensory neurons (PLM) to command motor interneurons (AVB and PVC) to motor circuits for forward movement (Chalfie, et al., 1985; Rankin and Wicks, 1995). With recent advances in optical neurophysiology and optogenetics, it has become possible to directly monitor or manipulate neuronal activity with high spatial and temporal resolution throughout the nervous system of behaving animals. Here, we sought to leverage optical neurophysiology to determine how neuronal dynamics and synaptic connectivity in the worm connectome might encode the full fixed action pattern of the escape response to anterior touch.

To obtain a map of neuronal activity dynamics during the escape response, we generated a set of transgenic animals that express the genetically encoded calcium indicator GCaMP (GCaMP3 and GCaMP6) in individual neurons of the putative circuit (Tian, et al., 2009; Chen, et al., 2013). Each worm's behavior and neuronal dynamics were tracked with a dual camera setup. One camera monitored behavioral dynamics while another camera simultaneously monitored neuron fluorescence at higher magnification (Movie II-1). To induce the backward-turning-forward motor sequence, we subjected

individual worms to short vibrations of the assay plate during periods of basal forward movement (Giles and Rankin, 2009).

The AVA and AVD are typically characterized as premotor interneurons that control backward locomotion (Chalfie, et al., 1985; Chronis, et al., 2007; Guo, et al., 2009; Pirri, et al., 2009; Ben Arous, et al., 2010; Kawano, et al., 2011). We found that AVA and AVD, exhibit distinct patterns of calcium dynamics during the reversal component of the escape response. The AVD neurons are electrically coupled to the ALM mechanosensory and have synaptic inputs onto the AVA neurons. AVD calcium levels rise rapidly at the onset of the stimulus-evoked reversal, remained elevated, and returned to prestimulus levels when forward locomotion resumed (Figure II-3). In contrast, AVD calcium levels do not rise during spontaneous reversals, suggesting a specific role in escape responses (Kawano, et al., 2011). AVA calcium levels followed the rise in AVD during reversals and remained elevated for a longer period after forward movement resumed before returning to basal levels (Figure II-3). The RIM neurons are electrically coupled to the AVA neurons, and have been shown to inhibit forward locomotion and head movements thought the release of tyramine. RIM calcium levels paralleled those in the AVA at the onset of the reversal, but rapidly returned to a basal level when forward movement and lateral head movements resumed (Figure II-3). Although the AIB neurons have not previously been implicated in the escape response, AIB are electrically coupled to the RIM has been shown to be active during reversals of navigating worms (Piggott, et al.,

2011; Chalasani, et al., 2007). The AIB have synaptic outputs onto the AVA, AVB premotor interneurons and the RIM. Similarly to the RIM, AIB calcium levels begin to rise at the onset of the reversal and fell after the omega turn (Figure II-3). Therefore, our experiments indicate that electrical synapses between the AVA, RIM and AIB neurons synchronize their activity. The AVB and PVC are characterized as premotor interneurons that control forward movement (Chalfie, et al., 1985; Kawano, et al., 2011; Pirri, et al., 2009). AVB calcium levels dropped slightly during reversals, but increased after the omega turn when the animal resumed forward movement at increased speed. PVC calcium levels showed no significant changes throughout the stimulus-evoked escape response (Figure II-3), even though the PVCs are electrically coupled to the AVA neurons. Chemical inhibitory inputs from the ALM/AVM and AVD onto the PVC, may exclude certain electrically coupled cells from synchronous firing.

The omega turn at the end of the reversal involves neck contraction and a deep ventral bend of the head. Calcium transients in the neck muscles show an increase in ventral neck muscle activity during the omega turn (Figure II-4, Movie II-2). Several motor neurons connect with the neck muscles. The RIM, SMD and RMD innervate both ventral and dorsal neck muscles, but the RIV is the only motor neuron class that exclusively innervate the ventral neck muscles (Figure II-5A) (White, et al., 1986). Laser ablation studies implicated the SMD and RIV in spontaneous turning during navigation behavior (Gray, et al., 2005; Iino and Yoshida, 2009). Acetylcholine is the primary excitatory neurotransmitter utilized

by *C. elegans* motor neurons. We found that the RIV, SMD expressed an acetylcholine transporter marker (P*unc-17*::mCherry/GFP), indicating that these are cholinergic motor neurons (Figure II-5B). Calcium imaging experiments showed RIV calcium levels increase sharply at the onset of the omega turn – exhibiting peak activity shortly after peak RIM activity – and rapidly return to basal levels after turn completion (Figure II-3). Additionally, SMDV calcium activity is anti-correlated to RIM activity in immobilized animals (Michael Hendricks personal communication). These experiments indicate that muscle contraction triggered through ACh release from the RIV and SMD initiate the omega turn.

To determine their role in the execution of the omega turn during the stimulus-evoked escape response, we ablated the RIV and the ventral pair of the SMD motor neurons (SMDV). Laser ablation of each of these neurons lowered the likelihood of exhibiting an omega turn at the end of each stimulus-evoked reversal (mock ablated, 48.2 +/- 2.9% executing omega turns after touch, n=64; -SMDV 30.7 +/- 3.6%, n=16; -RIV 25.49 +/- 3.69%, n=41). Ablation of both RIV and SMDV resulted in a more severe omega turn defect (-SMDV & -RIV, 7.3 +/- 2.2%, n=9) (Figure II-5C). Killing the SMDV also lengthened the reversal during the stimulus-evoked escape response; while killing the RIV or both the RIV and SMDV shortened the reversal (-SMDV: 5.5 +/- 0.4 body bends, n=16; -RIV: 3.3 +/- 0.2 body bends, n=11; -SMDV & -RIV: 3.6 +/- 0.4 body bends, n=9) (Figure II-6).

How are motorneurons that initiate for the omega turn connected to premotor interneurons that drive forward and backward locomotion? The *C. elegans* wiring diagram suggests pathways by which neurons active during the reversal phase of the escape response might trigger the ventral neck muscles. The RIM has inhibitory synaptic outputs to the SMD, which are electrically coupled to the RIV motor neurons (Pirri, et al., 2009). The AIB are electrically coupled to the RIV and has chemical and electrical synapses to DB/VB motor neurons that drive forward locomotion. Since the AIB and RIM are uniquely positioned to link the direction of locomotion and the activation of the ventral head bend, we hypothesized that signaling from the RIM and AIB to the SMD and RIV might mediate the transition from backward movement to the omega turn during the stimulus-evoked escape response (Figure II-8). We performed laser ablation analysis to test the roles of individual neurons in mediating potential links between the reversal and the omega turn. Killing the AVB or PVC had no impact on the animals' ability to make omega turns during stimulus-evoked escape responses (mock ablated: 48.2 +/- 2.9%, n=64; -AVB: 37.0 +/- 5.3%, n=14; -PVC: 52.1 +/- 4.8%, n=12), with just a modest decrease in reversal length in AVB ablated animals. Killing the AVA or RIM shortened reversals during the escape response (mock ablated: 4.7 +/- 0.2 body bends, n=28; -AVA: 2.8 +/- 0.2 body bends, n=13; -RIM: 2.5 +/- 0.1 body bends n=22), but only killing the RIM significantly decreased the likelihood that the reversal ended in an omega turn (-AVA: 36.3 +/- 4.5%, n=12; -RIM: 30.1 +/- 2.9%, n=27). In contrast, killing

the AIB only slightly shortened reversals during the escape response (-AIB: 3.8 +/- 0.3 body bends), and greatly reduced the likelihood that the reversal ended in an omega turn (-AIB: 17.2 +/- 5.7%, n=13). Ablation of both the RIM and AIB decreased the likelihood that a reversal ended in an omega turn (-RIM & -AIB: 16.3 +/- 3.5% n=10) and shortened the reversals during the escape response (-RIM & -AIB: 2.3 +/- 0.2 body bends, n=10) (Figures II-5C, II-6). Thus, the AIB and RIM appear to play key roles in mediating the transition from the reversal to omega turn during the escape response. Our results further suggest that manipulating the escape response circuit can disrupt the strict dependence between reversal length and the likelihood of executing an omega turn during the escape response.

Our calcium imaging data indicate that the *C. elegans* escape response arises from the coordinated activity of independent circuits that control distinct sub-motorprograms (Figure II-1A). Is it possible to dissect a fixed action pattern into its components parts? We used optogenetics to determine if activity in distinct sensory-, motor- and inter-neurons is sufficient or required for the execution of sub-motor programs of the escape response. Activation was achieved by illuminating neurons expressing Channelrhodopsin-2 (ChR2) with blue light stimulation (Nagel, et al., 2005). Inhibition was achieved by illuminating neurons expressing Archaerhodopsin-3 (Arch) with green light (Okazaki, et al., 2012). In addition to whole body illumination experiments, we also used a digital micro-mirror device to more precisely control illumination patterns and timing

during behavior when necessary (Leifer, et al., 2011; Shipley, et al., 2014). Animals were stimulated with light during basal forward movement. Blue light activation of the ALM and AVM mechanosensory neurons induced a response that mimicked the escape response to anterior touch (Figure II-7A, Movie II-3). The animals suppressed head movements (73.2 +/- 10.1% suppressed head movements) and made long reversals (3.0 +/- 0.4 body bends) that often culminated in an omega turn (35.1 +/- 8.0% reversals ended in omega turn, n=37 trials) (Figure II-7B). Whereas activation of the mechanosensory neurons was sufficient to induce a complete escape response, individual activation of specific interneurons recapitulated parts of the overall escape response. The AVA and RIM interneurons are both active during the reversal phase of the escape response (Figure II-3). Optogenetic activation of the AVA suppressed head movements (48.3 +/- 9.4%) but triggered very short reversals less than one body bend in length (0.4 +/- 0.1 body bends, n=29 trials) (Movie II-4). Optogenetic activation of the RIM suppressed head movements (78.3 +/- 8.8%) and triggered longer reversals (2.7 +/- 0.3 body bends, n=23 trials) than AVA activation (Figure II-7B, Movie II-5). This indicates that the suppression of head movements can be uncoupled from long reversals. Our data showed that during the course of the escape response, the AVB interneurons are inhibited during reversals and activated at the resumption of forward movement (Figure II-3). Neither optogenetic activation of the AVB with ChR2 nor inhibition with Arch produced notable responses (with ChR2, 0.2 +/- 0.1 body bends, 0% suppression of head

movements, n=20 trials; with Arch, 0.2 +/- 0.1 body bends, 0% suppression of head movements, n=27 trials) (Figure II-7B).

RIM and AVA share gap junctions, but have different effects when optogenetically activated. Optogenetic activation of RIM could induce long reversals and omega turns, whereas optogenetic activation of AVA induced short reversals without omega turns (Figure II-7B). This difference might be explained by the RIM's inhibitory synaptic output to the AVB in addition to its gap junctions with the AVA (Pirri, et al., 2009). We hypothesized that signaling from the circuit for the backward motor program to the circuit for the forward motor program is critical for the normal escape response. Indeed, simultaneously activating AVA and inhibiting AVB evoked significantly longer reversals than separate optogenetic manipulations of each neuron (1.3 +/- 0.2 body bends, n=39 trials) (Figure II-7B, Movie II-6). Even though AVB inhibition or activation alone did not induce a notable behavior, its inhibition enhances the backward locomotion motor program driven by the AVA activation. Our results suggest that synaptic communication from pre-motor interneurons for backward movement to neurons for forward movement is required for the reversal phase of the escape response. Unlike the AVA (3.4 +/- 3.4% reversals ended in omega turn, n=29 trials), RIM activation induced omega turns following the reversal (30.4 +/- 9.8%, n=23 trials) (Figure II-7B, Movie II-5). These results further suggest that synaptic communication from the RIM to the SMDV and RIV are required to engage the neurons that control head movement during the escape response (Figure II-8).

To determine if RIV activation is sufficient to induce an omega turn, we expressed ChR2 in a subset of head neurons that include the RIV using the *lim-4* promoter. Blue light stimulation induced a ventral neck bend and this ventral bending of the head was decreased in transgenic animals where the RIV was ablated (mock ablated: 63.3 +/- 15.9%, n=30 trials, -RIV: 22.1 +/- 5.7%, n=95 trials) (Figure II-7B). The activation of the RIV did not affect the direction of locomotion, demonstrating that we could uncouple the steep ventral turn that is normally preceded by a reversal. Interestingly, the animals' ventral turn rarely resulted in the execution of a complete omega turn where the tip of the nose slides down the length of the body. Rather, blue light stimulation induced a transient ventral bend of the neck that ended as soon as the stimulus ended and only moderately reoriented the animal's trajectory (Movie II-7). Our data suggests that the RIV may be necessary but not sufficient to induce a complete omega turn, and that the initiation of the ventral turn is just one motor program involved in the coordination of a full omega turn. AIB stimulation produced long reversals that ended in omega turns but did not result in the suppression of head movements (3.2 +/- 0.2 body bends; 75.0 +/- 11.2% executing omega turns; 25.0 +/- 11.2% suppressing head movements during the reversal, n=16 trials) (Figure II-7B, Movie II-8). This disruption in head movement suppression is likely due to the inhibitory glutamatergic inputs from the AIB onto the RIM (Piggott, et al., 2011), disrupting the RIM signaling that controls head movements during the reversal but not the omega turn that occurs at the end of the reversal.

We asked whether optogenetic dissection could be used to uncouple components of the escape response motor sequence. The omega turn only occurs after long reversals and always occurs ventrally (Ben Arous, et al., 2010) (Figures II-1E, II-2B). We expressed Arch specifically in the RIV of P*mec-4::*ChR2 animals using a *lim*-4 promoter fragment, and induced escape responses with blue light activation of the ALM/AVM. After the induced reversals reached at least 2-3 body bends in length, green light was applied to inhibit the RIV for the remainder of the reversal. This inhibition of the RIV resulted in a higher number of reversals that did not culminate in an omega turn, suggesting that RIV activation is necessary for the turn phase of the escape response (Figure II-7B, Movie II-9).

Finally, we sought to identify the molecular mechanism that initiates the ventral turn. During an escape response, tyramine signaling through the tyramine gated chloride channel, LGC-55, regulates backward locomotion and the suppression of head movements (Phase II) (Pirri, et al., 2005). During an omega turn, tyramine signaling through the GPCR, SER-2, regulates the magnitude of the ventral turn to reorient forward locomotion in the opposite direction (Phase IV) (Donnelly and Clark, et al., 2013). However, the mechanism for initiating the ventral turn (Phase III) is unknown.

Our data suggests that synaptic communication from the tyraminergic RIM to the SMDV and RIV is required in the ventral head bend. To test the connection between these neurons, we used animals expressing either a tyramine-gated

anion or cation channel post-synaptic to the RIM. Wild-type animals express the tyramine-gated chloride (anion) channel, LGC-55, post-synaptic to the RIM in the SMD (Pirri, et al., 2009). In Pirri, et al. (submitted 2014), the ion-selectivity of LGC-55 was engineered to be permeable to cations instead of anions. Reversing the ion-selectivity also reversed the behavioral outputs of tyramine signaling through LGC-55. In response to touch, animals expressing the LGC-55 cation channel made short, uncoordinated reversals and had hyper-contracted necks. Additionally, when LGC-55 cation animals were placed on exogenous tyramine, their necks became hypercontracted in a ventrally biased manner (Pirri, et al., submitted 2014). This suggests that hyperactivated SMD motor neurons expressing LGC-55 cation channel activate the RIV through gap junctions resulting in a ventral neck contraction.

To determine if initiation of the omega turn is mediated by tyramine signaling from the RIM, we optogenetically activated the RIM in *unc-3* mutant animals. Head movements can be isolated in *unc-3* mutants because they are immobile from the neck down (Prasad, et al., 1998). Their ability to move their head and neck, however, is unperturbed. While they do not make reversals, *unc-3* mutants suppress their head movements and make deep ventral head bends in response to gentle anterior touch. We measured turning behavior in animals expressing either the wild-type LGC-55 anion channel or the transgenic LGC-55 cation channel. RIM activation in wild-type animals expressing the LGC-55 anion channel resulted in head relaxation followed by a ventral turns (ventral turn after

8.06 +/- 0.53s, n=70) (Figure II-9, Movie II-10). These optogenetically induced turns occurred well after the stimulus was removed. The timing mimicked escape behavior during which the omega turn only occurs after a long reversal. RIM activation in *lgc-55* null mutants resulted in ventral turns that occurred without much of a delay (ventral turn after 4.03 +/- 0.31s, n=64) (Figure II-9) suggesting that tyramine signaling through LGC-55 may control the timing of the omega turn. RIM activation in animals expressing the LGC-55 cation channel resulted in immediate ventral neck contractions (ventral turn after 3.00 +/- 0.39s, n=44) (Figure II-9, Movie II-11). Based on the circuit model, tyramine release from the RIM activates the LGC-55 cation channels in the SMD which activates the RIV through gap junctions (Figure II-8). We hypothesize that the timing of the omega turn in wild type animals is delayed to follow the tyramine/LGC-55 anion channel inhibition of the SMD.

Optogenetic activation of the RIM indicated that tyramine signaling is involved in the timing of the omega turn. However, when we looked at the behavior of tyramine signaling mutants, we found that they made omega turns at the same rate as the wild type. Mutants defective for the biosynthesis of tyramine, *tdc*-1, and mutants for the tyramine-gated chloride channel, *lgc*-55 were able to make omega turns in response to anterior touch with similar frequencies as the wild type (Figures II-9, II-10A). This suggests an alternative neuronal signaling pathway initiates the omega turn. Looking at the escape response neural circuit, there is another neural path for sensory input to reach

neck motor neurons. The AIB are gap junction connected to the RIM and have outputs to the SMD and RIV (Figure II-8) The AIB interneurons play a role in turning behavior and are active during the omega turn (Gray, et al., 2005; Iino and Yoshida, 2009; Piggott, et al., 2011) (Figures II-3, II-5C, II-7B). To determine if signaling from the AIB plays a role in initiating the omega turn, we looked at the nature of the connections made by the AIB. The gap junction innexin, INX-1, is expressed in muscle and only two pairs of head neurons, the AIY and AIB (Altun, et al., 2009, Liu, et al., 2013). Since the AIB make gap junctions with the RIM and RIV we looked at the behavior of *inx-1* mutants. *inx-1* mutant animals made significantly fewer omega turns in response to touch. They were still able to make relatively long reversals suggesting the defect was specific for the omega turn (Figure II-10A, B). We made *tdc-1; inx-1* double mutants to disrupt signaling to neck motor neurons from both the RIM and AIB. These mutants rarely made omega turns in response to touch suggesting that omega turns are regulated by both innexin gap junctions and tyramine (Figure II-10A). Interestingly, this effect of tyramine on *inx-1* mediated omega turns does not appear to require the tyramine-gated chloride channel, LGC-55. There was no difference between the omega turn frequency of *inx-1* mutants and *lgc-55; inx-1 double* mutant animals (Figure II-10A). While LGC-55 is expressed in the SMD and neck muscles, the other three *C. elegans* tyramine receptors, SER-2, TYRA-2, and TYR-3 are expressed throughout the head ganglia and in head muscles (Pirri, et al., 2009); Rex and Komuniecki, 2002; Rex, et al., 2005; Wragg, et al., 2007; Rex, et al.,

2004; Donnelly and Clark, et al., 2013). The function of these tyramine GPCRs in head neurons is largely unknown. SER-2 has been shown to modulate turning behavior (Donnelly and Clark, et al., 2013), so it is not implausible to consider a role for any of these three GPCRs in initiating the ventral turn during escape behavior.

Discussion

Our results provide direct functional and structural mapping of a synaptic chain organizing multiple phases of a complex motor sequence. The escape response circuit of *C. elegans* is not comprised of two feed-forward reflex arcs by which stimulation of anterior or posterior touch receptors trigger gait changes in backward or forward movement, respectively (Proctor and Holmes, 2010). Instead, the complex motor sequence that follows anterior touch – backward, turning, and forward movement – is carried out by a progression of neuronal activity across synaptically connected neurons. Strikingly, many neurons of the escape circuit, AVA-RIM-AIB-RIV-SMD, are connected through gap junctions but do display distinct calcium dynamics. Our data suggest that electrical synapses mobilize neurons within the escape circuit and synchronize their activity. Chemical synapses may provide inhibitory feed forward and feedback mechanism to fine tune the peak activity of these neurons. For instance, we hypothesize that inhibitory tyramine signaling from the RIM onto the SMD and electrically coupled RIV (Pirri, et al., 2009) delays the onset of SMD/RIV activity

during the reversal. The continued rise in AIB activity and electrical coupling with the RIV may eventually overcome the tyramine mediated inhibition of the SMD/RIV leading to their subsequent firing and the initiation of the omega turn. Feedback inhibitory output of the AIB onto the RIM (Piggott, et al., 2011) may reset the activity of the RIM, AVA and AVB premotor interneurons and thus allowing forward locomotion to resume.

Our data show that neurons across the synaptic chain have distinct roles in regulating each motor program that makes up the escape response, as well as regulating transitions between motor programs. Mapping neuronal dynamics correlated with animal movements across the connectomes of freely moving animals provides direct insight into the neuronal computations that organize complex behaviors.

Materials and Methods

Strains:

N2; CB151: *unc-3(e151)*; QW284: *tdc-1(n3420)*; QW245: *lgc-55(tm2913)*; CR2172: *inx-1(tm3425)*; QW1135: *tdc-1(n3420); inx-1(tm3425)*; QW1150: *lgc-55(tm2913); inx-1(tm3425)*; QW625: *zfIs42*[P*rig-3*::GCaMP3::SL2::mCherry, *lin-15*+]; QW743: *zfIs64*[P*cex-1*::GCaMP3::SL2::mCherry, *lin-15*+]; QW1056: *zfEx427*[P*nmr-1*::mCherry::SL2::GCaMP6, *lin-15*+]; *lin-15(n765ts), lite-1(ce314)*; QW697: *zfIs53*[P*lgc-55(-120-+773)*::mCherry::SL2::GCaMP3, *lin-15*+]; QW783: *zfIs68*[P*lim-4(-3328--2174)*::mCherry::SL2::GCaMP3, *lin-15*+]; QW1112:

zfIs118[P*npr-9*::mCherry::SL2::GCaMP6s, *lin-15*+]; *lite-1(ce314);* AQ2953: *ljIs131*[P*myo-3*::GCaMP3::UrSL::RFP]; QW1153: *zfIs68*[P*lim-4(-3328--2174)*::mCherry::SL2::GCaMP3]; *zfIs4*[P*lgc-55*::mCherry, *lin-15*+]; QW310: *zfIs21*[P*lim-4*::GFP, *lin-15*+]; QW322: *mgIs19*[P*lim-4*::GFP; *rol-6*] X; *ufIs53*[P*unc-17*::ChR2::mCherry]; QW775 *vsIs48*[P*unc-17*::GFP]; *zfIs2*[P*lgc-55*::mCherry, *lin-15*+]; QW2: *zfIs1*[P*tdc-1*::GFP, *lin-15*+], *lin-15(n765ts)*; QW1052: *zfIs106*[*Plgc-55*::LGC-55::GFP, *lin-15*+]; VM484: *akIs3*[P*nmr-1*::GFP]; QW373: *zfIs18*[P*mec-4*::ChR2::YFP, *lin-15*+]; *lite-1(ce314)*; QW912: *zfIs46*[*Pnmr-1*::ChR2::GFP, *lin-15*+]; *lite-1(ce314)*; QW804: *zfIs74*[P*rig-3*::ChR2::mCherry, *lin-15*+]; *lite-1(ce314)* QW910: *zfIs9*[P*tdc-1*::ChR2::GFP, *lin-15*+]; *lite-1(ce314)*; QW805: *zfIs75*[P*lgc-55(-120-+773)*::ChR2::mCherry, *lin-15*+]; *lite-1(ce314)*; QW911: *zfIs66*[P*lim-4(-3328--2174)*::ChR2::GFP, *lin-15*+]; *lite-1(ce314)*; QW372: *zfEx63*[P*lim-4*::ChR2::GFP, *lin-15*+]; *lin-15(n765ts)*; QW1097: *zfIs112*[P*npr-9*::ChR2::GFP, *lin-15*+]; *lite-1(ce314)*; QW945: *zfIs91*[P*lgc-55(-120-+773)*::Arch::GFP, *lin-15*+]; *lite-1(ce314)*; QW973: *zfIs74*[P*rig-3*::ChR2::mCherry, *lin-15*+]; *zfIs89*[P*lgc-55(-120-+773)*::Arch::GFP, *lin-15*+]; QW974: *zfIs12*[P*rig-3*::ChR2::GFP, *lin-15*+]; *zfIs76*[P*lgc-55(-120-+773)*::ChR2::mCherry, *lin-15*+]; *lite-1(ce314)*; QW972: *zfIs18*[P*mec-4*::ChR2::YFP, *lin-15*+]; *zfIs89*[P*lgc-55(-120-+773)*::Arch::GFP, *lin-15*+]; QW1110: *zfIs18*[P*mec-4*::ChR2::YFP, *lin-15*+]; *zfIs110*[P*npr-9*::Arch::GFP, *lin-15*+]; *lite-1(ce314)*; QW971: *zfIs18*[P*mec-4*::ChR2::YFP, *lin-15*+]; *zfIs88*[P*lim-4(-3328--2174)*::Arch::GFP, *lin-15*+]; *lite-1(ce314);* QW333: *unc-3(e151)*; *zfIs9*[P*tdc-1*::ChR2::GFP, *lin-15*+]; QW327: *unc-3(e151)*; *lgc-55(tm2913)*;

zfIs9[P*tdc-1*::ChR2::GFP, *lin-15*+]; QW1283: *unc-3(e151)*; *lgc-55(tm2913)*; *zfIs9*[P*tdc-1*::ChR2::GFP, *lin-15*+]; *zfEx275*[P*lgc-55*::LGC-55Cation, P*ceh-22*::GFP]; QW1145: *unc-3(e151)*; *zfIs112*[P*npr-9*::ChR2::GFP, *lin-15*+].

Behavioral assays

Behavioral assays were performed on young adult animals at room temperature on NGM agar plates seeded with OP50 *E.coli* as a food source unless otherwise noted (Brenner, 1974). Touch assays were performed on plates seeded with a thin lawn of OP50 to prevent any physical restraint that may occur when the animals move through thick bacteria. To induce escape responses in laser ablated animal, the worms were touched just behind the posterior bulb of the pharynx with a fine hair or eyelash. Locomotion was quantified by manual observation. Worm tracking experiments were performed using the Multi-Worm Tracker with an additional plugin for detecting omega turns kindly designed by Rex Kerr. Analysis was done using Choreography software and custom designed Matlab (Mathworks) scripts (Swierczek, et al., 2011). All behavioral experiments were performed on NGM plates which were seeded with one drop of spread OP50 that was allowed to grow overnight at room temperature to form a thin bacterial lawn. 40 young adult worms were transferred to each assay plate and allowed to rest for 5 min. For experiments involving a plate tap, the mechanical stimulus was a 20 tap burst with 10ms between each tap. Plates were stimulated 2-4 times with a 5 min interstimulus interval. Reversals were considered tap

induced if they occurred within 1s of the stimulus. Ventral turns were considered tap induced if they occurred within 10s of the stimulus. Body bending angles for kymographs was measured using WormLab software (MBF Bioscience) and plotted with Matlab's contour function.

Strain generation

Transgenic strains were generated by microinjection of plasmid DNA. The pL15EK (*lin-15*+) rescue plasmid was co-injected at 80ng/µl with our transgenic plasmids into *lin-15(n765ts)* mutant animals. Optogenetic plasmids were injected a concentration of 80-100ng/µl. GFP and mCherry reporter plasmids were injected at 100ng/µl. GCaMP plasmids were injected at 50ng/µl. Integration of extra-chromosomal arrays was done with 10 minutes of 120kV X-ray irradiation. Integrated strains were backcrossed into either the N2 Bristol wild type or *lite-1(ce314)* mutants that are insensitive to short wavelength light (Edwards, et al., 2008).

Cell identification

Imaging of the RIV and SMD motor neurons was done using a P*lim-4::*GFP and a P*lgc-55*::mCherry reporter, respectively. Coexpression images with GFP or mCherry expressed under the *unc-17* promoter labeled cholinergic neurons were collected using confocal microscopy (Alfonso, et al., 1993; Pirri, et al., 2009; Sagasti, et al., 1999).

Laser Ablation:

Animals were anesthetized on an agar pad in a drop of 20mM sodium azide. Laser ablation of neurons was done on L2 and L3 larva using standard methods (Bargmann and Avery, 1995). The promoters used for fluorescent reporters used in cell identification were *nmr-1, rig-3, glr-1, lgc-55, tdc-1, cex-1, npr-9* and *lim-4*. Cells were identified using location, morphology, and fluorescent reporter expression. The animals were allowed to recover for 1-2 days following the ablations before they were used for behavioral assays.

Calcium Imaging

Single animals expressing GCaMP3 and mCherry in targeted neurons were imaged while moving freely on a 100mm square NGM agar plate containing a thin lawn of OP50 bacteria. Animals were imaged on a motorized stage with a custom dual image-path spinning disk confocal microscope that allowed for simultaneously recording the animal's behavior and red- and green-channel fluorescence.

Briefly, the microscope employs two imaging paths: the fluorescence imaging path uses a 20x objective to record calcium transients and mCherry fluorescence through a spinning disk confocal microscope while a second low magnification imaging path records the animal's posture and orientation under dark-field illumination. The system is built upon a modified Nikon Eclipse LV 100 upright microscope with a Yokogawa CSU22 Confocal Spinning Disk Unit

capable of rotating at 5000rpm. Illumination for fluorescence imaging is provided by blue (445nm) and green (561nm) lasers housed in an Andor Technologies Laser Combiner System 5000. The lasers are fiber-coupled into the spinning disk system using a quad-band dichroic. Laser power was set such that the sample was illuminated with 10mW/mm^2 of blue and 3mW/mm^2 of green laser light. Images were recorded with an Andor iXon+ EMCCD camera fitted with a dual-channel DV2 Dual-View imager by Photometrics. Fluorescent images were acquired using AndoriQ or Nikon Elements software.

To image behavior, a separate imaging path from the bottom of the microscope was used. A custom-made ring of 100 individual infrared LEDs (850nm) illuminate the sample perpendicular to the imaging path to create dark-field illumination. The microscope's condenser lens was removed to make space for the behavior imaging path. A prism located below the sample reflects light from the through a telescope and a long-pass filter (Thorlabs, FEL0750) so as to form an image of the sample on a CCD camera (DMK31BU03 from the Imaging Source). The behavior imaging path loosely approximated that of a microscope with a 4x objective. A modified version of the MindControl software (Leifer, et al., 2012; Shipley, et al., 214) was used to record the animal's behavior and to implement real-time tracking to control the motorized stage so as to keep the worm's head centered under the high magnification imaging path.

Behavior images were recorded at 30fps (33ms exposure). For the majority of trials, fluorescent images were acquired using a 20x objective at 20fps

with an exposure time of 50ms. Dual-channel images were recorded side-by-side simultaneously. In some trials, fluorescent images were instead recorded using a 10x objective for a larger field of view at the cost of spatial resolution. In a small number of trials fluorescence images were acquired with a 20x objective and temporally alternating laser illumination was used to achieve a greater effective field of view at the cost of temporal resolution. During those trials spectral unmixing was employed to infer relative mCherry and GCaMP fluorescence intensity.

In all trials, a brief vibration (approximately 1s) was applied to the edge of the plate by either directly vibrating the side of the plate with an electric toothbrush or by hitting the motorized stage with a screwdriver. Neurons coexpressing GCaMP3 and mCherry were imaged before, during and after the mechanosensory stimulus. Due to the nature of the vibration to the entire substrate, animals would either sprint forward or escape backwards. Only animals that executed backwards escape responses that culminated in omega turns were included in analysis. Single animals were stimulated 1-4 times with at least a three minute interstimulus interval.

Neural activity is reported as normalized deviations from baseline of the ratio between GCaMP3 and mCherry fluorescence, $\Delta R/R_0=(R-R_0)/R_0$ as described in detail in (Shipley, et al., 2014). Briefly, the baseline R_0 is defined as the mean of R during a time window spanning the start of the recording to the onset of vibration. We have chosen to report fluorescence intensity as a frame-

by-frame ratio of green fluorescence from GCaMP3 to red fluorescence from mCherry so as to better account for artifacts from the animal's motion. The ratio is defined as $R=(I_{GCaMP3}- B_{Green}) / (I_{mCherry}- B_{red})$. Where I_{GCaMP3} and $I_{mCherry}$ are the fluorescence intensities of GCaMP3 and mCherry, respectively, calculated by taking the median intensity value of pixels selected as the 40% brightest red-channel pixel intensities in a circular ROI centered on the neuron of interest. B_{green} and B_{red} are the background in the green and red, respectively, calculated as the median intensity of the local background defined by an annulus surrounding the neuron of interest. Custom MATLAB scripts were used to calculate the $\Delta R/R_0$ for each frame, and the time series was smoothed with a low-pass Gaussian filter (σ = 5 frames).

Occasionally the neuron of interest was obscured through motion artifact, change in z-position, or through tracker malfunction. If the mCherry signal fell below an intensity threshold, this signified that the neuron was out of focus and the fluorescence signal was tossed out for those frames. Gaps in fluorescence data of less than 0.5s are interpolated, while larger gaps are shown in the data as whitespace. The 0.5s cutoff was chosen because GCaMP3 has roughly a fall time of half a second.

Optogenetics

Single animals were transferred from NGM agar plates containing OP50 supplemented with 0.2-0.4nmol of *all-trans* retinal to NGM agar plates with no

food. The animals were washed in M9 buffer during the transfer to remove food. Food on the plate compromised image quality and tracking efficiency. The plates were placed on a motorized stage and the animals were tracked under infrared illumination (Leifer, et al., 2011; Shipley, et al., 2014). The animals were left to acclimate to the transfer for approximately ten minutes. Blue or green laser light stimulation was provided for 2.5-5s to activate the optogenetic proteins expressed in the nervous system. Targeted illumination was used when necessary to avoid off-target illumination, otherwise the entire field of view was illuminated. Behavior was measured before and during the response to stimulation. For animals that received stimulation of both colors, the colors were either applied simultaneously or staggered for varying durations. The events with staggered stimulations received 1.5s of blue light followed by green light that was applied manually depending on the magnitude and duration of the reversal observed. Single animals were stimulated 1-4 times with at least a three minute inter-stimulus interval.

Behavioral assays of *unc-3(e151)* animals were done on NGM agar plates containing OP50 supplemented with *all-trans* retinal. Each plate contained assayed contained approximately 20-60 animals. Animals were was stimulated once with blue light. Blue light stimulation was done one animal at a time until approximately 20-40 animals per plate were stimulated. Behavior was video recorded for analysis.

Acknowledgments

We thank the *Caenorhabdits* Genetics Center (CGC), Mei Zhen, Yun Zhang, Vincent Pieribone and Adam Cohen nematode strains and reagents. This work was supported by funding research conducted in laboratories of M.J.A, A.D.T.S and A.M.L.

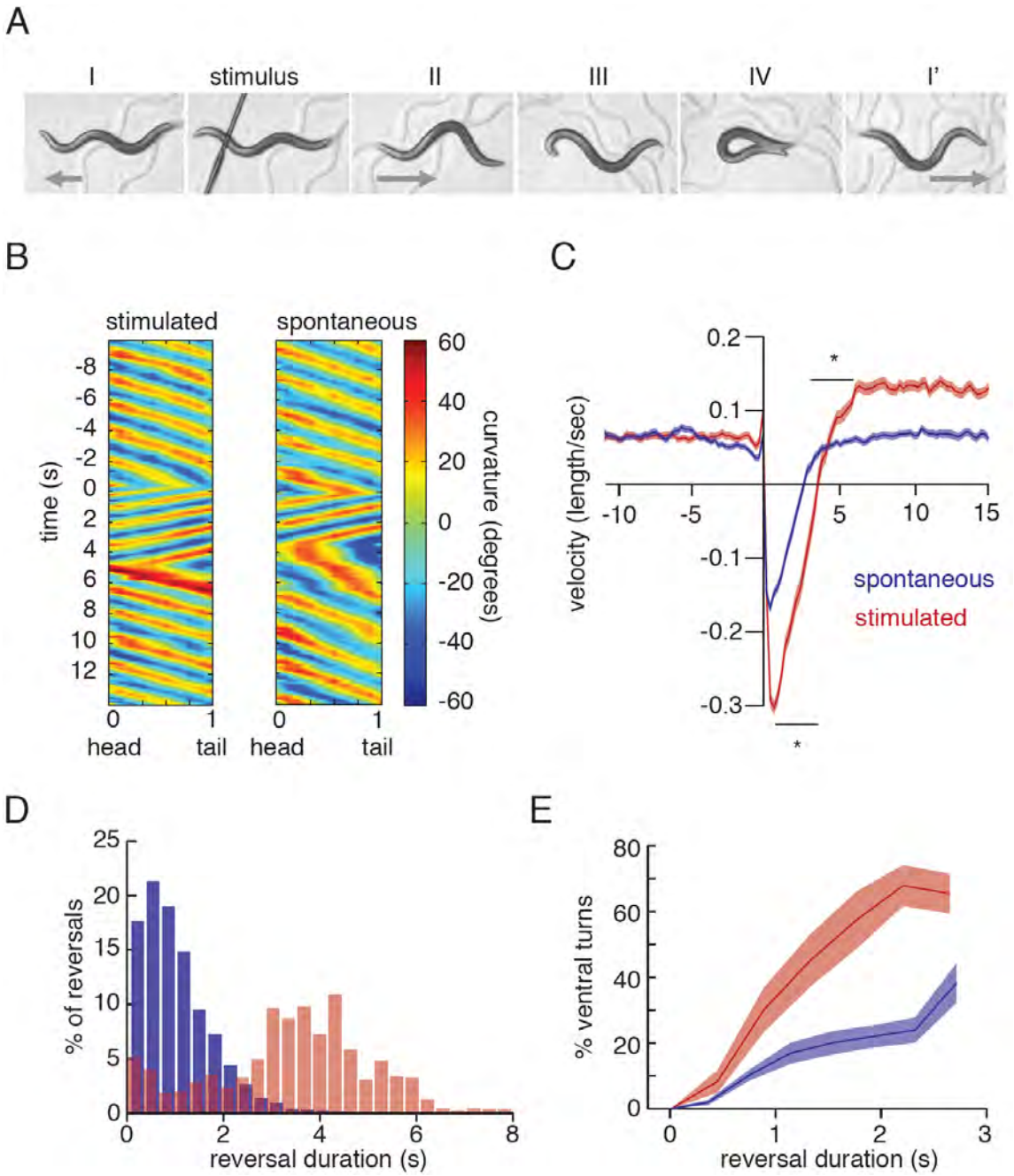

Figure II-1. The *C. elegans* escape response is a compound motor sequence.

(A) *C. elegans* executes an escape response to mechanical stimulation. The individual phases (I-IV) of a *C. elegans* escape response are shown beginning

with basal forward locomotion accompanied with foraging head movements (I). Gentle anterior touch (stimulus) induces a reversal and the suppression of head movements (II), which culminates in a deep ventral bend of the head (III) followed by the deep ventral body bend (omega turn, IV). Forward locomotion and foraging head movements are reinitiated after the omega turn (I'). Gray arrows indicate locomotion trajectory. (B) Kymographs of body bend amplitude (degrees) during a reversal in response to a tap stimulus and a spontaneous reversal. Onset of the reversal is at t=0s. (C) Mean (+/- SEM) instantaneous velocity (worm lengths/second) during escape responses to a tap stimulus (red line) and during spontaneous reversals (blue line). Instantaneous velocity traces were aligned to the onset of the reversal (t= 0s) (n for stimulated and spontaneous responses >1500). p values: *<0.05, two-tailed Student's t test. (D) Distribution of reversal durations for tap induced reversals and for spontaneous reversals (n for stimulated and spontaneous responses >1500). (E) Probability (+/- SEM) of a reversal culminating in an omega turn over increasing reversal durations following responses to a tap stimulus (red line) and following spontaneous reversals (blue line) (n=40 days of experiments).

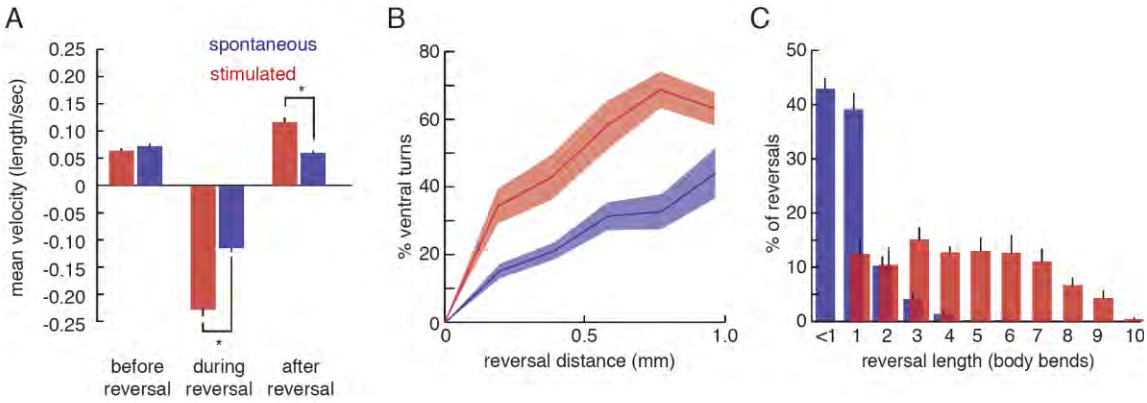

Figure II-2. Spontaneous reversals and stimulated reversals are distinct behaviors.

(A) Mean instantaneous velocity (worm lengths/second) of different aspects of stimulated (red) and spontaneous (blue) reversals (See Figure II-1C). Pre-reversal velocity is measured as a two second window before the onset of the reversal (t = -2 to 0s). Reversal velocity is measured as a two second window beginning at the onset of the reversal (t = 0 to 2s). Post-reversal velocity is measured as a two second window beginning 5s after the onset of the reversal at (t = 5 to 7s) (n for stimulated and spontaneous responses >1500). Error bars indicate SEM; p-values: *<0.05, two-tailed Student's t test. (B) Probability (+/- SEM) of a reversal culminating in an omega turn over increasing reversal distances (mm) following responses to a tap stimulus (red line) and following spontaneous reversals (blue line) (n=40 days of experiments). (C) Distribution of reversal lengths (body bends) for gentle anterior touch induced reversals (red bars, n=299) and spontaneous reversals (blue bars, n=453). Error bars indicate SEM.

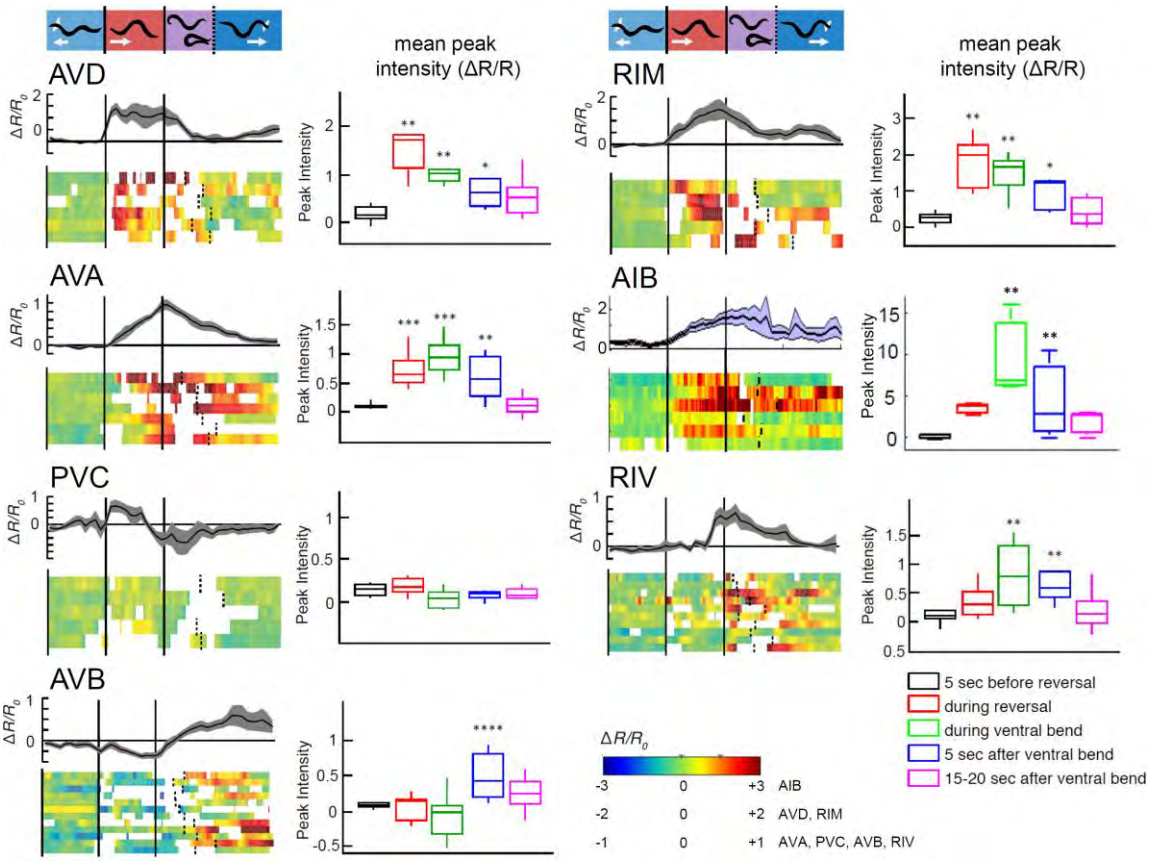

Figure II-3. Calcium dynamics in a neural network that orchestrates a compound motor sequence.

Schematic of vibration induced escape response is shown on the top (blue: forward locomotion, red: reversal, purple: ventral bend and omega turn, arrows indicate locomotion trajectory). Neural activity was measured as a fluorescence ratio of the calcium indicator GCaMP to mCherry in an unrestrained behaving animal ($\Delta R/R_0$). Neural activity traces and heat maps are aligned to the onset of the stimulated reversal (first vertical black line). Time (x-axis) is arbitrary as all traces were fit and aligned to a fixed reversal length ending with a ventral bend

(second vertical black line). The end of the omega turn is indicated with the third vertical black line (dotted). Each heat map row represents a single trial (AVD: n=6, AVA: n=7, PVC: n=5; AVB: n=12, RIM: n=5, AIB: n=6, RIV: n=10). Mean (+/- SEM) instantaneous $\Delta R/R_0$ values over time are plotted above the heat maps. Mean (+/- SEM) peak $\Delta R/R_0$ intensity during different time windows are shown in box plots to the right: 5s prior to stimulation and reversal onset (black box), during the reversal (red box), during the omega turn (green box), 5s after the omega turn during forward locomotion (blue box), 15s after the omega turn (purple box). The heat map range of $\Delta R/R_0$ values for each neuron is shown on the bottom right. The AVD, AVA, RIM, PVC, RIV and AVB neurons expressed GCaMP3 and the AIB neurons expressed GCaMP6s. Statistical significance to 5s prior to stimulation and reversal onset (black box); P-values: *<0.05, **<0.01, ***<0.001, ****<0.0001, Wilcoxon test.

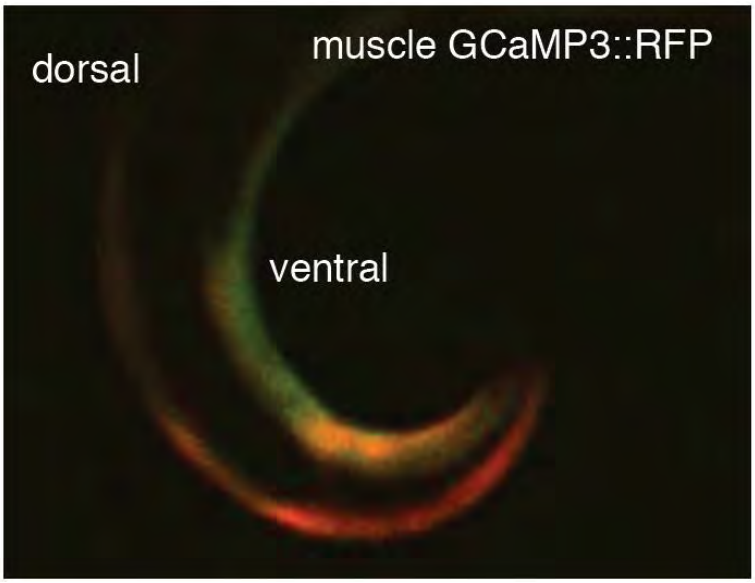

Figure II-4. Calcium activity in neck muscles during an omega turn. GCaMP3 fluorescence increases in ventral head and neck muscles during in omega turn. RFP expression in muscles is used as an activity independent fluorescent control. Muscle expression is driven by the *myo-3* promoter. See Movie II-2.

A

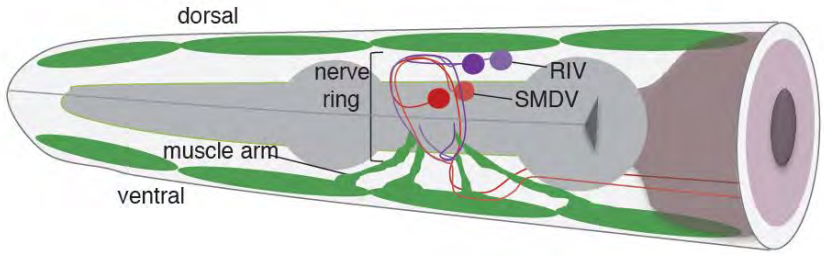
dorsal
nerve ring
RIV
SMDV
muscle arm
ventral

B

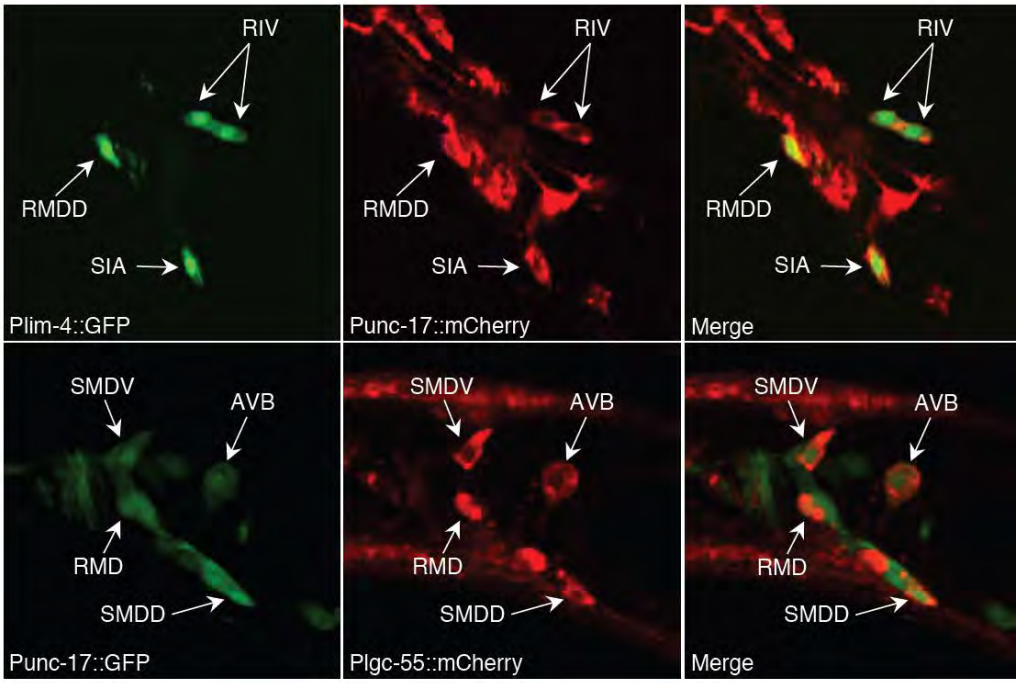
RIV
RMDD
SIA
Plim-4::GFP
RIV
RMDD
SIA
Punc-17::mCherry
RIV
RMDD
SIA
Merge
SMDV
AVB
RMD
SMDD
Punc-17::GFP
SMDV
AVB
RMD
SMDD
Plgc-55::mCherry
SMDV
AVB
RMD
SMDD
Merge

C

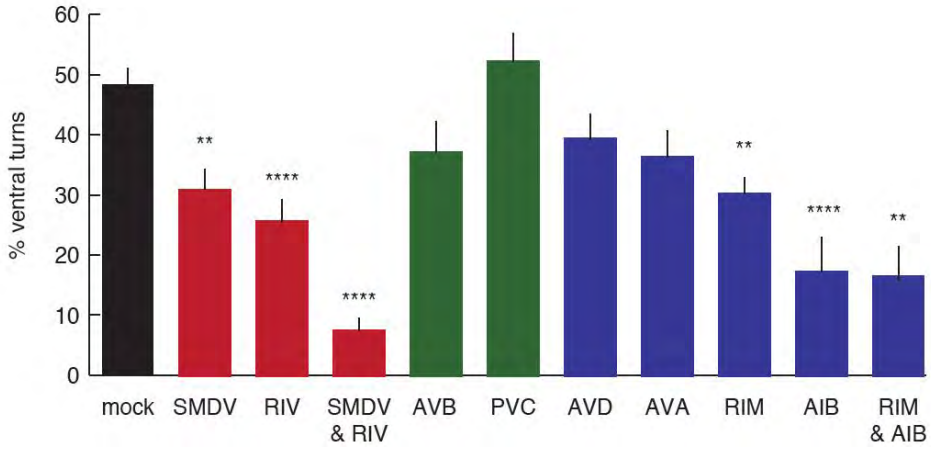
% ventral turns
60
50
40
30
20
10
0
**
****
****
**
****
**
mock
SMDV
RIV
SMDV & RIV
AVB
PVC
AVD
AVA
RIM
AIB
RIM & AIB

Figure II-5. Initiation of the omega turn requires the cholinergic SMD and RIV motor neurons.

(A) Cartoon of SMDV (red) and RIV (purple) motor neuron anatomy in the worm's head. The SMDV and RIV make neuromuscular junctions with the ventral neck muscle arms. Muscles are shown in green; the pharynx is shown in dark gray. (B) Fluorescent images of cell bodies in the nerve ring. Co-expression of SMDV and RIV reporters (P*lgc-55* and P*lim-4* respectively) with an acetylcholine vesicular transporter marker (P*unc-17*) indicates that the SMDV and RIV are excitatory cholinergic motor neurons. (C) Mean percentage of animals making a ventral turn in response to gentle anterior touch. Laser ablation of neurons in the neural circuit for the escape response results in omega turn defects. Ablation of the RIM, SMDV, RIV or AIB impaired an animal's ability to execute an omega turn in response to gentle anterior touch (mock: n=64, -SMDV: n=16, -RIV: n=41, -SMDV & -RIV: n=9, -AVB n=14, -PVC: n=12, -AVD: n=14, -AVA: n=12, -RIM: n=27, -AIB: n=13, -RIM & -AIB: n=10). Error bars indicate SEM. Statistical significance to mock ablated animals; p-values: **< 0.005, ****< 0.0001, two-tailed Student's t test.

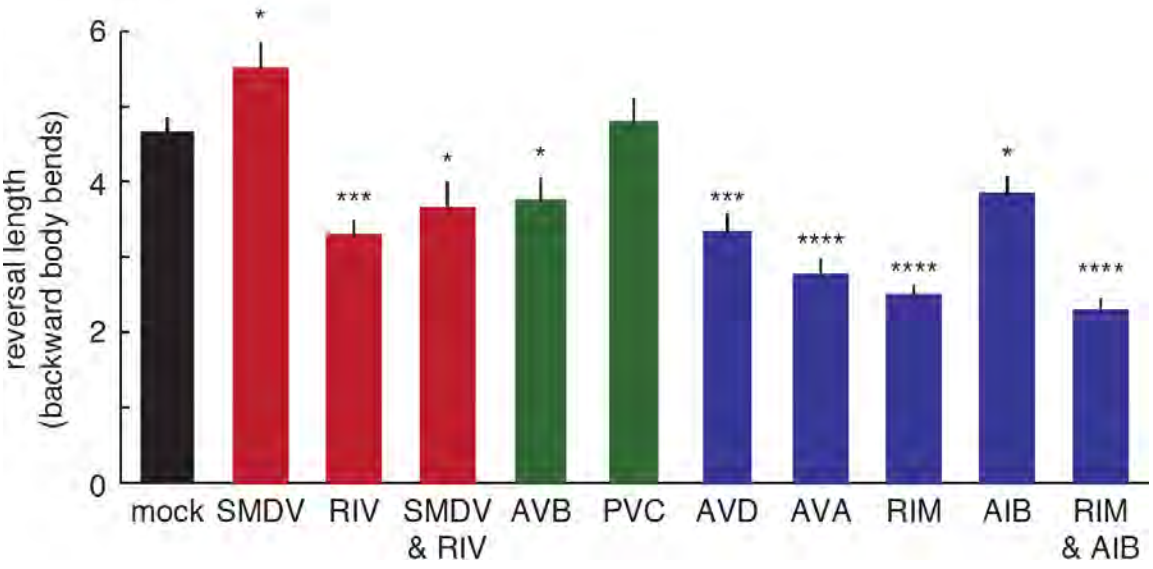

Figure II-6: Touch response reversal length after neuron ablation.

Laser ablation of neurons in the escape response neural circuit had varying impacts on the length of a reversal (body bends) in response to gentle anterior touch (mock: n=28; -AVD: n=14; -AVA: n=12; -AVB: n=14; -PVC: n=12; -RIM: n=22; -AIB: n=13; -RIV: n=41; -SMDV: n=16; -SMDV & -RIV: n=9, -RIM & -AIB: n=10). Error bars indicate SEM. Statistical significance to mock ablated animals; p-values: *< 0.5, ***< 0.005, ****< 0.0001, two-tailed Student's t test.

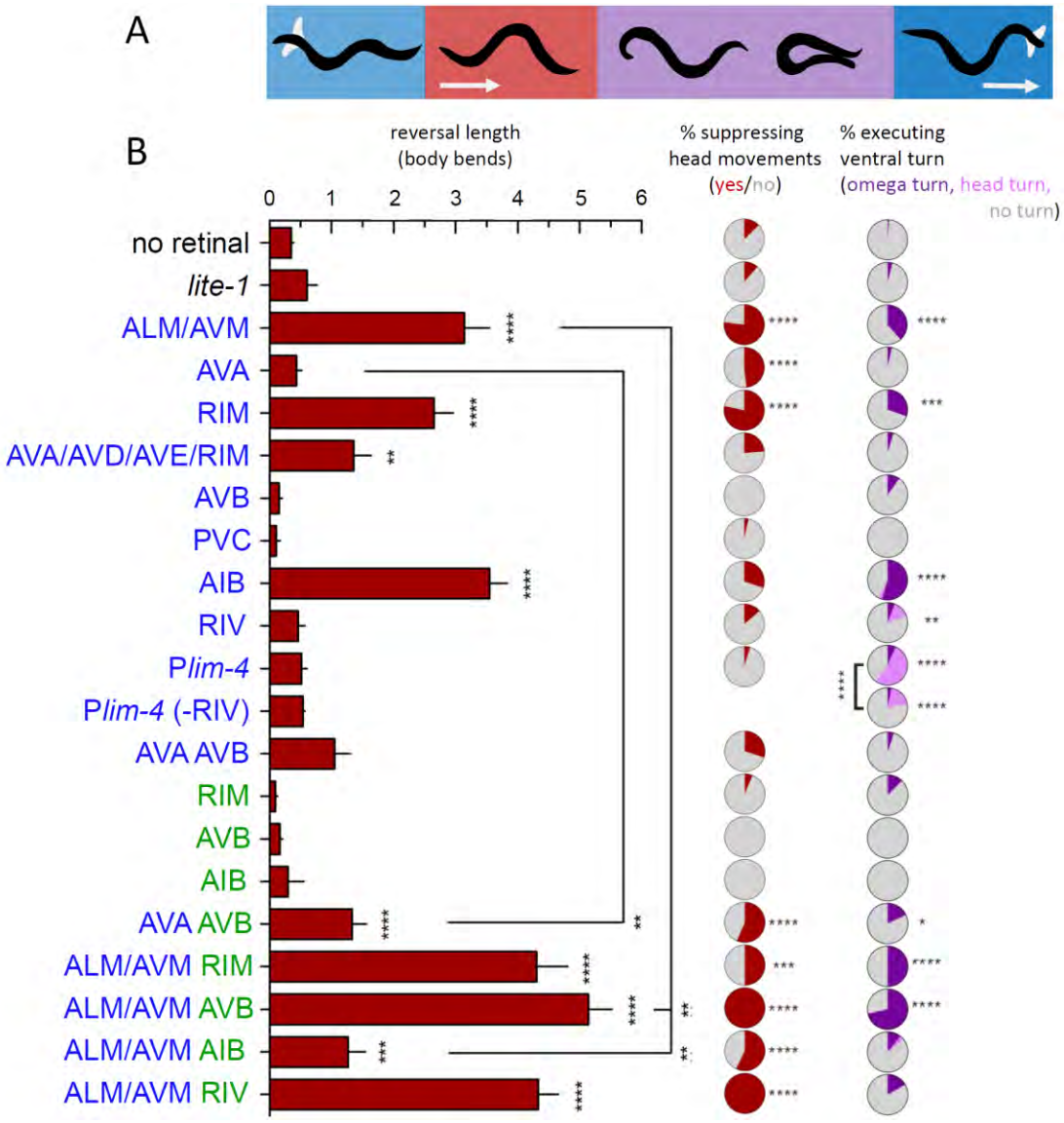

Figure II-7. Optogenetic stimulation of individual neurons induces sub-motor programs of the escape response.

(A) Schematic of escape response (blue: forward locomotion, red: reversal, purple: ventral bend and omega turn, arrows indicate locomotion trajectory). (B) Stimulation of neurons expressing the optogenetic proteins ChR2 (blue) and Arch (green) elicited aspects of escape response behavior. Blue indicates blue light

stimulation of ChR2 expressing neurons. Green indicates green light stimulation of Arch expressing neurons. Mean reversal length (backward body bends, red bars), mean fraction of animals suppressing head movements (red pie charts), and mean fraction of animals executing ventral turns (purple pie charts) were measured after neuron stimulation (rows). The fraction of ventral turns is divided into omega turns that occurred after a reversal (dark purple) and ventral head bends that did not accompany a reversal (light purple). Blue light stimulation of animals expressing ChR2 a subset of neurons (P*lim-4*) that included the RIV resulted ventral bending. Ablation of the RIV in these animals resulted in ventral turning defect. Each row represents at least 3 animals tested. Number of trials: no retinal: n=247; *lite*-1: n=52; ALM/AVM ChR2: n=39; AVA ChR2: n=29; RIM ChR2: n=23; AVA/AVD/AVE/RIM ChR2: n=21; AVB ChR2: n=20; PVC ChR2: n=28; AIB ChR2: n=33; RIV ChR2: n=51; P*lim-4*::ChR2 mock ablation: n=30; P*lim-4*::ChR2 RIV ablation: n=95; AVA/AVB ChR2: n=20; AVB Arch: n=27; RIM Arch: n=16; AIB Arch: n=15; AVA ChR2; AVB Arch: n=39; ALM/AVM ChR2, AVB Arch: n=14; ALM/AVM ChR2, RIM Arch: n=18; ALM/AVM ChR2, AIB Arch: n=28; ALM/AVM ChR2, RIV Arch: n=6. *lite-1(ce314)* mutants supplemented with retinal were tested to show the basal light response. Statistical difference from the blue light stimulated control group of animals not supplemented with *all-trans* retinal unless otherwise noted. Error bars indicate SEM; p-values: *<0.05, **<0.01, ***<0.001, ****<0.0001, two-tailed Student's t test.

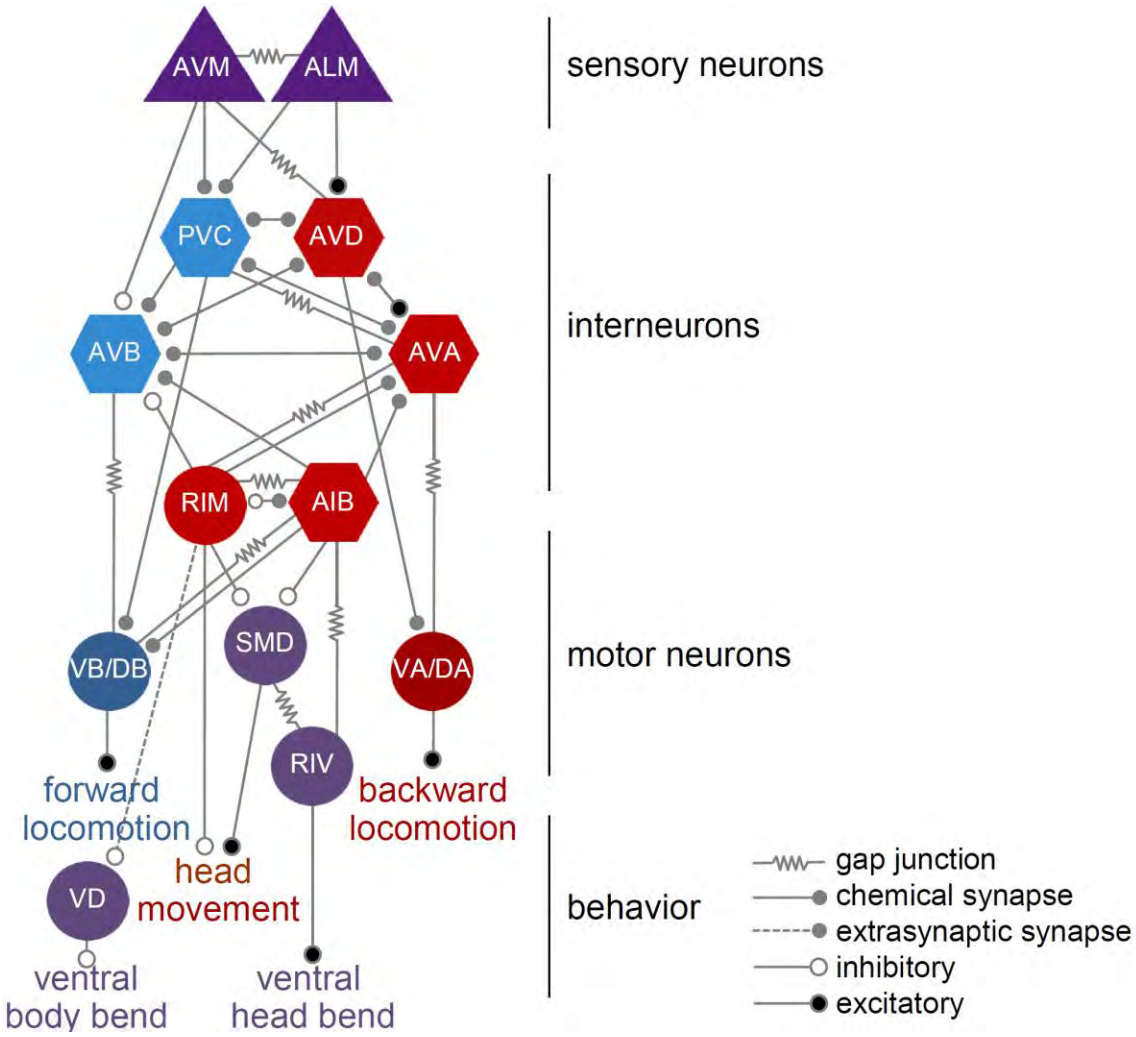

Figure II-8. The neural circuit for the *C. elegans* escape response.

Mechanosensory neurons (purple triangles) transduce mechanical stimulation from gentle anterior touch to locomotion interneurons (hexagons) and motor neurons (circles) to coordinate phases of the escape response. Red neurons are associated with backward locomotion. Blue neurons are associated with forward locomotion. Purple motor neurons are associated with ventral bending. White circles indicate inhibitory synaptic connections and black circles indicate

excitatory synaptic connections. The nature of the synaptic connections indicated with gray circles is unknown. Zig-zag lines indicate gap junctions. Dotted lines indicate extra-synaptic signaling to non-postsynaptic neurons.

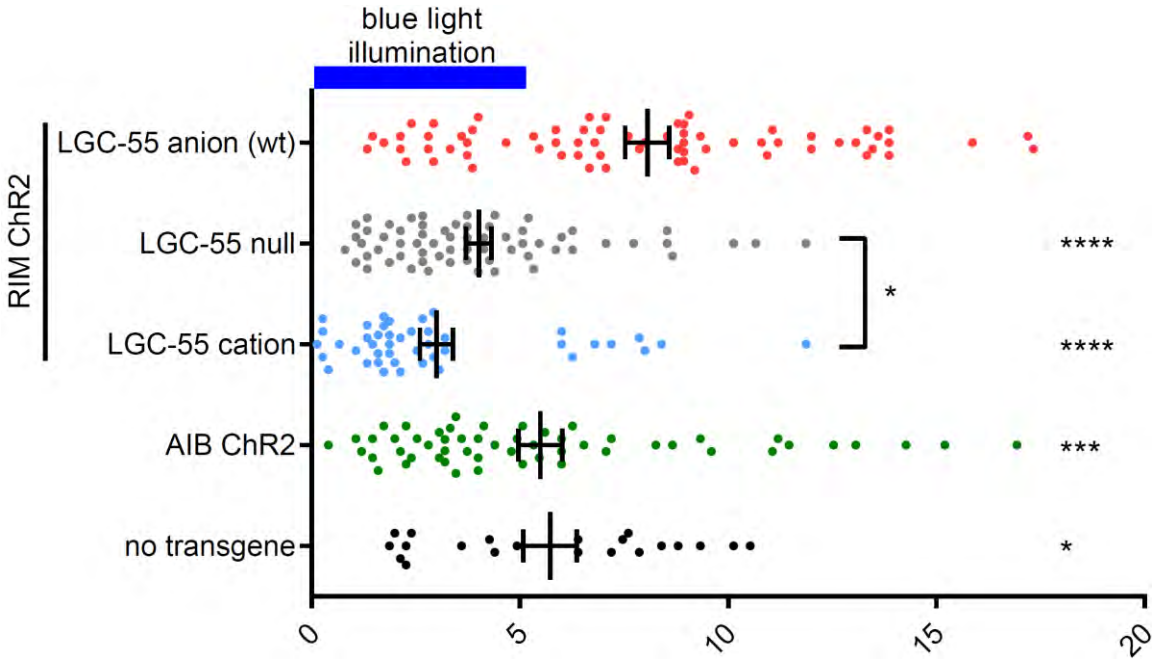

Figure II-9: The timing of the ventral turns induced by optogenetic stimulation.

Ventral turns that occurred independent of reversals were measured in *unc-3(e151)* mutants expressing ChR2 in the RIM (P*tdc-1*) or AIB (P*npr-9*). Animals were stimulated with blue light for 3-5 seconds (blue bar) to activate ChR2. The timing of the induced ventral bends was measured from the onset of blue light stimulus (t=0s). wt indicates *unc-3* mutants that are wild type for head movements [RIM::ChR2(*zfIs9*); LGC-55 anion (wt)]: n=70; [RIM::ChR2(*zfIs9*); LGC-55 null (*tm2913*)]: n=64; [RIM::ChR2(*zfIs9*); LGC-55 cation (*zfEx275*)]: n=44; [AIB::ChR2(*zfIs112*)]: n=55; no transgene: n=21. Error bars indicate SEM. Statistical difference from [RIM::ChR2(*zfIs9*); LGC-55 anion (wt)] unless otherwise noted; p-values: ****< 0.0001, ***< 0.001, *< 0.05, two-tailed Student's t-test.

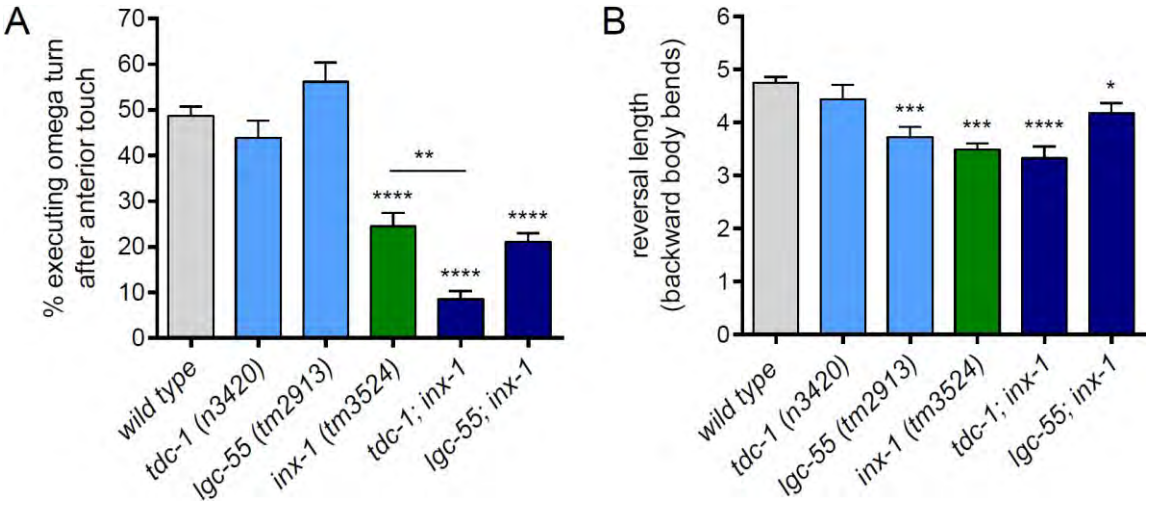

Figure II-10: Touch response behaviors of tyramine and gap junction signaling mutants.

(A) The percentage of animals that executed an omega turn in response to gentle anterior touch is shown. (B) The mean reversal length (backward body bends) of escape responses from gentle anterior touch is shown, wild type: n=853, *tdc-1(n3420)*: n=475(omega turns), n=331(reversal length), *lgc-55(tm2913)*: n=226, *inx-1(tm3524)*: n=208, *tdc-1; inx-1*: n=173, *lgc-55; inx-1*: n=312. Error bars indicate SEM. Statistical difference from wild type unless otherwise noted; p-values: ****< 0.0001, ***< 0.001, **< 0.005; *< 0.05, two-tailed Student's t-test.

Movie II-1:

Calcium activity of neurons during the escape response in a live, behaving animal. GCaMP3 and mCherry are expressed in the RIV motor neurons (left panels). The ratio of GCaMP3 to mCherry fluorescence is measured during a behavioral response to a mechanical (vibration) stimulus. Behavior of the worm is tracked (left panel) using dark field infrared illumination to keep the head of the worm centered in the field of view.

Movie II-2:

Calcium activity of muscles during the escape response in a live, behaving animal. GCaMP3 and RFP are expressed in muscles. An escape response is induced with a mechanical (vibration) stimulus. Behavior of the worm is tracked using dark field infrared illumination to keep the worm centered in the field of view.

Movie II-3:

Optogenetic activation of the ALM and AVM mechanosensory neurons expressing ChR2 using a spatially controlled illumination pattern.

Movie II-4:

Optogenetic activation of the AVA premotor interneurons expressing ChR2 using a spatially controlled illumination pattern.

Movie II-5:

Optogenetic activation of the RIM tyraminergic neurons expressing ChR2 using a spatially controlled illumination pattern.

Movie II-6:

Optogenetic activation of the AVA expressing ChR2 and inhibition of the AVB expressing Arch using a spatially controlled illumination pattern of blue and green light.

Movie II-7:

Optogenetic induction of ventral head bending behavior in an animal expressing ChR2 under the *lim-4* promoter.

Movie II-8:

Optogenetic activation of the AIB interneurons expressing ChR2 using a spatially controlled illumination pattern.

Movie II-9:

Optogenetic activation of the ALM and AVM expressing ChR2 and inhibition of the RIV expressing Arch using a spatially controlled illumination pattern of blue and green light. Green light stimulation was not applied until the blue light induced reversal response reached several body bends in length.

Movie II-10:

Optogenetic activation of the RIM induced delayed ventral bending behavior in animals expressing the wild-type tyramine-gated anion channel, LGC-55. RIM activation was done in *unc*-3 mutant animals to genetically uncouple turning behavior from reversals.

Movie II-11:

Optogenetic activation of the RIM induced immediate ventral bending behavior in animals expressing the tyramine-gated channel, LGC-55, that was engineered to be a cation channel. RIM activation was done in *unc*-3 mutant animals to genetically uncouple turning behavior from reversals.

PREFACE TO CHAPTER III

The work presented in this chapter demonstrates how the biogenic amine, tyramine, functions to coordinate different phase of a compound behavior. Tyramine is a neurotransmitter that is released from the RIM interneurons during the *C. elegans* escape response and functions as an extrasynaptic neurotransmitter in addition to its role as a classical synaptic neurotransmitter. . Tyramine activates ionotropic receptors, LCG-55, expressed in neurons post-synaptic to the RIM. In this study, we show that tyramine also activated neurons that are not post-synaptic to the RIM through the extrasynaptic GPCR, SER-2. Following a mechanical stimulation, tyraminergic activation of the fast acting LGC-55 ionotropic receptor coordinates the reversal and suppression of head movements while tyraminergic activation of the slower acting SER-2 metabotropic receptor facilitates the deep ventral bend that reorients the worm's locomotion trajectory. Through this bimodal activation mechanism, a single neurotransmitter, tyramine, can orchestrates of a compound motor sequence.

Jamie Donnelly, Jennifer Pirri and Mark Alkema performed the genetic screen and pharmacological assays. Jamie Donnelly, Jennifer Pirri and Christopher Clark generated the transgenic strains used in the GPCR signaling experiments. Jamie Donnelly and Christopher Clark performed the fluorescent imaging experiments. Marian Huburcak and Michael Francis performed the electrophysiology experiments. Christopher Clark performed the laser ablations

and subsequent navigation experiments. Jamie Donnelly and Christopher Clark generated the transgenic strains used in the optogenetic experiments. Jamie Donnelly, Andrew Leifer and Christopher Clark performed the DD optogenetic experiments in the lab of Aravinthan Samuel. Jamie Donnelly and Christopher Clark performed the behavioral experiments measuring the features of omega turns. Michael Francis, Aravinthan Samuel and Mark Alkema designed the experiments. Jamie Donnelly, Christopher Clark and Mark Alkema co-wrote the manuscript. All authors discussed the results and commented on the manuscript**.** This work was published in the journal *PLoS Biology* in 2013.

CHAPTER III: MONOAMINERGIC ORCHESTRATION OF MOTOR PROGRAMS IN A COMPLEX *C. ELEGANS* BEHAVIOR

Jamie L Donnelly[1†], Christopher M Clark[1†], Andrew M Leifer[2], Jennifer K Pirri[1], Marian Haburcak[1], Michael M Francis[1], Aravinthan DT Samuel[2] and Mark J Alkema[1]

1. Department of Neurobiology, University of Massachusetts Medical School, 364 Plantation Street, Worcester, MA 01605, USA
2. Department of Physics & Center for Brain Science, Harvard University, 17 Oxford Street, Cambridge, MA 02138, USA

† Authors contributed equally

Published in *PLoS Biology* (2013) 11: e1001529.

Summary

How the nervous system controls complex innate behaviors has intrigued neurobiologists for decades. There are many examples where the sequential motor patterns that comprise these complex behaviors have been described in great detail. However, the neural mechanisms that orchestrate a behavioral sequence are poorly understood. Gentle touch to the head of the roundworm *C. elegans* elicits an escape response in which the animal quickly moves backward. The reversal is followed by a deep turn that allows the animal to change its direction of locomotion and move away from the threatening stimulus. We found that the neurotransmitter tyramine controls the initial reversal phase of the escape response through the activation of a fast-acting ion channel and the later turning phase through the activation of a slow-acting G-protein coupled receptor (GPCR). We show that this tyramine GPCR is expressed in neurons that make contacts with the ventral muscles of the animal. Activation of this receptor facilitates the contraction of ventral muscles and thus allows the animal to turn and resume locomotion in the opposite direction during its escape. Our studies show how a single neurotransmitter coordinates sequential phases of a complex behavior through the activation of distinct classes of receptors: the synaptic activation of a fast-acting ion channel and extra-synaptic activation of a slow-acting G-protein coupled receptor.

Abstract:

Monoamines provide chemical codes of behavioral states. However, the neural mechanisms of monoaminergic orchestration of behavior are poorly understood. Touch elicits an escape response in *Caenorhabditis elegans* where the animal moves backward and turns to change its direction of locomotion. We show that the tyramine receptor SER-2 acts through a $G\alpha_o$ pathway to inhibit neurotransmitter release from GABAergic motor neurons that synapse onto ventral body wall muscles. Extra-synaptic activation of SER-2 facilitates ventral body wall muscle contraction, contributing to the tight ventral turn that allows the animal to navigate away from a threatening stimulus. Tyramine temporally coordinates the different phases of the escape response through the synaptic activation of the fast-acting ionotropic receptor, LGC-55, and extra-synaptic activation of the slow-acting metabotropic receptor, SER-2. Our studies show how a sensory input recruits the action of a monoamine to change neural circuit properties and orchestrate a compound motor sequence with single-cell resolution.

Introduction

Complex behaviors require the temporal coordination of independent motor programs in which neurotransmitters and neuromodulators orchestrate the output of neural circuits. How the nervous system directs sequential activation and inhibition of assemblies of neurons, however, is largely unclear. Neurotransmitters can directly activate ligand-gated ion channels at synapses inducing rapid changes in

the electrical activity of post-synaptic cells. Neuromodulators generally act through G-protein coupled receptors (GPCR) that activate intracellular signaling cascades with slower but longer lasting effects. The release of neuromodulators can activate or refine basic motor patterns generated by fast acting neurotransmitters in a neural network (Marder and Bucher, 2001; Grillner and Jessell, 2009; Harris-Warrick, 2011).

In mammals, monoamines such as serotonin, dopamine and noradrenaline are associated with specific behavioral states. Adrenergic modulation provides one of the most striking examples of the coordination of behavior and physiology to reflect an internal state of stress. Adrenergic transmitters stimulate the amygdyla and increase heart rate, muscle tone, oxygen supply to the brain and the release of glucose from energy stores to prepare for a fight-or-flight response (Brede, et al., 2004). Noradrenaline and adrenaline are not used by invertebrates but the structurally related monoamines octopamine and tyramine are often considered as the invertebrate counterparts of these adrenergic transmitters (Roeder, 2005). Octopamine and tyramine have been implicated in subordinate behavior in lobsters (Kravitz, 1988), the honey bee sting response (Burrell and Smith, 1995), the energy metabolism of flight in locusts (Adamo, et al., 1995), aggression in crickets and fruit flies (Baier, et al., 2002; Certel, et al., 2007; Stevenson, et al., 2005; Zhou, et al., 2008), and the escape response of *C. elegans* (Alkema, et al., 2005). Pioneering studies in the locust (Pfluger, 1999), mollusks (Katz, 1998) and crustaceans (Bicker and

Menzel, 1989) have supported an “orchestration hypothesis” (Hoyle, 1985) where monoamines control behavioral states through the recruitment of distinct neural circuits. However, the sensory input that triggers the release of monoamines and the molecular and neural coding of these behaviors remain poorly understood.

The *C. elegans* escape response consists of a behavioral sequence used by the animal to navigate away from a threatening stimulus. *C. elegans* moves on its side by propagating a sinusoidal wave of ventral-dorsal muscle contractions along the length of its body (Croll, 1975). Locomotion is normally accompanied by exploratory head movements in which the tip of the nose moves rapidly from side to side. Gentle touch to the head elicits a backing response and the suppression of exploratory head movement (Alkema, et al., 2005; Chalfie, et al., 1985). The backing response is usually followed by a deep ventral head bend, allowing the animal to make a sharp (omega) turn and change its direction of locomotion. The completion of the entire escape response takes approximately 10 seconds and requires sensory processing, decision-making, and sequential inhibition and activation of distinct motor programs. Therefore, the anterior touch response is a highly orchestrated motor sequence with complexity far beyond that of a simple reflex.

The neural wiring diagram in combination with genetic and laser ablation experiments has provided a framework for the neural circuit that controls the initial phase of the escape response (Chalfie, et al., 1985; White, et al., 1986; Wicks and Rankin, 1995). *C. elegans* has a single pair of tyraminergic motor

neurons that are essential in coordinating the backing response with suppression of head movements (Alkema, et al., 2005). Synaptic activation of the tyramine-gated chloride channel, LGC-55 inhibits forward locomotion and induces the relaxation of neck muscle (Pirri, et al., 2009) (see also Figure III-13). The coordination of these motor programs increases the animals' chances of escaping from predacious fungi that use constricting rings to catch nematodes, illustrating the vital importance of monoaminergic motor control (Maguire, et al., 2011; Pirri and Alkema, 2012). How this initial phase of the escape response is temporally linked to later stages in which the animal makes a sharp turn to navigate away from the stimulus is unknown. To elucidate how monoamines may orchestrate the activity of specific neural circuits in complex behaviors, we analyzed the role of tyramine in *C. elegans* locomotion during the escape response. We show that the extra-synaptic activation of a G-protein coupled tyramine receptor generates asymmetry in a locomotion program, thus allowing the animal to execute a deep ventral turn and navigate away from the stimulus.

Results

ser-2 mutants are resistant to exogenous tyramine

C. elegans become immobilized on plates containing exogenous tyramine in a dose-dependent manner (Figure III-1A and Figure III-2, Pirri, et al., 2009). Three GPCRs have been shown to bind tyramine with high affinity: TYRA-2, TYRA-3, and SER-2 (Rex and Komuniecki, 2002; Rex, et al., 2005; Wragg, et al.,

2007; Rex, et al., 2004). To determine whether the effects of tyramine are mediated by these GPCRs, we examined the locomotion of *ser-2(pk1357* and *ok2103)*, *tyra-2(tm1815)* and *tyra-3(ok325)* deletion mutants on agar plates containing exogenous tyramine. Wild-type, *tyra-2* and *tyra-3* mutant animals become immobilized on 30 mM tyramine within 5 minutes (Figure III-3). However, *ser-2* mutant animals sustained movement on plates containing exogenous tyramine (Figure III-1A-C and Figure III-2). Sensitivity to exogenous tyramine is restored back to wild-type levels in *ser-2* mutants containing a *ser-2* genomic transgene (Figure III-1B, C and Figure III-3). This indicates that exogenous tyramine mediates its paralytic effects through the hyperactivation of endogenous tyramine signaling pathways that are at least in part dependent on SER-2.

We have previously shown that activation of the tyramine-gated chloride channel, LGC-55, inhibits head movements and forward locomotion (Pirri, et al., 2009). Exogenous tyramine initially induced backward locomotion and the inhibition of head movements in both the wild type *and ser-2* mutants. However, unlike the wild type, *ser-2* mutants recovered and resumed forward locomotion and head movements within minutes. Body movements of *lgc-55* mutants are inhibited, similar to the wild type, but head movements are sustained on exogenous tyramine (Figure III-1C, D). *lgc-55; ser-2* double mutants largely persisted both head and body movements on exogenous tyramine, however, locomotion remained slightly uncoordinated. This indicates that while the activation of the ionotropic LGC-55 and metabotropic SER-2 receptor are

required for paralysis, exogenous tyramine may affect locomotion through the activation of other receptors.

Head movements and body movements are controlled by distinct groups of muscles and motor neurons (Alkema , et al., 2009; White, et al.,1986). In wild type animals the inhibition of head movements occurred rapidly (half time to immobilization, t_{i50} = 77 ± 2 s) and was followed by the slower inhibition of body movement (t_{i50} = 149 ± 3 s). This suggests that signaling pathways with distinct kinetics contribute to tyramine's effects. The sustained body movements of *ser-2* mutants on exogenous tyramine make it difficult to dissect the effects of exogenous tyramine on head movements. Therefore, we analyzed the effect of tyramine on head movements in an *unc-3(e151)* mutant background. *unc-3* mutants display few body movements, but have normal head movements (Prasad, et al., 1998). Head movements of *ser-2 unc-3* double mutants were inhibited on exogenous tyramine, like those in the wild type and *unc-3* mutants Figure III-1D). Consistent with our previous observation (Pirri, et al., 2009), head movements were sustained in *lgc-55: unc-3* double mutants. The kinetics and distinct inhibition of head and body movements of *lgc-55* and *ser-2* mutants indicates that exogenous tyramine induces the fast immobilization of head movements mainly through the hyper-activation of the ionotropic tyramine receptor LGC-55 followed by the immobilization of body movements through hyper-activation of the metabotropic tyramine receptor SER-2.

$G\alpha_o$ signaling pathway mutants are resistant to exogenous tyramine

To identify genes involved in tyramine signaling, we performed a genetic screen for mutants that are resistant to the immobilizing effects of exogenous tyramine on body movements. Four isolates from this screen, *zf47*, *zf97, zf98 and zf133* sustained movement on plates containing 30 mM tyramine. Genetic mapping, complementation tests and sequence analysis showed that *zf47* was an allele of *goa-1. goa-1* encodes the *C. elegans* ortholog of the neural G protein-alpha subunit of the $G\alpha_o$ class. GOA-1/$G\alpha_o$ is expressed throughout the nervous system and is thought to negatively regulate synaptic transmission through the inhibition of EGL-30, the *C. elegans* $G\alpha_q$ ortholog (Brundage, et al.,1996; Lackner, et al., 1999; Miller, et al., 1999). We found that *zf97, zf98* and *zf133* were alleles of *dgk-1*, which encodes the *C. elegans* ortholog of the vertebrate brain diacylglycerol kinase theta (DAGθ) (Miller, et al., 1999; Nurrish, et al., 1999). *dgk-1* mutants have a reduced ability to deplete DAG generated by the *egl-30/*$G\alpha_q$ pathway (Nurrish, et al., 1999; Jose and Koelle, 2005). Previously characterized null mutants for *goa-1* and *dgk-1* were also resistant to the paralytic effect of tyramine on both head and body movements (Figure III-1B). We found that *egl-30*/$G\alpha_q$ gain-of-function mutants and mutants for *eat-16,* which encodes a Regulator of G-protein Signaling (RGS) protein that inhibits EGL-30 (Hajdu-Cronin, et al., 1999) are resistant to exogenous tyramine (Figure III-1B). Unlike *goa-1* and *dgk-1* mutants, which exhibit hyperactive locomotion and egg-laying behavior, *ser-2* mutants did not have obvious behavioral defects (Tsalik, et

al., 2003). Therefore, mutations that reduce GOA-1/$G\alpha_o$ signaling or increase EGL-30/$G\alpha_q$ signaling confer resistance to exogenous tyramine. The resistance of *goa-1* and *ser-2* mutants to exogenous tyramine, suggest that SER-2 signals through GOA-1/$G\alpha_o$ to modulate locomotion.

SER-2 acts in GABAergic neurons

Where does SER-2 act to confer resistance to exogenous tyramine? A *ser-2* genomic rescuing transgene restored sensitivity of *ser-2* mutants to exogenous tyramine, indicating that the transgene is expressed in the cells that confer sensitivity to exogenous tyramine (Figure III-1B and Figure III-3). The *ser-2* genomic locus is large and complex and encodes several splice variants (Rex and Komuniecki, 2002; Tsalik, et al., 2003). To analyze the *ser-2* expression pattern we expressed mCherry under the control of an 11.8 kb *ser-2* promoter sequence that included the four alternative first exons. We found that our *Pser-2*::mCherry reporter was expressed in head muscles, as well as several neurons in the head and ventral cord. The *ser-2* reporter was expressed in the first and second row of muscle cells, which are distinct from neck muscles (third and fourth row of muscle cells) that express the tyramine-gated chloride channel LGC-55 (Figure III-4). *lgc-55* mutants fail to suppress head movements in response to touch but head movements were suppressed normally in *ser-2* mutants, indicating that only LGC-55 is required for tyramine induced head relaxation. The *ser-2* reporter was not expressed in interneurons that control

locomotion, as expression did not overlap with *Pglr-1*::GFP and *Plgc-55*::GFP reporters that are expressed in the locomotion command neurons (data not shown). *ser-2* reporter expression was also observed in 13 cells in the ventral cord (Figure III-5A) that send commissures to the dorsal cord. The ventral cord is composed of excitatory cholinergic and inhibitory GABAergic motor neurons that innervate body wall muscles and control locomotion. Coexpression analysis with GFP reporters that specifically label cholinergic or GABAergic neurons showed that *Pser-2*::mCherry was highly expressed in a subset GABAergic motor neurons (Figure III-5B-D). The same set of GABAergic motor neurons were labeled in transgenic line (*Pser-2a*::GFP) that expressed a reporter for the SER-2A isoform (data not shown) (Tsalik, et al., 2003). GABAergic ventral nerve cord neurons are subdivided into 13 VD motor neurons that synapse onto the ventral body wall muscles, and 6 DD motor neurons that synapse onto the dorsal body wall muscles. The cells that highly express the *ser-2* reporter do not co-label with a *Pflp-13*::GFP reporter, which is expressed in the DD motor neurons (Kim and Li, 2004) (data not shown). This indicates SER-2 is specifically expressed in the GABAergic VD motor neurons.

Since GABAergic motor neurons are required for normal locomotion, we tested if SER-2 acts in these cells to mediate the inhibitory effects of tyramine on movement. No other promoters have been described that specifically drive expression in the GABAergic VD neurons. The complexity and size of the *ser-2* promoter did not allow us to define promoter elements that specifically drive

expression in the VD neurons. We therefore expressed *ser-2* cDNA in all GABAergic neurons using the *unc-47* promoter (*Punc-47::*SER-2). *ser-2* expression in GABAergic neurons of *ser-2* mutants restored normal sensitivity to exogenous tyramine (Figure III-5E).

To determine if GABA signaling affects tyramine sensitivity, we tested GABA-deficient mutants for sensitivity to exogenous tyramine. We found that *unc-25* mutants, that lack glutamate decarboxylase required for GABA synthesis (Jin, et al., 1999), were slightly hypersensitive to the immobilizing effects of exogenous tyramine (Figure III-5E, Figure III-6). This suggests that reduced GABA signaling increases the sensitivity to exogenous tyramine, likely through the hyperactivation of other tyramine receptors, such as LGC-55 and TYRA-2. GABA deficiency suppressed the resistance phenotype of *ser-2* mutants, since *unc-25; ser-2* double mutants were nearly as sensitive to tyramine as *unc-25* single mutants (Figure III-5E). These epistasis experiments indicate that SER-2 acts upstream or in parallel to GABAergic signaling and are consistent with the hypothesis that SER-2 acts in the VD neurons to inhibit GABA signaling and control locomotion.

We performed cell specific rescue experiments to determine whether G-protein signaling components are required in the GABAergic neurons to mediate sensitivity to the exogenous tyramine. Expression of *goa-1* or *eat-16* in the GABAergic neurons (*Punc-47::*GOA-1/Gα_o and *Punc-47::*EAT-16/RGS) of *goa-1* and *eat-16* mutants, respectively, did not rescue the hyperactive locomotion

phenotype. However, *goa-1* expression in GABAergic neurons of *goa-1* mutants largely restored sensitivity to exogenous tyramine (Figure III-5E, Figure III-6). Similarly, rescue expression of *eat- 16* in GABAergic neurons partly restores sensitivity to exogenous tyramine. The activation of the $G\alpha_q$ pathway in other cells may contribute to tyramine resistance phenotype in G-protein signaling mutants since the sensitivity to tyramine is not completely restored to wild type levels. Nonetheless, the increased sensitivity of GABA-neuron specific rescue of G-protein signaling mutants suggest that exogenous tyramine induces body immobilization through the activation of SER-2A and a $G\alpha_o$ pathway in GABAergic neurons.

SER-2 inhibits neurotransmitter release

To test the hypothesis that SER-2 modulates neurotransmitter release from ventral cord motor neurons, we analyzed mutants for their sensitivity to the acetylcholinesterase inhibitor aldicarb. Aldicarb increases acetylcholine (ACh) concentration at the neuromuscular junction (NMJ), causing muscle contraction and eventual paralysis. Mutants with impaired ACh release are resistant to aldicarb-induced paralysis (Nonet, et al., 1993). *egl-30*/$G\alpha_q$ mutants are resistant to aldicarb, whereas *goa-1* mutants are hypersensitive to aldicarb-induced paralysis, indicating that EGL-30/$G\alpha_q$ stimulates and GOA-1/$G\alpha_o$ inhibits ACh release from motor neurons (Lackner, et al., 1999; Miller, et al., 1999; Nurrish, et al., 1999). Since body wall muscles also receive inhibitory GABA inputs,

hypersensitivity to aldicarb can also be caused by decrease in GABA release at the NMJ (Jiang, et al., 2005; Loria, et al., 2003; Vashlishan, et al., 2008). The time course of paralysis of *ser-2* mutants induced by aldicarb was similar to the wild type (Figure III-7A). This may be due to the restricted expression of *ser-2* in a subset of GABAergic neurons or insufficient endogenous tyramine signaling to modulate GABA release under regular assay conditions. We therefore generated transgenic lines that overexpressed *ser-2* in all cholinergic motor neurons (*Pacr-2*::SER-2) or GABAergic (*Punc-47*::SER-2) motor neurons and analyzed the rate of aldicarb-induced paralysis. In the absence of exogenous tyramine, the time course of paralysis of transgenic animals that express SER-2 in cholinergic or GABAergic ventral nerve cord motor neurons was similar to the wild type (Figure III-7A). However, on plates that contained both aldicarb and tyramine, animals that overexpressed *ser-2* in cholinergic neurons (*Pacr-2*::SER-2) were more resistant to the paralytic effects of aldicarb than the wild type. Conversely, animals that overexpressed *ser-2* in all GABAergic neurons (*Punc-47*::SER-2) were hypersensitive to paralysis on plates containing aldicarb and tyramine (Figure III-7B). These data are consistent with the hypothesis that SER-2 couples to the GOA-1/$G\alpha_{io}$ pathway to inhibit neurotransmitter release.

Tyramine-mediated reduction in GABA synaptic release requires SER-2

The GABAergic VD motor neurons that express *ser-2* make synaptic contacts onto the ventral musculature (Figure III-8A). Therefore, to directly

evaluate whether tyramine modulates synaptic release of GABA from motor neurons, we measured the frequency of endogenous inhibitory post-synaptic currents (IPSCs) in whole-cell recordings from ventral body wall muscle cells (Figure III-7C-H). To isolate GABA currents, recordings were made from *unc-29; acr-16* double mutants (+/+) that lack excitatory neurotransmission at the NMJ (Francis, et al., 2005; Touroutine, et al., 2005). In *unc-29; acr-16* double mutants, the only remaining currents are mediated through chloride permeation of the $GABA_A$-like receptor UNC-49 (Francis, et al., 2005; Richmond and Jorgensen, 1999). In these animals, we observed high levels of endogenous IPSC activity (~13 events/s) that gradually declined over the time course of the recording period (~10 minutes). This basal level of inhibitory activity is consistent with previous reports that have used other, non-genetic approaches to isolate IPSCs. After recording an initial 60 second period of basal activity, we switched to a bath solution containing tyramine. Within 30 seconds of tyramine exposure we noted a clear decrease in IPSC frequency (Figure III-7E, G). The magnitude of this decrease was significantly greater than the slight decrease in IPSC frequency we observed over the same time course in control experiments without tyramine (+ tyramine: 34 ± 4% decrease; no tyramine: 13 ± 6% decrease). These results indicate that tyramine can inhibit GABA-mediated transmission at the NMJ. The tyramine-induced red uction was not reversible within the time course of our recordings, which may suggest that tyramine is acting through a high affinity receptor. To test whether the reduction in IPSC frequency involved SER-2, we

examined the effects of tyramine exposure in recordings from *unc-29; acr-16; ser-2* triple mutants (Figure III-7F, G). The amplitude of endogenous GABA IPSCs was not significantly different between +/+ animals and *ser-2* mutants (+/+: 29.5 ± 1.4 pA, *ser-2*: 31.9 ± 3.9 pA) and was not significantly affected by tyramine exposure for either strain (+/+: 26.9 ± 1.2 pA, *ser-2*: 30.7 ± 4.4 pA), indicating that clustering and function of postsynaptic GABA receptors are normal in *ser-2* mutants, and not affected by tyramine (Figure III-7H). The basal IPSC frequency prior to tyramine exposure was also not changed significantly in *ser-2* mutants (+/+: 13.2 ± 1.2 Hz, *ser-2*: 12.5 ± 2 Hz). However, the tyramine-mediated reduction in IPSC frequency we observed in +/+ animals was significantly attenuated in *ser-2* mutant animals (*ser-2*: 17 ± 4% reduction, +/+: 35 ± 4% reduction) such that it was indistinguishable from that observed in our control recordings without tyramine (control (no tyramine): 13 ± 6 % reduction). After normalization, tyramine application reduced IPSC frequency by 25 ± 5% in +/+ compared to 5 ± 5% reduction in *ser-2* mutants (Figure III-7G). Taken together, our data show that tyramine inhibits GABA release onto ventral body wall muscles in a SER-2 dependent manner.

Ablation of subsets of GABAergic motor neurons induces a navigational bias

C. elegans moves on its side by propagating a sinusoidal wave of ventral-dorsal flexures along the length of its body. GABAergic VD motor neurons synapse onto ventral muscles and receive synaptic inputs from DA/DB

cholinergic motor neurons that synapse onto dorsal body wall muscles (Figure III-8A) (McIntire, et al., 1993). Conversely, GABAergic DD motor neurons synapse onto dorsal muscles and receive synaptic inputs from VA/VB cholinergic motor neurons that synapse onto ventral body wall muscles. This arrangement suggests that a body bend is generated by ACh mediated muscle contraction on one side and GABA mediated relaxation on the contralateral side. This hypothesis is supported by the observation that animals in which the VD and DD neurons are killed by laser ablation move with a reduced wave amplitude (McIntire, et al., 1993). The *Pser-2*::GFP and *Pflp-13*::GFP fluorescent markers, which specifically label the 13 VD and 6 DD neurons, respectively, allowed us to further test the role of the VD and DD neurons in laser ablation experiments. Animals in which only the VD neurons were ablated still propagated a sinusoidal wave along the anterior-posterior axis, but displayed deeper ventral than dorsal flexures (Movies III-1 and III-2). As a consequence VD ablated animals moved in ventrally directed circles (radius 2.20 ± 0.29 body lengths, n=5, Figure III-8B, C). Conversely, animals in which the DD neurons were ablated exhibited deeper dorsal than ventral flexures and moved in dorsally directed circles (radius 0.61 ± 0.11 body lengths, n=10). GABA deficient *unc-25* mutants made shallow body bends, but showed no directional bias in their locomotion pattern. Thus, the specific ablation of the VD or DD GABAergic neurons indicate that asymmetric relaxation of either the ventral or dorsal body wall muscles results in a directional bias in locomotion.

Induction of turning behavior through optogenetic control of GABAergic motor neurons

Our data suggest that the modulation of the activity of either the VD or DD motor neurons allows the animal to bend and steer in either a ventral or dorsal direction. To determine if acute activation or inhibition of a specific subclass of GABAergic neurons could induce turning behavior, we used optogenetic stimulation and inhibition. The complexity of the *ser-2* promoter, which contains coding sequences and alternative start sites, did not allow us to highly express light activated channels in the VD neurons. To test whether the differential activity of the VD and DD motor neurons can induce bending, we generated transgenic animals that co-expressed the light-activated cation channel Channelrhodopsin-2 (ChR2) (Nagel, et al., 2005) and light-activated chloride pump Halorhodopsin (NpHR) (Zhang, et al., 2007) in the six GABAergic DD motor neurons that synapse onto the dorsal muscles (*Pflp-13*::ChR2; *Pflp-13*::NpHR). ChR2 is activated by blue light and depolarizes neurons, while NpHR is activated by green light and hyperpolarizes neurons. We found that blue light activation induced a deep ventral turn (Figure III-9 and Movie III-3). In contrast, green light inhibition induced a deep dorsal turn. This turning behavior was not observed in non-transgenic animals or in transgenic animals raised on plates without all-*trans*-retinal, the chromophore of ChR2 and NpHR. To quantify turning behavior we calculated a bending index as the fraction of animals that turned

ventrally or dorsally in response to light exposure (Figure III-9A). A bending index of zero indicates no directional bias, whereas a negative or positive fraction indicates a ventral or dorsal bias, respectively. The bending index of *Pflp-13*::ChR2/NpHR transgenic animals was -0.45 ± 0.04 with exposure to blue light and 0.41 ± 0.06 for animals with to exposure to green light. The *flp-13* promoter also drives expression in a small set of head neurons in addition to the DD neurons. To determine if the activation or inhibition of the DD neurons was sufficient to induce bending, we used an optogenetic illumination system capable of tracking and stimulating individual regions of a freely moving animal (Leifer, et al., 2011). Targeted illumination of the animal's ventral nerve cord which harbors the DD neuronal cell bodies induced a tight ventral bend in response to blue light activation and a tight dorsal bend in response to green light inhibition (Figure III-9B and Movie III-3). Switching between blue and green light exposure enabled the remote control of ventral and dorsal turning behavior in freely moving *Pflp-13*::ChR2/NpHR transgenic animals. Thus, the acute stimulation of GABA release on the dorsal side induced relaxation of the dorsal muscles resulting in a ventral turn. Conversely, the acute inhibition of GABA release onto the dorsal muscles resulted in hypercontraction of dorsal muscles and a dorsal bend. Our data indicate that modulating the activity of subsets of GABAergic neurons synapsing onto either the dorsal (DD) or ventral side (VD) of the animal can induce navigational bias.

ser-2 facilitates the execution of omega turns in the escape response

The expression of *ser-2* in the GABAergic VD neurons suggested a possible role in *C. elegans* navigation. However, *ser-2* mutants moved normally and did not display a ventral or dorsal directional bias (Figure III-8B) possibly through a lack of basal tyramine to activate SER-2 during regular locomotion. We have previously shown that tyramine coordinates the timing of backing locomotion and the suppression of head movements in the escape response (Alkema, et al., 2005). Gentle anterior touch triggers tyramine release from the RIM neurons and the synaptic activation of the tyramine-gated chloride channel, LGC-55 (Pirri, et al., 2009). Is SER-2 also required in the execution of the escape response? Touch induced reversals are often coupled to a sharp omega turn, which allows the animal to change locomotion in a direction opposite to its original course (Croll, 1975) (Figure III-10E and Figure III-13A). The omega turn is initiated by a steep ventral bend of the head when the animal reinitiates forward locomotion. While the sharp bend is propagated posteriorly along the body, the head usually slides along the ventral side of the body. We analyzed turning behavior in response to gentle anterior touch. We found that the likelihood of engaging in an omega turn (> 90° turn initiated by the first forward head swing) was correlated with the length of the reversal (Figure III-10A). Short reversals most often resulted in shallow head bends and modest deflections from the original trajectory. In contrast, escape responses that included reversals of 4 or more body bends most often ended in an omega turn. These results are

consistent with previous studies of reversals where omega turns tend to occur after a long reversal (Zhao, et al., 2003; Gray, et al., 2005; Huang, et al., 2006).

Omega turns that occurred in response to anterior touch were exclusively made on the ventral side of the animal (n ≥ 250). In response to touch, animals in which the GABAergic DD neurons were ablated initiated omega turns with a deep ventral head bend, but often their head failed to touch the ventral side of the body to close the omega turn (Figure III-11). Animals with ablated GABAergic VD neurons did not have a defect in the execution of closed omega turns. The initiation of the omega turn may be triggered by the RIV head motorneurons that innervate ventral neck muscles (Gray, et al., 2005). The failure of DD ablated animals to fully close their omega turns indicates that the propagation of a sharp bend along the body requires the hyper-contraction of ventral muscles and relaxation of dorsal muscles.

Tyramine deficient *tdc-1* mutants or RIM ablated animals fail to suppress head movements, make short reversals and less frequently engage in the execution of omega turns (Alkema, et al., 2005; Gray, et al., 2005). In contrast, in response to anterior touch, *ser-2* mutants suppressed head movements and reversed similar to wild-type animals (Figure III-12). Furthermore, *ser-2* mutants initiated an omega turn with a steep ventral head bend at the same frequency as the wild-type (Figure III-10A). However, once *ser-2* mutants initiated the omega turn, the ventral turn was less deep than the wild-type. Whereas most wild-type animals' heads touched the ventral side of the body (86 % ± 3.6%, n=51) during

an omega turn, *ser-2* mutant animals failed to fully close the omega turn (27% ± 7.8%, n=62) (Figure III-10B, C and Movies III-4 and III-5). Like the *ser-2* mutants, *tdc-1* mutants that are unable to synthesize tyramine and octopamine (Alkema, et al., 2005) failed to fully close the omega turn during the escape response (*tdc-1* 32% ± 5.5%, n=144). In contrast, *tbh-1* mutants, that only lack octopamine, executed closed omega turns (*tbh-1* 72% ± 7.9%, n=153), comparable to the wild type. We measured the angle of the omega turn (omega angle) from the deepest most contracted region of the body to the closest or touching points in the head and tail (Figure III-10B, D). Wild-type animals typically fully closed their omega bend, while *ser-2* mutants often failed to close omega bends, averaging an omega angle of 24°± 2.3° (n=62). Animals lacking tyramine and octopamine (*tdc-1)* averaged an omega angle of 25° ± 3.6°, while animals lacking octopamine (*tbh-1)* alone closed their omega turn. Since touch stimuli in these assays have some inherent variability, we also induced reversals by optogenetic activation of the touch sensory neurons. Light induces an escape response in *Pmec-4*::ChR2 transgenic animals that express the ChR2 in the touch sensory neurons (Nagel, et al., 2005; Leifer, et al., 2011; Stirman, et al., 2011). We analyzed omega turns of *Pmec-4*::ChR2 transgenic animals in response to blue light in both wild-type and *ser-2* mutant backgrounds. The light induced escape response of *ser-2* mutants showed a similar defect in omega turns as with reversals induced by touch and had a lower frequency of closed omega turns than the wild-type, (Figure III-10C, D). The turning defects of *ser-2* mutants caused an alteration in

the direction of reinitiated forward movement, or escape angle. In response to touch, wild-type animals and *tbh-1* mutants completely reversed their direction of locomotion with an escape angle of 179° ± 5° (n=42) and 177° ± 11° (n=16) respectively. In contrast, in response to touch *ser-2* mutants and *tdc-1* mutants made a more shallow escape angle, changing their direction from the point of stimulus by 150° ± 5° (n=46) and143° ± 6° (n=35) (Figure III-10E, F). Genomic rescue lines partially restore the omega angle defect of the mutants and restored the escape angle to wild type levels. Our data indicate that tyraminergic activation of SER-2 facilitates the execution of a tight ventral bend in the escape.

Discussion

The concept of monoaminergic coding of behaviors originated from work in crustaceans and insects where fully coordinated behavioral sequences can be elicited by the injections of specific monoamines into the nervous system (Kravitz, 1988; Bicker and Menzel, 1989; Hoyle, 1985). However, understanding how sensory inputs recruit the action of monoamines and how changes in circuit properties affect behavior remains a tremendous challenge in the mammalian and even insect nervous systems. Tyramine release from a single pair of neurons, acting on few tyramine receptors in the *C. elegans* nervous system with single-cell resolution provides unique insights into how monoamines orchestrate independent motor programs in a complex behavior. In this study we analyzed how the G-

protein coupled receptor SER-2 modulates the output of a neural circuit in a compound motor sequence.

Tyramine inhibits GABA release

Our genetic data suggest that the tyramine receptor SER-2 acts in a $G\alpha_o$ (GOA-1) pathway. The $G\alpha_o$/GOA-1 is expressed in all *C. elegans* neurons where it antagonizes $G\alpha_q$/EGL-30 function in many behaviors including locomotion, egg laying and pharyngeal pumping (Mendel, et al., 1995; Segalat, et al., 1995). Dopaminergic and serotonergic G-protein coupled receptors are expressed in *C. elegans* ventral cord neurons and their hyperactivation with exogenous dopamine or serotonin can induce paralysis within minutes (Horvitz, et al., 1982; Schafer and Kenyon, 1995; Chase, et al., 2004; Harris, et al., 2009). However, *ser-2* and other individual biogenic amine receptor mutants have no obvious locomotion defects. This indicates that $G\alpha_o$/GOA-1 and $G\alpha_q$/EGL-30 integrate monaminergic signals to modulate neurotransmitter release from the motor neurons to control locomotion (Figure III-1B). Dopamine, serotonin and tyramine may allow the animal to refine locomotory patterns during different behavioral states. $G\alpha_o$/GOA-1 activity is thought to reduce the abundance of the synaptic priming protein UNC-13 at the synapse in *C. elegans* ventral cord neurons (Nurrish, et al.,1999). Our data indicate that tyramine reduces GABA release from VD motor neurons in a SER-2-dependent manner to augment the reorientation component of the escape response. In this regard, SER-2 shares similarities with mammalian

alpha(2)-adrenergic receptors that inhibit neurotransmitter release and cause vasoconstriction during a “fight or flight” response (Brede, et al., 2004).

Tyramine acts through synaptic activation of ionotropic receptors and extrasynaptic activation of metabotropic receptors

Tyramine can act as a classical neurotransmitter in *C. elegans* through the synaptic activation of the tyramine-gated chloride channel, LGC-55 (Pirri, et al., 2009; Ringstad, et al., 2009). While LGC-55 is predominantly expressed in cells that are directly synaptic to tyraminergic RIM neurons, SER-2 expressing cells do not receive direct RIM innervation indicating that SER-2 activation occurs extra-synaptically, indicating that SER-2 activation occurs extra-synaptically (Rex, et al., 2004; Tsalik, et al., 2003). In addition, ionotropic and metabotropic receptors have distinct ligand affinity and signaling kinetics. Ligand-gated ion channels like LGC-55 have a relatively low affinity for ligand (Kd 0.1 to 1 mM) and affect post-synaptic potentials within milliseconds. This allows for fast localized signaling between neurons and their post-synaptic partners. In contrast, G-protein coupled receptors have a high affinity for their ligand (Kd 0.1-1μM) and operate on timescales from seconds to minutes (Hille, 1992). Synaptic spillover from the synaptic cleft and diffusion can activate these high affinity receptors that are distant from the release site. As tyramine is released from a single pair of head neurons that extend processes into the nerve ring, the activation of SER-2 in the GABAergic VD neurons depends upon the diffusion of tyramine through the

pseudocoelomic space to reach the VD processes along the length of the body. *C. elegans* has two other G-protein coupled receptors, TYRA-2 and TYRA-3, in addition to SER-2 that bind tyramine with high affinity (Rex, et al., 2005; Wragg, et al., 2007). *tyra-2 and tyra-3* are not expressed in cells that receive direct synaptic inputs from the tyraminergic RIM neurons (Bendesky, et al., 2011). Furthermore, no tyramine or octopamine reuptake transporter has been identified in either *C. elegans* or *Drosophila,* which suggests that tyramine diffusion from the synaptic cleft is part of its mechanism of action. Serotonin, dopamine and octopamine receptors are also expressed in many *C. elegans* cells that are not directly postsynaptic to the small number of monoaminergic neurons that release them (Tsalik, et al., 2003; Chase, et al., 2004). Similarly, in humans the monoaminergic cells are grouped in relative small nuclei that can affect large areas of the CNS or the periphery that do not receive direct synaptic inputs. Thus, monoamines are not confined to the anatomical connectome and can reconfigure outputs to large neuronal ensembles (Bargmann, 2012).

Tyramine temporally coordinates independent motor programs in a complex behavior

The translation of sensory input into goal directed behaviors requires the temporal coordination of independent motor programs. In response to gentle touch to the head, *C. elegans* engages in a compound motor sequence that allows the animal to retreat and navigate away from a touch stimulus (Figure III-13A). In the

base state, (I) forward locomotion is accompanied by exploratory head movements in which the tip of the nose moves from side to side. Gentle touch to the head of *C. elegans* elicits an escape response where the animal reverses its direction of locomotion while suppressing its exploratory head movements (II). Classic laser ablation experiments by Chalfie, et al. (1985) complemented by the known neural wiring diagram support a model in which the touch sensory neurons (ALM/AVM) inhibit the forward locomotion "command" neurons (PVC/AVB) and activate the backward locomotion "command" neurons (AVD/AVA) causing the animal to move backward away from the stimulus (Figure III-13B). The AVA backward locomotion "command" neurons activate the electrically coupled tyraminergic RIM motor neurons, which exhibit coactivated calcium transients with the AVA (Guo, et al., 2009; Kawano, et al., 2011). Tyramine release from the RIM induces the suppression of head movements through the activation of the fast acting inhibitory chloride channel, LGC-55, in neck muscles and cholinergic motor neurons that control head movements (Alkema, et al., 2005; Pirri, et al., 2009). Activation of LGC-55 in the AVB forward locomotion "command" neuron further inhibits forward locomotion, stimulating long reversals that are coupled to the initiation of an omega turn (Zhao, et al., 2003; Gray, et al., 2005). The reversal is followed by a deep ventral head bend (III) allowing the animal to make a sharp (omega) turn (IV) where the head of the animal slides along the ventral side of the body and resumes forward locomotion (I). Our data show that extrasynaptic activation of the G-protein coupled tyramine receptor SER-2 contributes to the proper execution of

the omega turn during the last stage of the escape response. The RIV and SMD head motor neurons have been implicated in the ventral head bend that initiates the omega turn (Gray, et al., 2005). *ser-2* mutants properly initiate the turn but bend less deep and the head often fails to touch the tail during the omega turn (IV).

C. elegans locomotion is controlled by cholinergic (A and B) and GABAergic (D) motor neurons that propel a wave of ventral-dorsal muscle flexures along the length of the body. We show that SER-2 inhibits neurotransmitter release from the GABAergic VD neurons. VD motor neurons release GABA on ventral body wall muscles and receive inputs from cholinergic DB neurons that synapse onto dorsal muscles. The DD motor neurons receive input from cholinergic VB motor neurons and release GABA on dorsal body wall muscles (Figure III-8A) (White, et al., 1986). This organization indicates that GABAergic motor neurons are essential for contralateral muscle relaxation, thus promoting local bending during wave propagation (McIntire, et al., 1993).

While spatial orientation in response to sensory stimuli is a fundamental component of animal behavior, the neural correlates are poorly understood. To change its direction of movement and navigate its environment, an animal needs to generate asymmetry in its locomotion pattern (Schoène, 1984; Lockery, 2011). We show that the ablation of GABAergic VD neurons induces ventrally directed movement likely through the failure to properly relax the ventral muscles. Conversely, ablation of GABAergic DD neurons induces dorsally directed movement. Our experiments provide functional evidence that VD and DD

neurons inhibit ventral and dorsal bending. Strikingly, the acute inhibition or activation of the DD motor neurons induces a sharp dorsal or ventral turn respectively. Optogenetic neuronal stimulation can elicit distinct motor responses in multiple systems (Nagel, et al., 2005; Lima and Miesenbock, 2005; Douglass, et al., 2008; Kravitz, et al., 2010). The optogenetic control of a single class of GABAergic neurons induces bi-directional steering and the remote control of animal navigation.

The ventral omega turn in the escape response occurs several seconds after the touch-induced reversal, which is within the time scale that GPCRs modulate neuronal activity. To make a tight turn the animals needs to generate an asymmetry in the excitation and inhibition of the ventral and dorsal muscle quadrants. Our data indicate that SER-2 mediated inhibition of GABAergic release onto the ventral muscles stimulates ventral muscle contraction and the proper propagation of the ventral body bend during the omega turn (Figure III-13B). The kinetics of synaptic activation of the ion channel LGC-55 and extrasynaptic activation of the G-protein coupled receptor SER-2 temporally coordinates different phases of the escape response. Interestingly, the tyramine GPCR TYRA-3 modulates responses to pain-like stimuli and decision making (Wragg, et al., 2007; Bendesky, et al., 2011). This indicates that tyramine much like the mammalian adrenergic signaling coordinates different aspects of a flight response.

Our results provide molecular and neural insights on how monoamines reconfigure the output of neural circuits and orchestrate complex behaviors. Many neurotransmitters, including serotonin, GABA, acetylcholine and glutamate act through both ion channels and GPCRs in animals ranging from worms to man. We hypothesize that the temporally coordinated activation of ionotropic and metabotropic receptors may be a common signaling motif employed across organisms to orchestrate behavioral responses. Furthermore, the different monoamines appear to play a strikingly conserved role in the specification of distinct internal states suggesting that the principles of neuronal modulation are conserved across species.

Materials and Methods

Strains

All *C. elegans* strains were grown at room temperature (22°C) on nematode growth media (NGM) agar plates with OP50 *E. coli* as a food source (Brenner, 1974). The wild-type strain used in this study was Bristol N2. G-protein coupled receptor and signaling component mutants used in this study were OH313: *ser-2(pk1357),* QW329: *ser-2(ok2103),* QW245: *lgc-55(tm2913),* QW42: *tyra-2(tm1815),* VC125: *tyra-3(ok325),* JT734: *goa-1(sa734),* JT748: *dgk-1(sa748),* JT609: *eat-16(sa609),* EG4532: *egl-30(tg26),* CB156: *unc-25(e156),* CB151: *unc-3(e151),* QW284: *tdc-1(n3420)*, MT9455: *tbh-1(n3247)*, QW542: *unc-25(e156); ser-2(pk1357),* QW40: *lgc-55(n4331); unc-3(e151),* QW41: *ser-*

2(pk1357) unc-3(e151), QW837*: lgc-55(tm2913); ser-2(pk1357),* QW838*: lgc-55(tm2913); ser-2(pk1357) unc-3(e151)*. The rescue strains used were QW198: [*Pser-2*::SER-2::GFP, *lin-15(+)*]*(zfEx34); ser-2(pk1357) lin-15(n765ts),* QW411: [*Pser-2*::SER-2::GFP, *lin-15(+)*]*(zfEx70); ser-2(pk1357) lin-15(n765ts),* QW412: [*Pser-2*::SER-2::GFP, *lin-15(+)*]*(zfEx301); ser-2(pk1357) lin-15(n765ts),* QW196: [*Punc-47*::SER-2*, lin-15(+)*]*(zfEx33)*; *ser-2(pk1357) lin-15(n765ts),* QW897: [*Punc-47*::GOA-1::SL2::mCherry, *unc-122*::GFP] (*zfEx347*); *goa-1(sa734),* QW895: [*Punc-47*::EAT-16::SL2::mCherry, *unc-122*::GFP] (*zfEx346*); *eat-16(sa609)*, QW194: [*Pacr-2*::SER-2, *lin-15(+)*]*(zfEx32); ser-2(pk1357) lin-15(n765ts).* The strains used for cell identification were EG1285: *Punc-47*::GFP*(oxIs12),* CX2835: *Pglr-1::GFP(kyIs29),* LX929: *Punc-17*::GFP*(vsIs48),* NY2037: *Pflp-13*::GFP*(ynIs37),* OH2246: *Pser-2::GFP(otIs107),* QW192: *Pser-2*::mCherry*(zfIs8),* QW122: *Plgc-55*::GFP*(zfIs6),* QW84: *Plgc-55*::mCherry*(zfIs4).* The strains used for electrophysiological analysis were IZ33*: unc-29(x29); acr-16(ok789), IZ598: unc-29(x29); acr-16(ok789); ser-2(pk1357).* The strains used for optogenetic assays were QW410: [*Pmec-4*::ChR2::YFP, *lin-15(+)*]*(zfIs18); ser-2(pk1357),* QW409: [*Pmec-4*::ChR2::YFP, *lin-15(+)*]*(zfIs18); ser-2(ok2103),* QW429: [*Pflp-13*::ChR2::GFP*; Pflp-13*::NpHR::CFP, *lin-15(+)*]*(zfIs32); lite-1(ce314).*

Transgenic strains were generated by microinjection of plasmid DNA into the germ line of *lin-15(n765ts*) mutants with the pL15EK rescuing plasmid. Extra-chromosomal arrays were integrated by X-ray irradiation (120kV) and resulting

transgenic strains were outcrossed at least four times to N2. A *Pser-2*::SER-2::GFP rescue construct was made by cloning 10.2 kb of genomic sequence including 2.2 kb upstream of the first translational start site into the pPD95.70 vector. The genomic rescue constructs used for exogenous tyramine and omega turn assays were injected between 10-20 ng/µl. A *Pser-2*::mCherry mini-gene reporter was constructed by cloning an 11.8 kb sequence that included the three start sites, first intron, and part of exon 2 into the pDM1247 vector. The GABAergic and cholinergic cell-specific rescue lines were cloned using *ser-2a* cDNA behind the *unc-47* (1.2 kb) (Eastman, et al., 1999) and *acr-2* (3.4 kb) promoters, respectively (Hallam, et al., 2000).

A *Pmec-4*::ChR2::YFP plasmid (Nagel, et al., 2005) was injected at 80 ng/µl. The integrated strain was crossed into two *ser-2* mutant allele backgrounds. *Pflp-13*::ChR2::GFP; *Pflp-13*::NpHR::CFP was cloned by inserting a 2 kb promoter from *Pflp-13*::GFP (Kim and Li, 2004) into ChR2 and NpHR vectors (Nagel, et al., 2005; Zhang, et al., 2007). The integrated strains carrying ChR2 or NpHR transgenes were cultured on NGM agar plates containing OP50 *E. coli* supplemented with 1.3 mM all-*trans*-retinal for one generation. Larval L4 animals were transferred to retinal plates 24 hours before behavioral assays.

Ventral nerve cord expression analysis was performed using *Pser-2*::mCherry, *Punc-47*::GFP and *Punc-17*::GFP transgenic animals. Head muscle analysis was done using *Pser-2::GFP* and *Plgc-55*::mCherry. Images were taken

using confocal microscopy (Zeiss and Pascal imaging software) and formatted using ImageJ software.

Behavioral Assays

Behavioral assays were performed at room temperature. Drug assays were conducted on young adult animals aged 24 hours post-L4 larval stage. Locomotion assays on were performed on agar plates containing 2 mM acetic acid with or without tyramine hydrochloride (Sigma-Aldrich). Approximately 10 animals were transferred to assay plates and scored for locomotion every minute over a 20 minute period. Animals were scored as immobilized if there was no sustained forward or backward locomotion in a 5 second interval. Aldicarb drug assays were performed using NGM agar plates supplemented with 0.5 mM aldicarb (Sigma-Aldrich) with or without 30 mM tyramine. Locomotion is not obviously affected on plates with 30 mM tyramine dissolved in NGM agar instead of the agar used in exogenous tyramine paralysis assays. Animals were scored as paralyzed when they did not move when prodded with a platinum wire.

Optogenetic blue and green light induced bending assays were performed with *Pflp-13*::ChR2::GFP; *Pflp-13*::NpHR::CFP; *lite-1(ce314)* transgenic animals. Bending behavior movies, worm tracking traces and kymographs were generated using the CoLBeRT worm tracking system as previously described (Leifer, et al., 2011). Animals were placed in between two glass slides in 200 µl of NGM containing 30% dextran. The space between the slides was approximately 0.127

mm and limited locomotion to two dimensions. The ventral nerve cord was illuminated with blue or green light using the micro-mirror control of the CoLBeRT system, and the behavior was analyzed using custom tracking software written in MATLAB. For assays used to calculate a bending index, young adult animals were transferred to NGM plates without food for 45 minutes. Food deprivation stimulated long forward runs, which facilitated the analysis of light induced bending. Animals were exposed to blue or green light, using GFP (525 nm) and Rhodamine (550 nm) filters for 3 seconds. A dorsal or ventral bend were scored if the bend was larger than 45°. The bending index was calculated as the fraction of dorsally bending worms minus the fraction of ventrally bending worms. A positive fraction indicates a dorsal bias, a negative fraction indicates a ventral bias and a zero value represents no directional bias or no response to light exposures.

Omega turns were analyzed on NGM agar plates two days post pouring to control for assay plate humidity. Assay plates (60 mm diameter) were seeded with 40 µl OP50 *E. coli* and grown overnight at 37°C to produce a thin bacterial lawn. Young adult worms were transferred to an omega assay plate and allowed to acclimate for at least 10 minutes. Omega turns were induced by gentle anterior touch with fine eyebrow hair while recording using a FireWire camera and Astro IIDC software. For *Pmec-4*::ChR2::YFP induced omega turns, animals were exposed to blue light for 5 seconds to induce a reversal. Bending angles and locomotion trajectories were calculated using Image J software analysis of

Movie stills. An omega turn was classified as a sharp turn larger than 90° from the initial trajectory, following a reversal of 3 or more body bends. The omega angle was measured using the deepest part of the bend as the apex with vectors extending to the closest points along the body. Angles larger than 60° were not scored. The escape angle was measured as the angle between the reversal trajectory and the trajectory of reinitiation of forward locomotion after the omega turn.

Laser Ablations

Animals were mounted on agar pads and anesthetized with 20 mM sodium azide. Laser ablations were done using standard methods (Bargmann and Avery, 1995). DD and VD motor neurons were identified in *Pflp-13*::GFP animals in the L2 larval stage and *Pser-2*::GFP animals in the L3-L4 larval stage respectively. Following a recovery period of one to three days post ablations, locomotion and omega turn assays were conducted on young adult animals. Locomotion patterns of animals that exhibited coordinated long runs were recorded at 7.5 fps. Movie analysis was done using MATLAB and the MATLAB Image Acquisition Toolbox (Ramot, et al., 2008). To determine directionality for each locomotion trace, the slope of instantaneous direction over time was measured for individual 360 degree turning events. Laser ablation of motor neurons was confirmed by lack of GFP expression in the cell body positions in adult animals following behavioral experiments.

Electrophysiology

Endogenous postsynaptic currents were recorded from body wall muscles as previously described (Francis, et al., 2005). All electrophysiology experiments were carried out at room temperature. Adult animals held at drop of bath solution were glued down to the sylgard coated glass coverslip with cyanoacrylate tissue adhesive (Skinstitch Corp.) applied along the dorsal side of the body. A longitudinal incision was made by sharp glass electrode tip in the dorsolateral area, the intestine and gonad were removed, and the cuticle flap along the incision was glued down in order to expose the ventral medial body wall muscles along the ventral nerve cord. The preparation was then washed briefly for ~20 second with a solution of collagenase type IV from Clostridium hystolyticum (Sigma-Aldrich) in extracellular bath solution (at a concentration of 1mg/ml) in order to remove the basement membrane overlying the muscles.
The extracellular solution consisted of 150 mM NaCl, 5 mM KCl, 4 mM $MgCl_2$, 1 mM $CaCl_2$, 15 mM HEPES, and 10 mM glucose (pH 7.4, osmolarity adjusted with 20 mM sucrose). The intracellular fluid (ICF) consisted of 115 mM K-gluconate, 25 mMKCl, 0.1 mM $CaCl_2$, 50 mM HEPES, 5 mM Mg-ATP, 0.5 mM Na-GTP, 0.5 mM cGMP, 0.5 mM cAMP, and 1 mM BAPTA (pH 7.4, osmolarity adjusted with 10 mM sucrose). For some experiments measuring GABA-mediated currents, the intracellular solution contained 115 mM KCl and 25 mM K-gluconate. At least 60-90 seconds of continuous data were used in the analysis. Whole-cell voltage clamp recordings from *C. elegans* body wall muscle cells (group of ventral medial

muscles 9, 11, 13) from +/+ and *ser-2* mutant strains were performed as previously described (Francis, et al., 2005) using an EPC-10 amplifier (HEKA). Data acquisition and voltage protocols were controlled by HEKA Patchmaster software. Patch-clamp electrodes were pulled from borosilicate glass with filament (Sutter Instrument), fire-polished to a resistance of 4-6 MΩ and filled with an internal solution. 1M KCl electrode with agarose bridge served as reference electrode. Leak currents and liquid junction potentials were not compensated, though pipette offset was zeroed immediately before getting a gigaohm seal. The membrane potential was clamped at -60 mV. Data were digitized at 6.67 kHz and low pass filtered at 3.3 kHz. Membrane capacitance and the series resistance (at least 20%, up to 60%) were compensated, and only recordings in which the series resistance was stable throughout the course of the recording were included. Endogenous synaptic activity data were collected in continuous mode (saved as 30 second recording sweeps). Typically, 60-90 seconds of control endogenous activity was recorded followed by a 90 second of bath tyramine application (100 μM), and subsequent tyramine wash-out (occasional). The muscle preparation was continuously perfused by extracellular solution with or without tyramine by gravity-flow at a perfusion rate of 2 ml/min. Cells were excluded from analysis if a leak current > 300 pA was observed. Only recordings with series resistance R_s < 15 MΩ were included in the analysis. Data analysis and graphing were performed using Excel (Microsoft), Igor Pro (WaveMetrics Inc.) and GraphPrism (GraphPad Software). Mini Analysis software (Synaptosoft

Inc.) was used to detect and analyze the endogenous events off-line. Parameters for detection of events were set as follows: amplitude threshold 12 pA, period to search local minimum 80 ms, time before a peak for baseline 20 ms, period to search a decay time 30 ms, fraction of peak to find a decay time 0.37, period to average a baseline 10 ms, area threshold 10, number of points to average for peak 3. In addition, following automatic detection of endogenous postsynaptic currents, traces were visually inspected, and all events were manually verified and accepted/rejected or recalculated, if necessary. Sixty seconds of continuous data were used in analysis. Segments of 60 seconds recording prior to tyramine application served as a control. The tyramine effect was evaluated in the last 60 seconds of a 90 second perfusion i.e. initial 30 seconds of recording with tyramine in bath solution were eliminated from analysis in order to allow enough time for adequate tyramine perfusion and stabilization effect. Data from each group were averaged, and statistical significance between the strains was determined by two-tailed unpaired Student's t-test. All chemicals were purchased from Sigma-Aldrich.

Acknowledgments

We thank the *Caenorhabdits* Genetics Center (CGC) for nematode strains, Andrew Fire, Chris Li, Michael Koelle, Alexander Gottschalk and Yuji Kohara for reagents, and Claire Bénard and Scott Waddell for comments and helpful discussions. This work was supported by the NSF and a Pioneer grant of

the National Institutes of Health to A.D.T.S., NIH grant NS064263 to M.M.F. and NIH grant GM084491 to M.J.A.

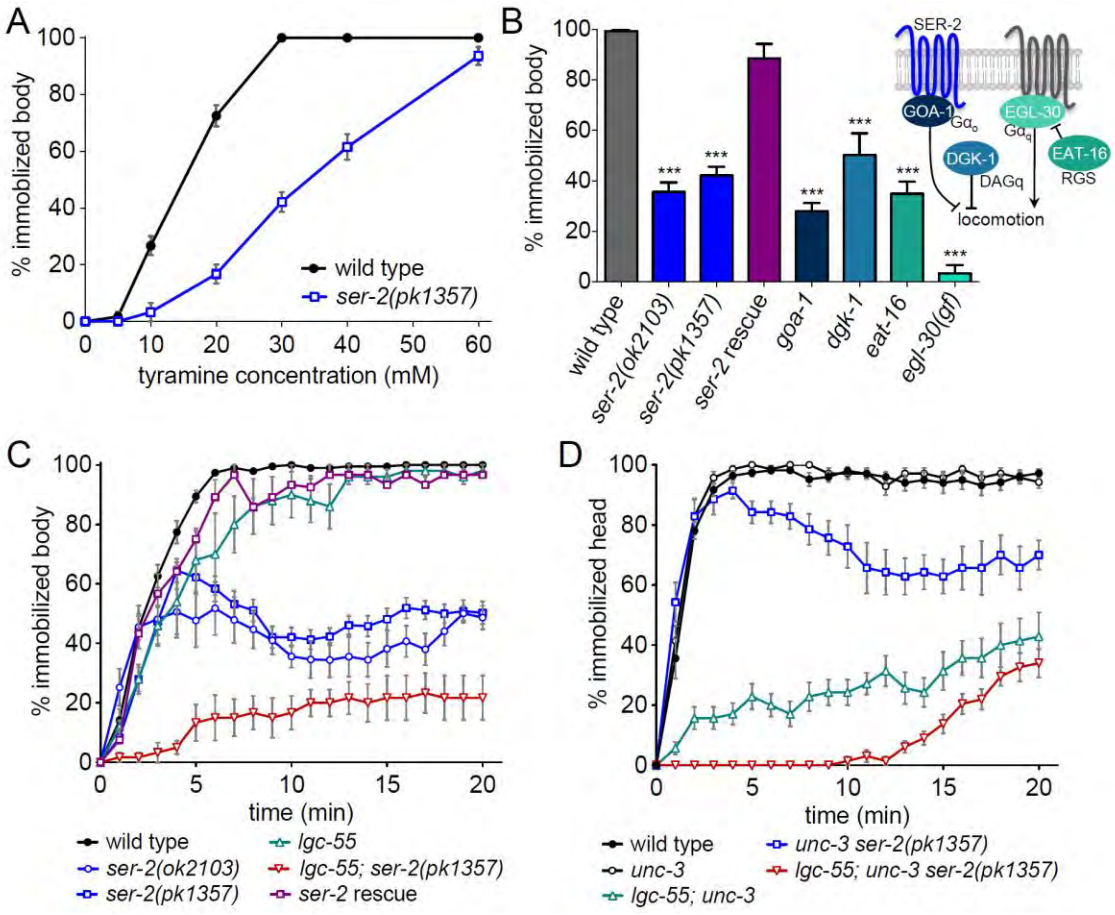

Figure III-1. *ser-2* mutants are partially resistant to the paralytic effects of exogenous tyramine.

(A) Tyramine induces immobilization in a dose-dependent manner. Shown is the percentage of animals immobilized after 10 minutes on agar plates supplemented with tyramine. Wild-type animals become fully immobilized at concentrations above 30 mM tyramine, while *ser-2* mutants continue sustained movement. Each data point represents the mean ± the standard error of the mean (SEM) for at least 3 trials, totaling a minimum of 30 animals. (B) G-protein

signaling mutants are resistant to the paralytic of effects of exogenous tyramine. Shown is the percentage of animals that become immobilized after 10 minutes on 30 mM tyramine. Each bar represents the mean ± SEM for at least 4 trials totaling a minimum of 40 animals. Inset: schematic representation of the $G\alpha_o$ and $G\alpha_q$ signaling pathways that modulate locomotion in *C. elegans*. The genetic data suggest that SER-2 acts in the $G\alpha_o$ pathway. The names of the human orthologs are shown. Rescue denotes the transgenic line *Pser-2*::SER-2; *ser-2(pk1357).* (C, D) Tyramine affects locomotion and head movements through different mechanisms. Shown is the percentage of animals with sustained body (C) or head (D) movements on 30 mM tyramine. *ser-2* mutants are partially resistant to the effects of tyramine on body movements, but not head movements. *lgc-55* mutants continue to move their heads through the duration of the assay. Each data point represents the mean percentage of animals that become immobilized by tyramine each minute for 20 minutes ± SEM for at least 6 trials, totaling a minimum of 60 animals. Head movements were analyzed in an *unc-3* mutant background (+/+). *unc-3* mutants make few body movements but display normal head movements, and are wild type for the *ser-2 and lgc-55* loci. Statistical significance to wild type: ***p< 0.0001, two-tailed Student's t test. See also Figures II-2 and II-3.

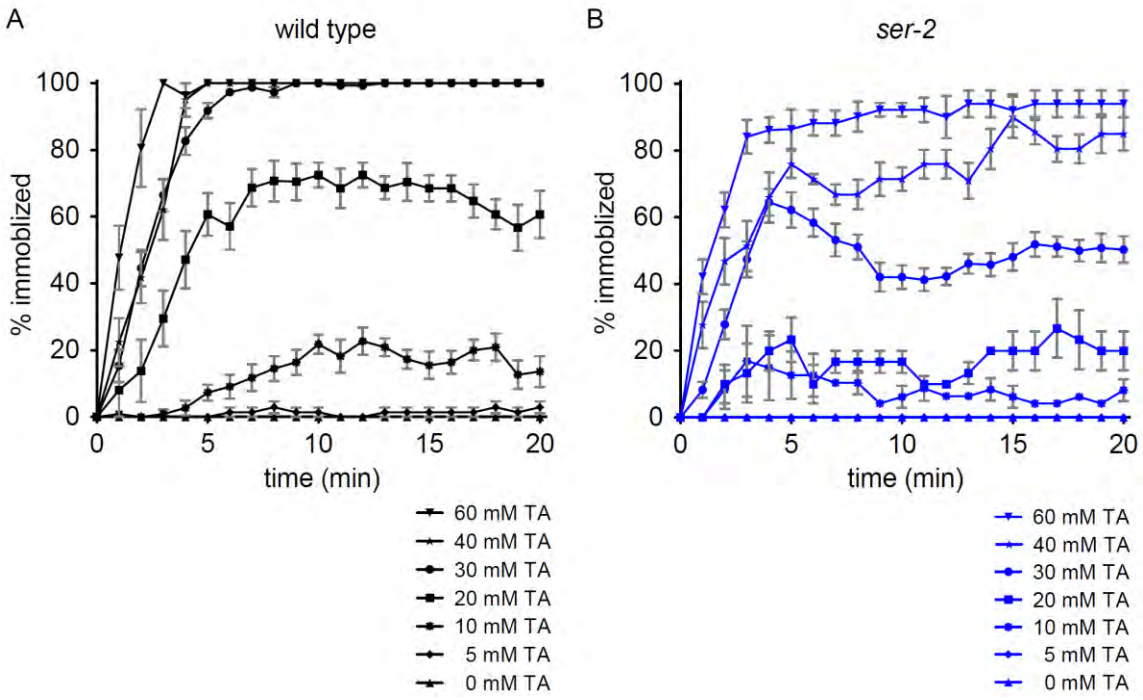

Figure III-2. *C. elegans* become immobilized on exogenous tyramine in a dose-dependent manner.

(A) Wild-type animals become immobilized within 5 minutes on 30 mM tyramine (also see Pirri, et al., 2009). (B) *ser-2* mutants are resistant to body immobilization compared to wild-type, but become immobilized by 60 mM tyramine. Each data point represents the mean ± SEM for at least 4 trials totaling a minimum of 40 animals.

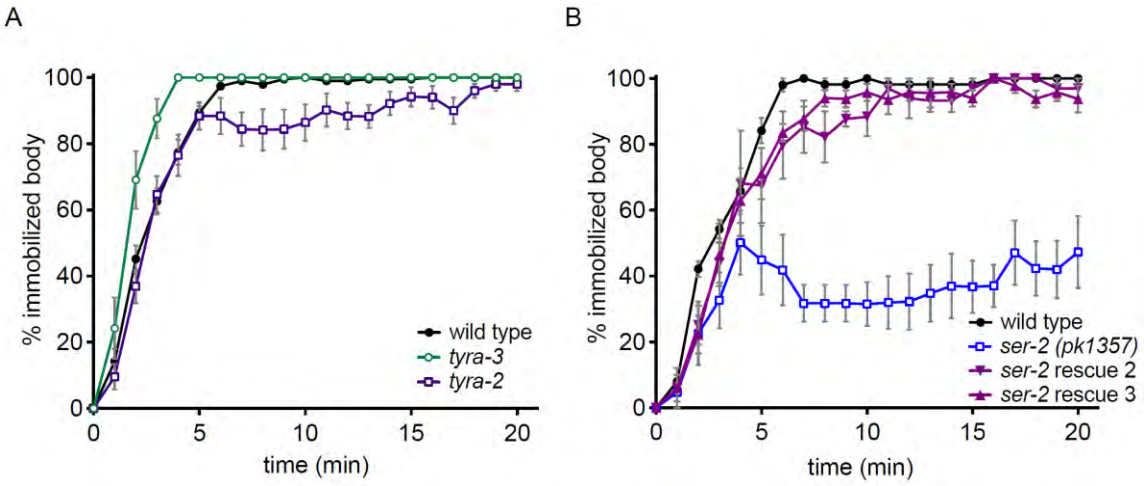

Figure III-3. *tyra-2* and *tyra-3* mutant animals paralyze on exogenous tyramine.

(A) *tyra-2* and *tyra-3* mutants become immobilized on plates containing 30 mM exogenous tyramine similar to wild type. (B) Two additional SER-2 rescue strains (10 ng/µl injection) also rescue the immobilization resistance phenotype of *ser-2* mutants. Rescue denotes the transgenic line *Pser-2*::SER-2*; ser-2(pk1357)*. Each data point represents the mean ± SEM for at least 5 trials totaling a minimum of 50 animals.

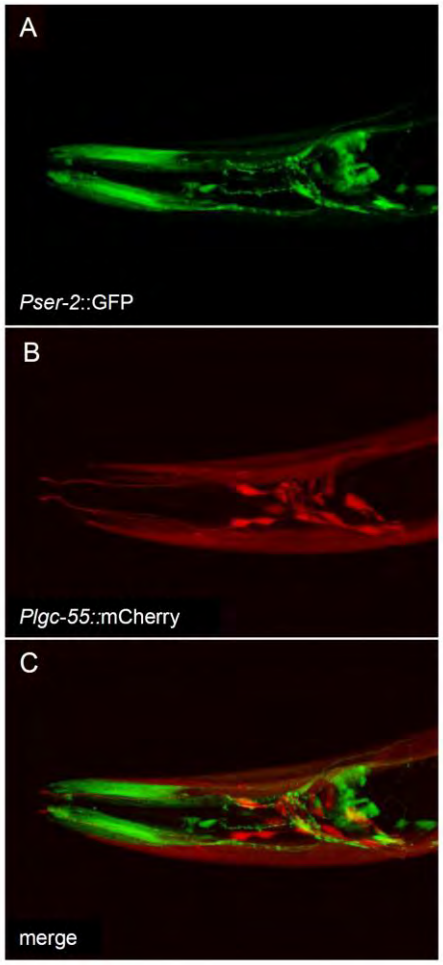

Figure III-4. *Pser-2*::GFP and *Plgc-55*::mCherry are expressed in different cells.

(A-C) Transgenic adult animal co-expressing (A) *Pser-2*::GFP and (B) *Plgc-55*::mCherry. (C) Merge. Head muscle expression of *Pser-2*::GFP does not overlap with neck muscle expression of *Plcg-55*::mCherry. Unlike *lgc-55* mutants, *ser-2* mutants do suppress head movements in response to touch. *ser-2* mutants occasionally reinitiate head movements before the reinitiation of forward locomotion (unpublished observation), which may suggests a role for *ser-2* in head muscles.

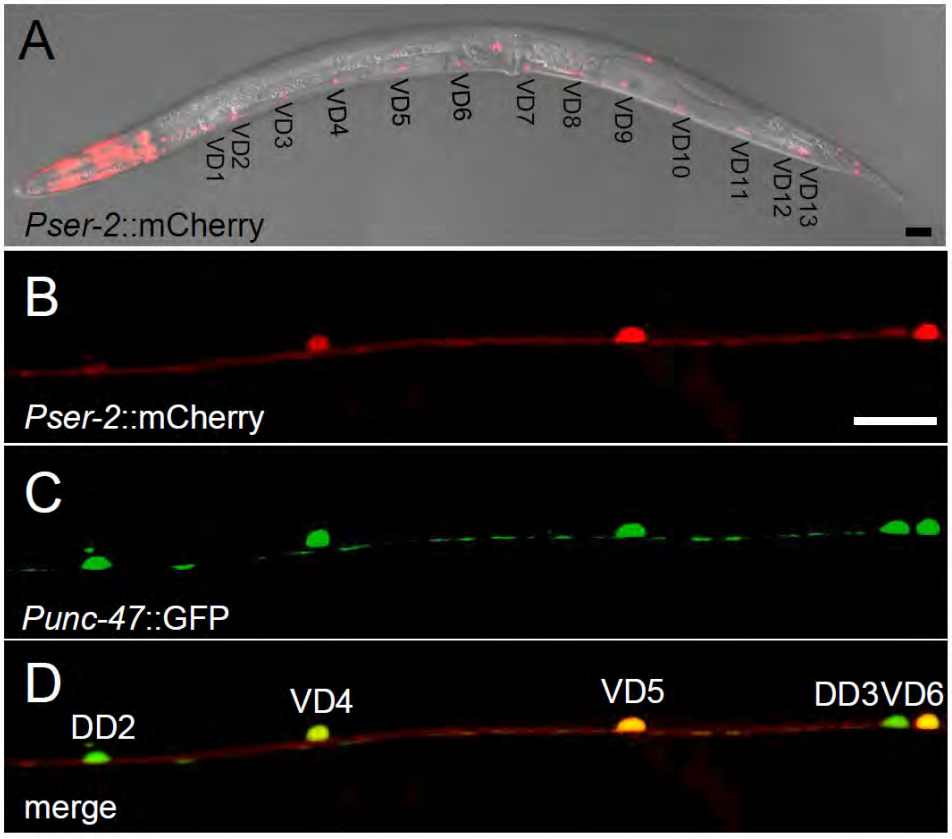
A
VD1
VD2
VD3
VD4
VD5
VD6
VD7
VD8
VD9
VD10
VD11
VD12
VD13
Pser-2::mCherry
B
Pser-2::mCherry
C
Punc-47::GFP
D
DD2
VD4
VD5
DD3VD6
merge

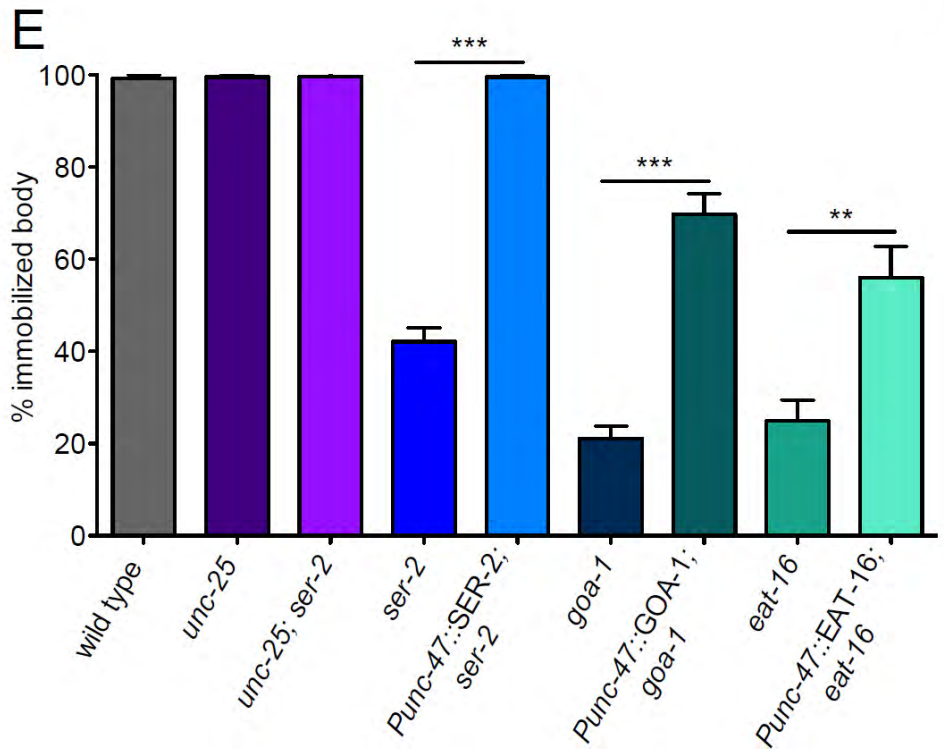
E
% immobilized body
100
80
60
40
20
0
***
***
**
wild type
unc-25
unc-25; ser-2
ser-2
Punc-47::SER-2; ser-2
goa-1
Punc-47::GOA-1; goa-1
eat-16
Punc-47::EAT-16; eat-16

Figure III-5. *ser-2* is expressed in a subset of GABAergic motor neurons. (A) A fluorescent *Pser-2::*mCherry transcriptional reporter is expressed in head muscles, head neurons and neurons in the ventral nerve cord. (B-D) Transgenic animal showing coexpression of *Pser-2::*mCherry (B) and *Punc-47::*GFP which labels all GABAergic motor neurons (C). *Pser-2::*mCherry is strongly expressed in the GABAergic VD neurons but not the DD neurons (D). Anterior is to the left. Scale bar is 20 μm. (E) Exogenous tyramine induces immobilization though the activation of SER-2 and $G\alpha_o$ signaling pathway in the GABAergic neurons. Shown is the percentage of animals that become immobilized after 10 minutes on 30 mM tyramine. Loss-of-function of *unc-25* (glutamic acid decarboxylase) suppresses the tyramine resistance of *ser-2* mutant animals. *unc-25* (GABA deficient) mutants and *unc-25; ser-2(pk1357)* double mutants are not resistant to the paralytic effects of exogenous tyramine. Expression of SER-2 in all GABAergic neurons (*Punc-47*::SER-2) restores sensitivity of *ser-2* mutants to exogenous tyramine. Expression of GOA-1/ $G\alpha_o$ or EAT-16/RGS in all GABAergic neurons (*Punc-47*::GOA-1 or *Punc-47*::EAT-16) partially restores sensitivity to exogenous tyramine in the respective *goa-1* and *eat-16* mutants. Each bar represents the mean ± SEM for at least 3 trials, totaling a minimum of 30 animals. Statistical differences calculated from wild type unless otherwise noted: $^{**}p < 0.005$, $^{***}p < 0.001$, two-tailed Student's t test.

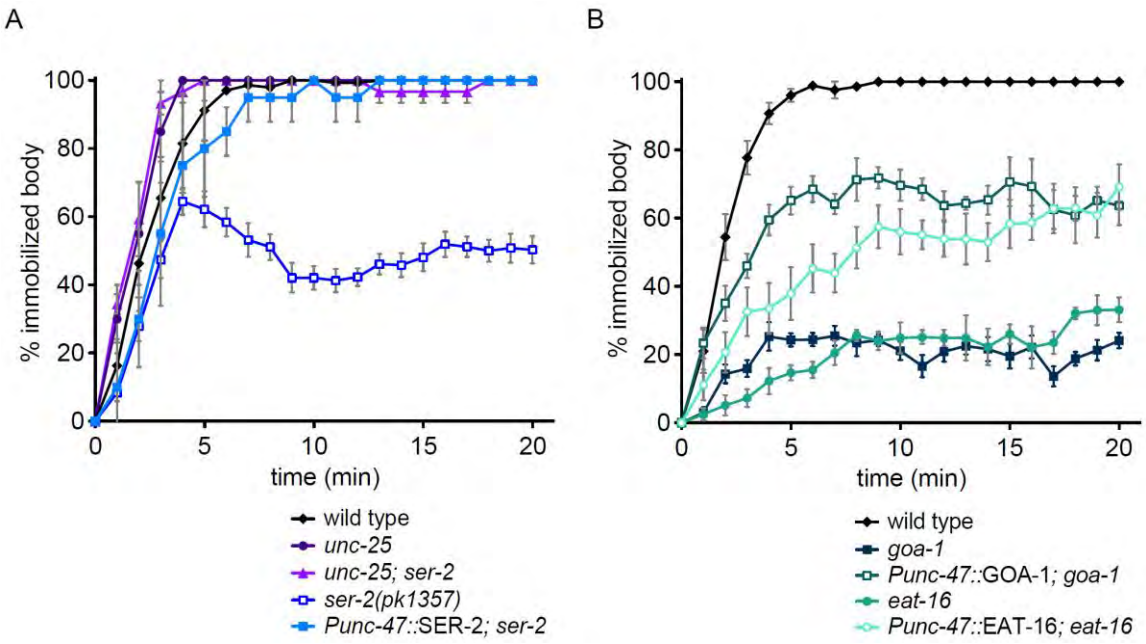

Figure III-6. SER-2 acts in a Gα$_o$ pathway in GABAergic neurons.

(A) Shown is the percentage of animals that display sustained locomotion on 30 mM exogenous tyramine (see also Figure III-5E). *unc-25* (GABA deficient) mutants and *unc-25; ser-2(pk1357)* double mutants are not resistant to the paralytic effects of exogenous tyramine. Expression of SER-2 in all GABAergic neurons (*Punc-47*::SER-2) restores sensitivity of *ser-2* mutants to exogenous tyramine. (B) Expression of GOA-1/ Gα$_o$ or EAT-16/RGS in all GABAergic neurons (*Punc-47*::GOA-1 or *Punc-47*::EAT-16) partially restores sensitivity to exogenous tyramine in the respective *goa-1* and *eat-16* mutants. Each data point represents the mean percentage of animals immobilized by tyramine each minute for 20 minutes ± SEM for at least 3 trials, totaling a minimum of 30 animals.

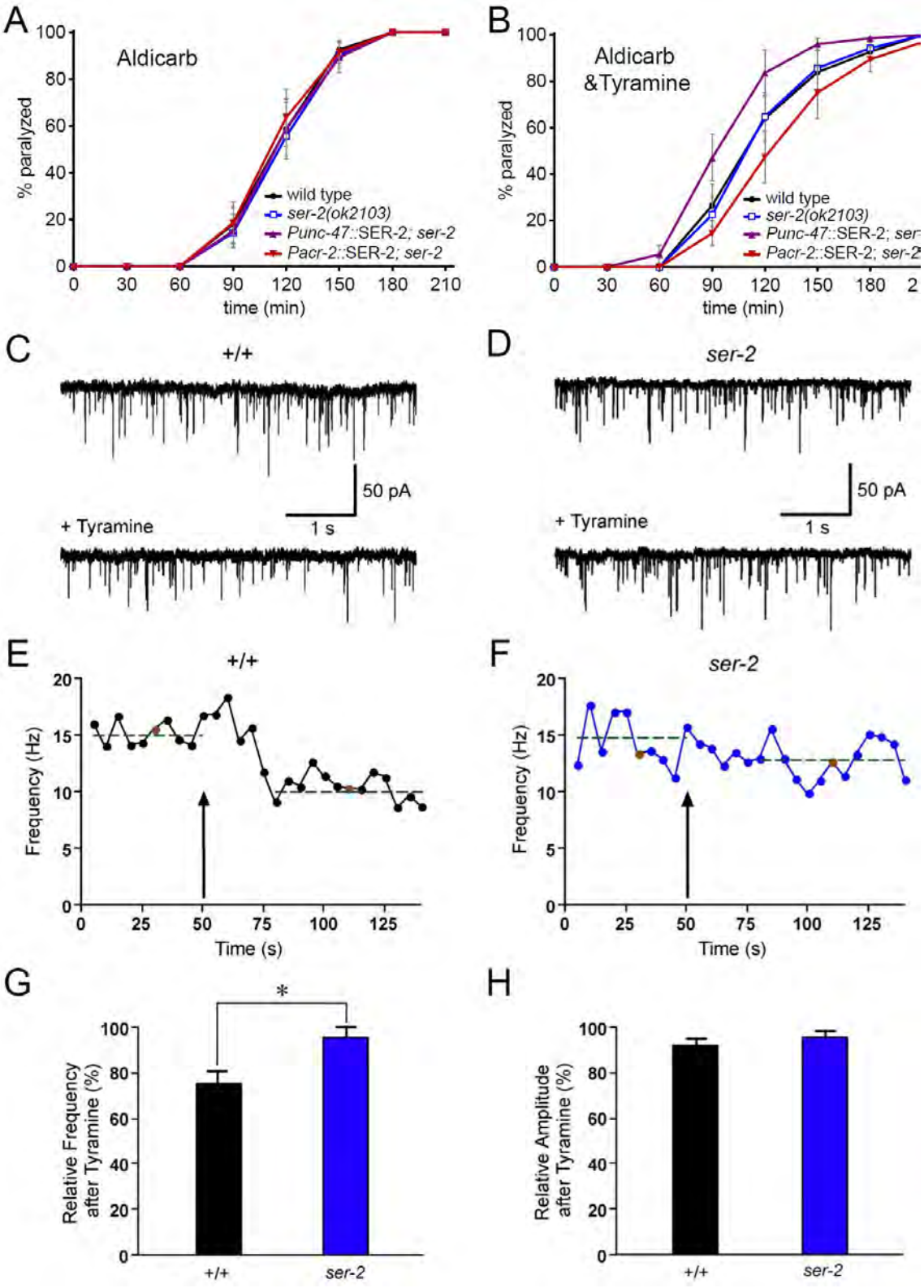
A
Aldicarb
% paralyzed
time (min)
wild type
ser-2(ok2103)
Punc-47::SER-2; ser-2
Pacr-2::SER-2; ser-2
B
Aldicarb
&Tyramine
% paralyzed
time (min)
wild type
ser-2(ok2103)
C
+/+
50 pA
1 s
+ Tyramine
D
ser-2
50 pA
1 s
+ Tyramine
E
+/+
Frequency (Hz)
Time (s)
F
ser-2
Frequency (Hz)
Time (s)
G
*
Relative Frequency after Tyramine (%)
+/+
ser-2
H
Relative Amplitude after Tyramine (%)
+/+
ser-2

Figure III-7. Tyramine-mediated reduction in GABA synaptic release requires SER-2.

(A, B) SER-2 expression in cholinergic (*Pacr-2::*SER-2*)* or GABAergic (*Punc-47::*SER-2*)* motor neurons alters the rate of paralysis of *ser-2* mutants on aldicarb drug plates. All genotypes paralyze at a similar rate on drug plates containing only 0.5 mM aldicarb (A), yet drug plates containing both 30 mM tyramine and 0.5 mM aldicarb causes paralytic resistance (*Pacr-2::*SER-2) or hypersensitivity (*Punc-47::*SER-2) (B). Aldicarb experiments were conducted on nematode growth media (NGM) plates. 30 mM tyramine dissolved in NGM agar does not inhibit locomotion. SER-2 was expressed in *ser-2(pk1357)* mutant animals. Each data point represents the mean percentage of animals immobilized by aldicarb scored every 30 minutes ± SEM for at least 4 trials, totaling a minimum of 60 animals. (C, D) Representative endogenous inhibitory post-synaptic currents (IPSCs) recorded from ventral body wall muscles. +/+: *unc-29; acr-16* double mutants that lack excitatory neurotransmission at the NMJ are wild type for the *ser-2* locus. *ser-2*: *unc-29; acr-16; ser-2(pk1357)* triple mutants. (E, F) Tyramine application decreased the rate of IPSCs in +/+ (n=6), but not *ser-2* mutants (n=5). Arrow depicts tyramine application time point. Each point represents the IPSC frequency calculated over a 5 second time window as indicated. The red points correspond to the displayed samples in C and D, respectively. Dashed lines show average frequency before tyramine application and during the stabilized tyramine response period. (G) Average IPSC frequency

after tyramine application plotted relative to IPSC frequency prior to tyramine exposure. Values were normalized to average frequency observed in control recordings in the absence of tyramine. (H) Average amplitude of IPSCs after tyramine application plotted relative to average amplitude prior to tyramine exposure. Error bars depict SEM. Statistical differences calculated from +/+: *$p < 0.05$, two-tailed Student's t test.

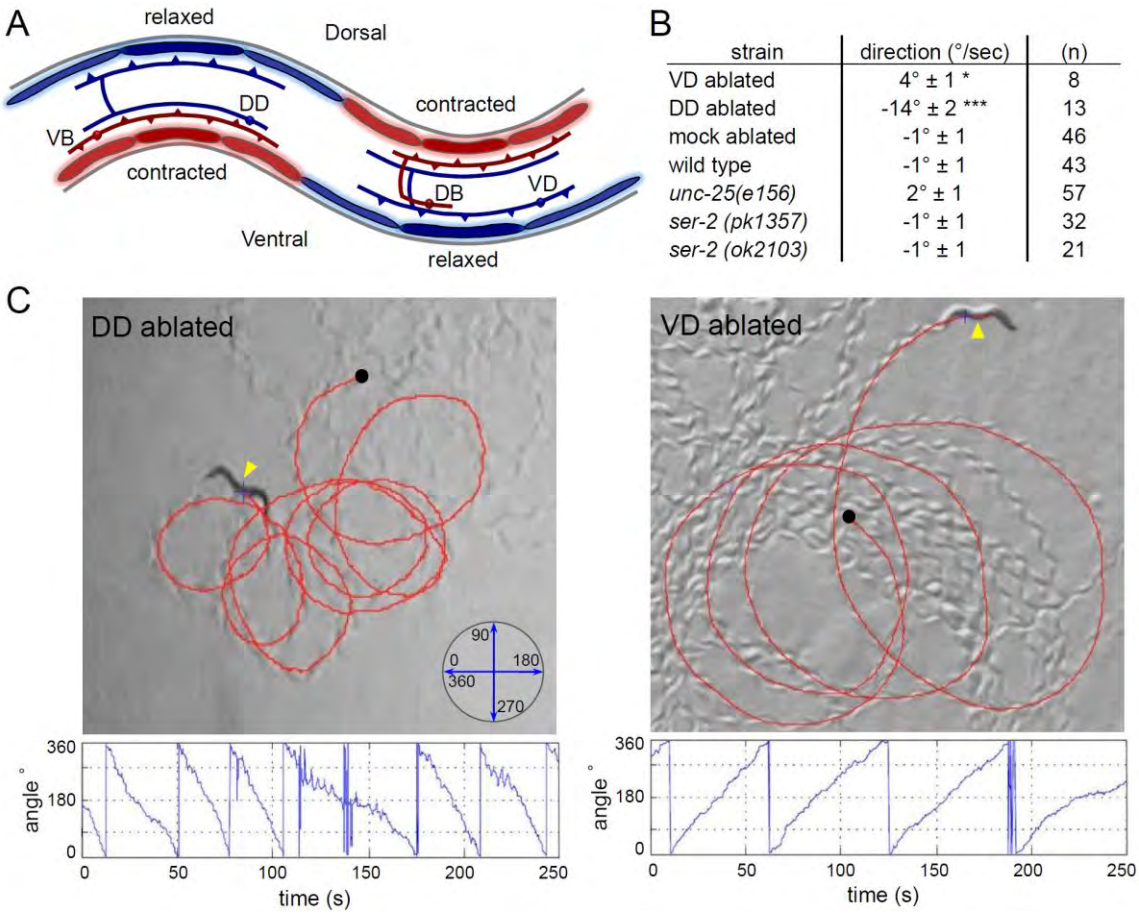

strain	direction (°/sec)	(n)
VD ablated	4° ± 1 *	8
DD ablated	-14° ± 2 ***	13
mock ablated	-1° ± 1	46
wild type	-1° ± 1	43
unc-25(e156)	2° ± 1	57
ser-2 (pk1357)	-1° ± 1	32
ser-2 (ok2103)	-1° ± 1	21

Figure III-8. Ablation of VD or DD motor neurons induces a navigational bias.

(A) Schematic of D-motor neuron wiring. VD motor neurons receive inputs from cholinergic DB motor neurons, and release GABA on ventral body wall muscles. DD motor neurons receive input from cholinergic VB motor neurons and release GABA on dorsal body wall muscles. Figure adapted from wormatlas.org. (B, C) Killing subsets of GABAergic motor neurons by laser ablation induced navigational biases. (B) Turning rate (°/sec ± SEM) is affected in animals where VD or DD neurons are ablated. DD ablated animals navigate with a dorsal bias.

VD ablated animals navigate with a ventral bias. Mock ablated animals, GABA deficient mutants (*unc-25*), and *ser-2* mutants did not show a change in turning rate. Turning angle was calculated by worm tracking software, n is indicated. (C) Representative locomotory path of a DD ablated (left panel) and VD ablated animal (right panel). DD ablated animals locomote in dorsally directed circles (Movie III-1). VD ablated animals locomote in ventrally directed circles (Movie III-2). The direction of locomotion (°) was determined from orientation of the animal's trajectory on the plate (inset). Red line traces the path of locomotion from the origin (black dot); yellow arrow designates the ventral side of the animal. Instantaneous turning angle is plotted for the duration of the locomotion path. Statistical differences calculated from mock ablations: *$p < 0.05$, ***$p < 0.001$, two-tailed Student's t test.

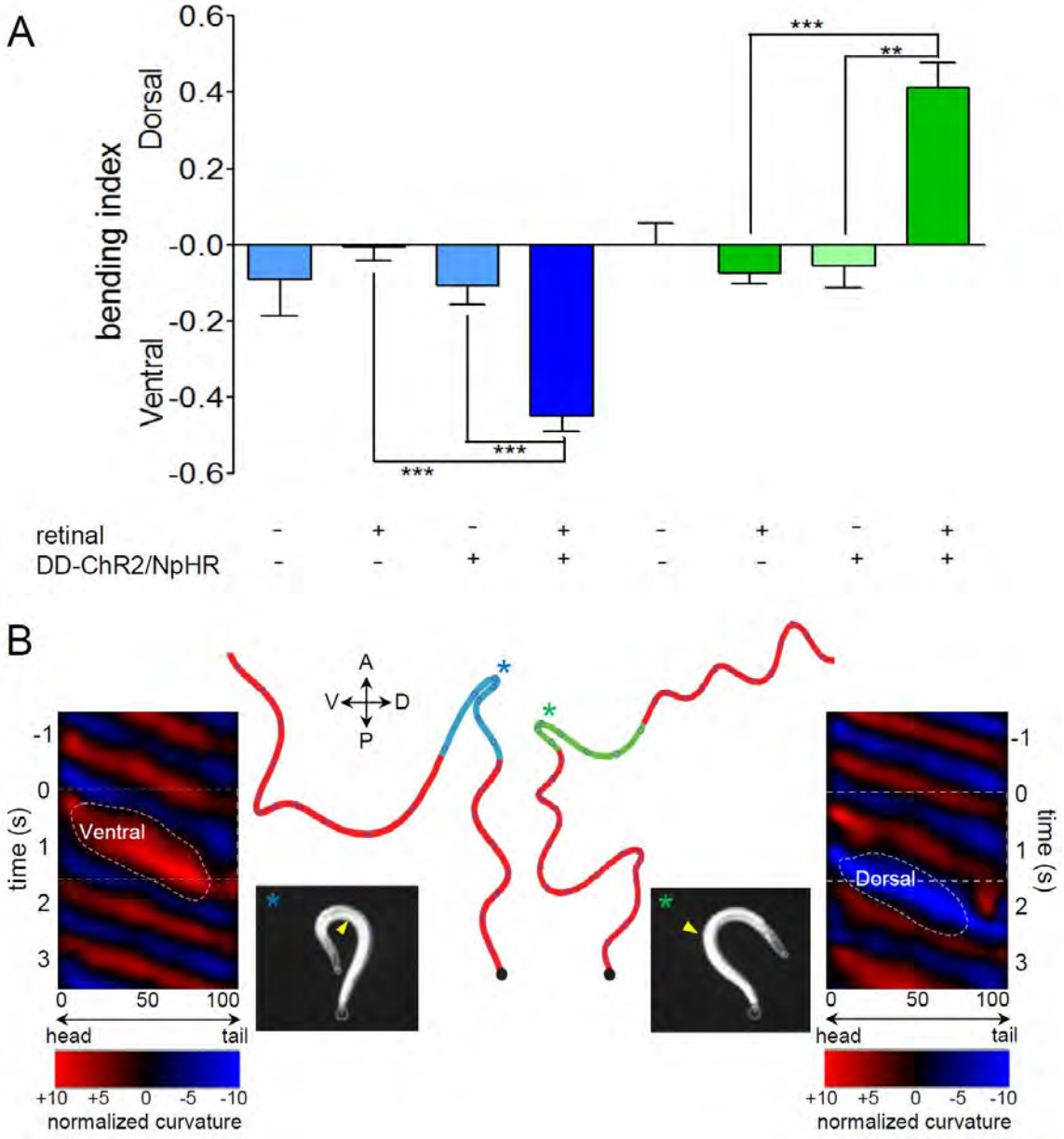

Figure III-9. Optogenetic control of navigation.

(A, B) Acute modulation of the activity of DD GABA neurons in transgenic animals expressing channelrhodopsin (ChR2) and halorhodopsin (NpHR) in DD motor neurons (*Pflp-13*::ChR2::GFP; *Pflp-13*::NpHR::CFP) induces turning

behavior. Blue light activation of GABAergic DD motor neurons that synapse onto dorsal muscles induces ventral turning. Green light inhibition of GABAergic DD motor neurons induces dorsal turning. (A) Quantification of bending behavior with green and blue light exposure. Bending bias was calculated as the fraction of dorsal turns – fraction of ventral turns after blue (DD activation, blue bars) or green (DD inhibition, green bars) light exposure. Each bar represents the mean bending bias for a minimum of 45 animals per genotype. Statistical significance as indicated: **$p < 0.001$ and ***$p < 0.0001$, two-tailed Student's t test. (B) Locomotion traces signify the time course of blue and green light exposure during forward movement (red). Open circles denote 1 second time marks. The compass indicates anterior (A), posterior (P), ventral (V) and dorsal (D) directions. Kymographs display sinusoidal bending wave amplitude before, during, and after light exposure. Normalized curvature is plotted at each point along the worm's centerline in units of inverse worm lengths. Color indicates curvature in either the ventral (red) or dorsal (blue) direction. The colored bands widen and brighten during deep turns induced by light exposure; white horizontal dotted lines indicate duration of light exposure, Ventral indicates a deep ventral bend, Dorsal indicates a deep dorsal bend. Still images were taken at * location on worm track (Movie III-3). Yellow triangle indicates the position of the vulva.

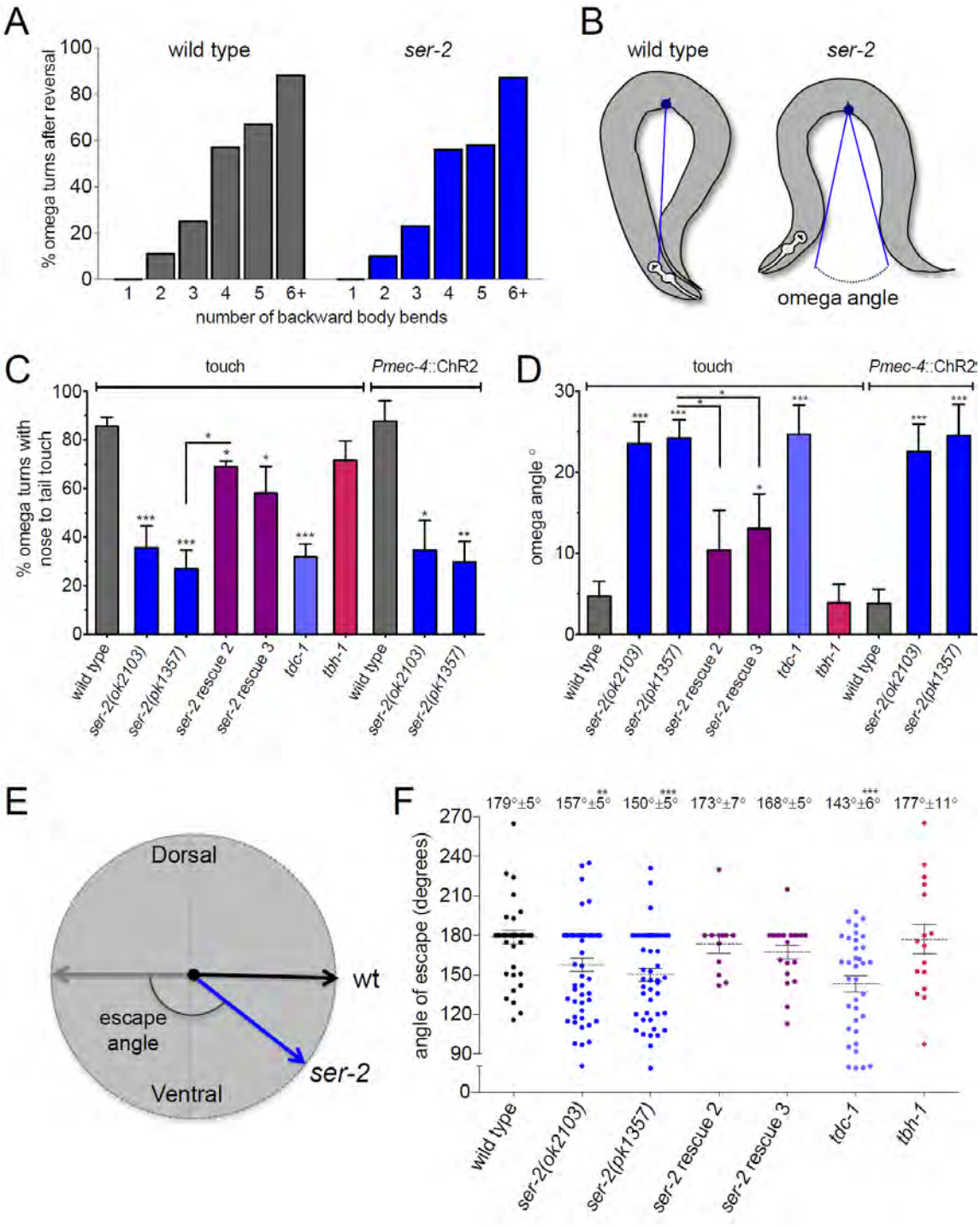
A
wild type
ser-2
% omega turns after reversal
number of backward body bends
B
wild type
ser-2
omega angle
C
touch
Pmec-4::ChR2
% omega turns with nose to tail touch
wild type
ser-2(ok2103)
ser-2(pk1357)
ser-2 rescue 2
ser-2 rescue 3
tdc-1
tbh-1
D
touch
Pmec-4::ChR2
omega angle °
E
Dorsal
wt
escape angle
ser-2
Ventral
F
179°±5°
157°±5°
150°±5°
173°±7°
168°±5°
143°±6°
177°±11°
angle of escape (degrees)

Figure III-10. *ser-2* mutants make shallow omega bends.

(A) Distribution of touch induced reversals ending in an omega turn. Omega turns are more likely to occur after longer reversals (> 3 body bends). Wild-type and *ser-2* mutant animals initiate omega turns at the same rate (n≥150 per genotype). (B) Schematic representation of the omega angle. The omega angle was measured as the angle from the deepest point in the ventral bend to the closest points anterior and posterior of the animal. Images were adapted from movies of animals in the most ventrally contracted state of the escape response. (C) Percent of omega turns where the animal's nose touches the tail during the execution of the turn (closed omega turn). *ser-2* mutants [*ser-2(ok2103),* n=52*; ser-2(pk1357),* n=62] touch nose to tail less frequently than wild-type (n=51) in omega turns induced by both touch (Movies III-4 and III-5) and blue light in a *Pmec-4*::ChR2 background [*Pmec-4*::ChR2, n=38; *ser-2(ok2103)*; *Pmec-4*::ChR2, n=43; *ser-2(pk1357)*; *Pmec-4*::ChR2, n=28]. Tyramine/octopamine deficient *tdc-1* mutants touch nose to tail less frequently than wild-type (*tdc-1(n3420)* , n=144) while octopamine deficient *tbh-1* mutants close omega turns like the wild type (*tbh-1(n3247)*, n=153). Genomic rescue lines partially restore this omega turning defect [*ser-2* rescue line 2, n=20; *ser-2* rescue line 3, n=21]. (D) Average omega angle measured after touch or exposure to blue light in a *Pmec-4*::ChR2 background [*Pmec-4*::ChR2, n=38; *Pmec-4*::ChR2; *ser-2(ok2103),* n=43; *Pmec-4*::ChR2; *ser-2(ok2103)*, n=28]. *ser-2* mutants [*ser-2(ok2103),* n=52; *ser-2(pk1357)*, n=62] and tyramine/octopamine deficient

mutants (*tdc-1(n3420)*, n=35) make a wider omega turn than wild-type (n=51). Octopamine deficient *tbh-1* mutants do not make wider omega turns (*tbh-1(n3247),* n=16*)*. Genomic rescue lines partially restore the omega angle defect of the mutants [*ser-2* rescue line 2, n=20; *ser-2* rescue line 3, n=21]. (E) Escape angles were measured from the direction of the reversal (induced by gentle anterior touch) to the direction of reinitiated forward locomotion. (F) Distribution of escape angles. Dashed grey line indicates average. Wild-type animals and *tbh-1* mutants escape in the opposite direction from the touch stimulus (wt: 179° ± 5°, n=42); *tbh-1(n3427)*: 177° ± 11°, n=16). *ser-2* mutants and *tdc-1* mutants make a shallower escape angle (*ser-2 (ok2103)*: 157.5° ± 5°, n=53; *ser-2(pk1357)*: 150° ± 5°, n=46; *tdc-1(n3420)*: 143.3° ± 6°, n=35). Genomic rescue lines restore the escape angle to wild type levels (*ser-2* rescue line 2: 173° ± 7°, n=12); *ser-2* rescue line 3 : 168.5° ± 5°, n=20)]. Rescue denotes the transgenic line *Pser-2*::SER-2; *ser-2(pk1357).* Error bars depict SEM. Statistical differences calculated from wild-type unless otherwise indicated: *p < 0.05, **p < 0.01, ***p < 0.001, two-tailed Student's t test.

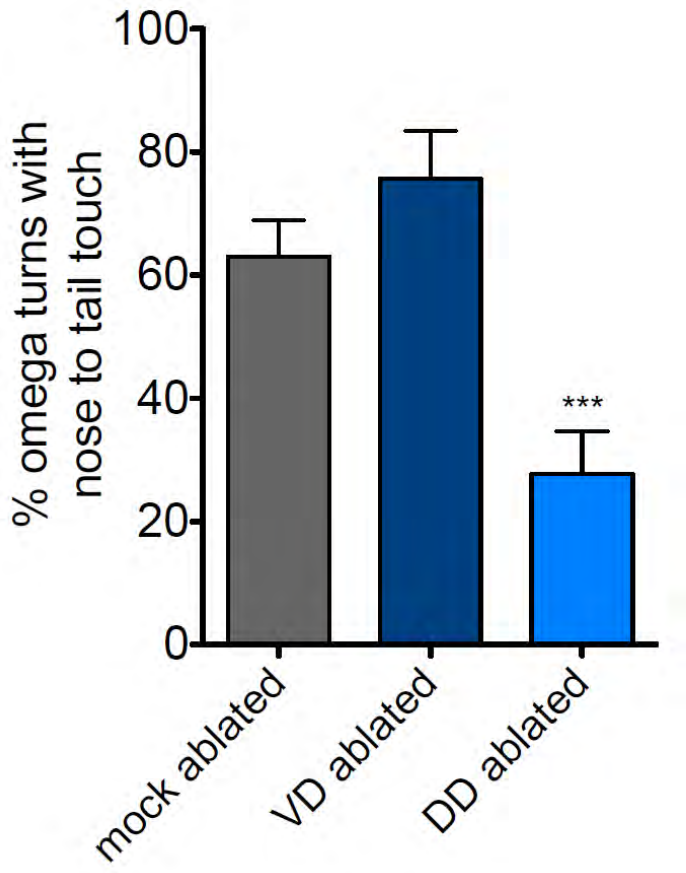

Figure III-11. Ablation of GABAergic DD neurons impair ventral omega turns.

Average number of closed omega turns made by animals with either VD (n=7) or DD (n=12) neurons ablated or mock ablated animals (n=13). Error bars represent SEM, ***p < 0.001, two-tailed Student's t-test.

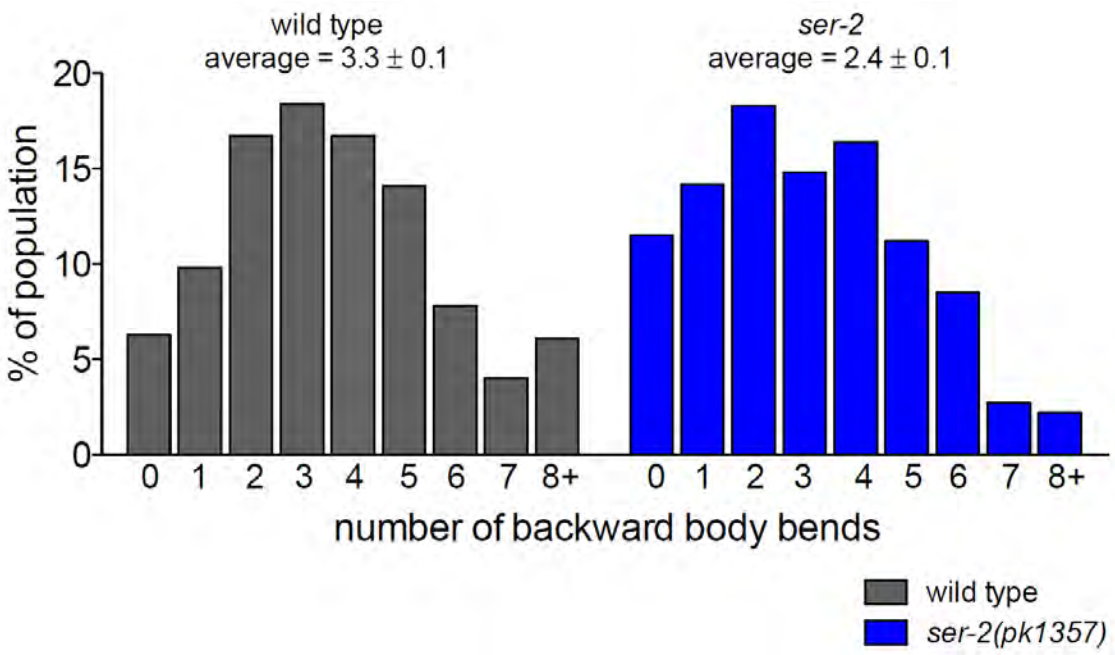

Figure III-12. Reversal length after gentle anterior touch.

Distribution of the number of backward body bends in response to anterior touch of wild-type and *ser-2* mutants. n≥250 animals per genotype.

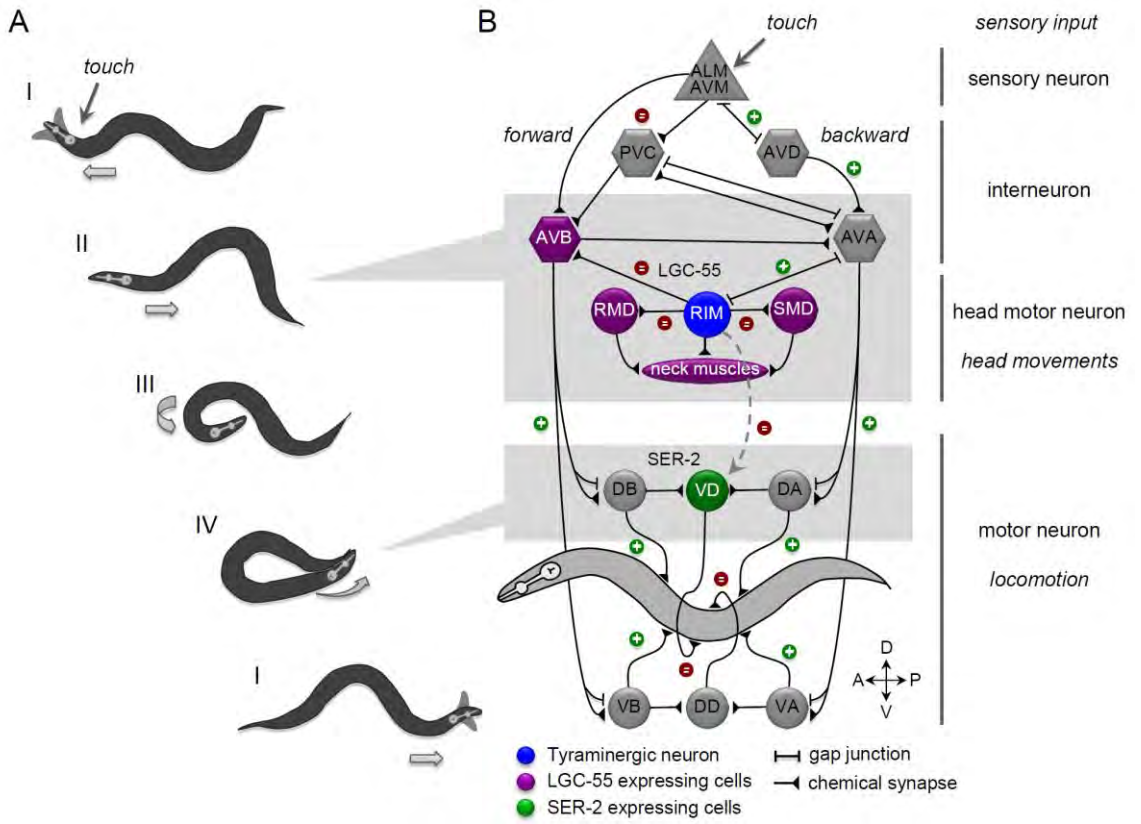

Figure III-13. Model: Tyramine orchestrates the *C. elegans* escape response through the activation of ionotropic and metabotropic receptors.

(A) Silhouettes of the four phases of the *C. elegans* anterior touch escape response. Images were adapted from a movie of an animal executing an escape response. See text for details. (B) Schematic representation of the neural circuit that controls the *C. elegans* escape response. Synaptic connections (triangles) and gap junctions (bars) are as described by White, et al. (1986). Green plus signs represent excitatory connections and red minus signs indicate inhibitory connections. Sensory neurons are shown as triangles, command neurons

required for locomotion are hexagons and motor neurons are depicted as circles. The compass indicates anterior (A), posterior (P), ventral (V) and dorsal (D) directions. *C. elegans* sinusoidal locomotion is propagated by alternatively contracting and relaxing opposing ventral and dorsal body wall muscles of the animal using cholinergic (DB and VB for forward and DA and VA for backward locomotion) and GABAergic (VD and DD) motor neurons. Anterior touch induces the activation of the tyramine release from the RIM motor neurons (blue cells). Solid lines represent synaptic activation of LGC-55 in neurons and muscles (purple cells) that result in the inhibition of forward locomotion and suppression of head movement in the initial phase of the escape response. Dashed lines represent extra-synaptic activation of SER-2 in the GABAergic VD motor neurons (green cells). The activation of SER-2 causes a decrease in GABA release on the ventral side animal. This allows the hypercontraction of muscles on the ventral side of the animal, thus facilitating the execution of a ventral omega turn.

Movie III-1.

Laser ablation of the DD GABAerigic motor neurons results in a dorsal bias during forward locomotion. The operated animal locomotes in a circular pattern with its ventral side (location of the vulva) facing the outside of the circles.

Movie III-2.

Laser ablation of the VD GABAerigic motor neurons results in a ventral bias during forward locomotion. The operated animal locomotes in a circular pattern with its ventral side (location of the vulva) facing the inside of the circles.

Movie III-3.

Tracking of a [*Pflp-13::*ChR2; *Pflp-13*::NpHR] single worm's locomotion and spatial illumination of the ventral nerve cord using the CoLBeRT system (Leifer, et al., 2011). Inhibition of the DD motor neurons with green light activation of NpHR causes a dorsal bend. Activation of the DD motor neurons with blue light activation of ChR2 causes a ventral bend.

Movie III-4.

A wild-type animal executing a complete omega turn in response to an anterior touch. Following a long reversal, the animal makes a deep ventral turn where the head of the animal touches and slides along the ventral side of the body and resumes forward locomotion in the direction opposite its original trajectory.

Movie III-5.

A *ser-2* mutant animal does not execute a complete omega turn in response to an anterior touch. Following a long reversal, the animal's head fails to touch the ventral side of the body.

CHAPTER IV: DISCUSSION

Mechanisms of neural circuit signaling

Synaptic chain models describe the organization of neural circuits that controls behavioral patterns comprised of a sequence of motor outputs. Karl Lashley (1951) postulated that associative chains were the mechanism by which nervous systems generated sequential behaviors. In this model, behaviors in a sequence are not activated as separate units; rather, they are activated together as a unit, and the timing of their execution is internally controlled as if by a chain of activity. This synaptic chain model is supported by electrophysiological analysis of zebra finch song circuits. Long, et al. (2010) showed that premotor neurons involved in singing behavior exhibit bursting activity that propagates through a chain of synaptically connected neurons. Zebra finch song behavior gives tremendous insight into the organization of neural circuits by electrically demonstrating the existence of synaptic chains. This principle can be applied to the simpler *C. elegans* nervous system to investigate the properties of synaptic chains with single cell resolution. The *C. elegans* escape response is a sequential compound behavior. In Chapter II, we show the neural activity patterns of neurons connected in a synaptic chain from sensory neurons to motor neurons, and how this chain orchestrates the motor programs of the escape response. Pirri, et al. (2009) and Donnelly and Clark, et al. (2013, Chapter III) describe the molecular mechanisms that modulate two phases of the escape response, the reversal with suppression of head movements (Phase II) and the deep ventral omega turn (Phase IV). However, the mechanism that initiates the

ventral bend (Phase III) is unclear. I hypothesize that ventral turn is initiated through a chain of excitatory and inhibitory connections.

The omega turn is a unique behavior that only occurs after a long reversal, and it always occurs in the ventral direction (Ben Arous, et al., 2010). In Chapter II, we showed that the SMD and RIV motor neurons are required to execute the ventral turn, but the mechanism that controls RIV and SMD activity is still unclear. INX-1 gap junctions play a role in executing the turn (Figure II-10) and tyramine signaling plays a role in the timing of the turn (Figure II-9). The AVA, RIM, AIB and RIV are coupled through a chain of gap junctions (White, et al., 1986, Figure II-8). We hypothesize that during an escape response, activation of the AVA results in the co-activation of the RIM, AIB, and RIV. This is observed in the elevated calcium signals in the AVA, RIM and AIB during the reversal. However, RIV activity does not increase until the omega turn occurs (Figure II-3). While the RIV may have been primed through gap junctions with AIB, its activity may be depressed through its gap junctions with the SMD. Tyramine release from the RIM inhibits the SMD through the tyramine-gated chloride channel LGC-55 (Pirri, et al., 2009). Additionally, the SMD express the inhibitory glutamate-gated chloride channel AVR-14 (data not shown). Glutamate release from the AIB inhibits the RIM through AVR-14 signaling (Piggott, et al., 2011). This inhibitory connection may also occur between the AIB and SMD. Dual inhibition of the SMD may delay to the activation of the electrically coupled RIV to occur at the appropriate time when initiating the omega turn. Calcium imaging of the SMD

and RIV motor neurons in mutant animals deficient for RIM tyraminergic signaling (*tdc*-1 and *lgc-55*) and for signaling from the AIB (*inx-1* and *avr-14*) will further uncover the nature of the connections that control the initiation of the omega turn.

The neurotransmitter tyramine is a regulator of the *C. elegans* escape response. The escape response is a compound behavior composed of multiple behavioral motifs, each of which is modulated by tyramine signaling. Since the RIM are the only neurons in the nervous system that are exclusively tyraminergic, they serve as the neural orchestrators of escape behavior. The RIM also have roles in navigation, egg laying, foraging behavior and learning and memory; and they receive inputs from interneurons involved in olfactory behavior and fat metabolism (Alkema, et al., 2005; Gray, et al., 2005; Lau, et al., 2013; Chalasani, et al., 2007; Piggott, et al., 2011; Cohen, et al., 2009). Interestingly, optogenetic activation of the RIM results in behavior that mimics the activation of the touch sensory neurons (Figure II-7). How can the activation of an interneuron deep in a neural circuit produce the same behavioral outputs as the stimulation of sensory neurons? The RIM inter/motor neurons likely serve as a neuromodulators for many behaviors by communicating the internal state the animal to locomotion interneurons and motor neurons. For example, Piggott, et al. (2011) used optogenetic inhibition and calcium imaging experiments to suggest that the RIM inhibits reversal behavior. Conversely, data in Chapter II and the work of others shows that RIM activity promotes reversals (Chronis, et al., 2007; Guo, et al., 2009). Alkema, et al. (2005) describes the RIM as the

coordinators of locomotion changes between forward and backward locomotion. The RIM do not necessarily drive backward and forward locomotion; rather, the RIM modulate the balance between AVA and AVB pre-motor interneuron activity that drives locomotion (Kawano et al., 2011). While tyramine may serve as the neuromodulator of many behaviors, optogenetic activation of the RIM may be the equivalent of a panic response, thus matching the response observed with ALM/AVM activation. Cation influx from the activation of overexpressed ChR2 is likely not a physiological process that resembles intrinsic synaptic signaling. Optogenetic activation may, however, mimic the stimulus threshold that releases the escape response fixed action pattern, thus facilitating survival behavior above all other internal states.

The *C. elegans* connectome shows all of the synaptic connections through which neurons can potentially communicate; and all of these connections are subject to neuromodulation from non-synaptic partners. Monoamine neurotransmitters like dopamine, serotonin and octopamine have been shown to have extrasynaptic signaling partners (Tsalik, et al., 2003; Chase, et al., 2004; Bargmann, 2012). Additionally, we defined a tyraminergic mechanism for the extrasynaptic modulation of GABA signaling in motor neurons (Donnelly and Clark, et al., 2013; Chapter III). Neuromodulation increases the flexibility of a neural circuit's output to reflect the animal's internal state. Neuromodulation also magnifies the complexity of interpreting a connectome. In addition to the modulatory roles of neurotransmitters, the *C. elegans* genome encodes over 200

neuropeptides (Bargmann, 2012). Studying modulation by specific neuropeptides can be difficult because different developmental stages, tissues and cellular compartments can utilize different cleavage products of the same neuropeptide (Li and Kim, 2008). Additionally, modulatory effects can be so subtle that they only experimentally manifest in sensitized genetic backgrounds (Bhattacharya, et al., 2014). It is plausible that a context specific behavior such as the omega turn may be modulated by neuropeptides, particularly because of its delayed timing after a mechanical stimulus. The *C. elegans* genome encodes a large number of neuropeptides and neuropeptide receptor that have not been fully characterized, but several genes have expression patterns that include neurons in the escape response neural circuit. One such example is FLP-18. FLP-18 is an FMRF-amide like neuropeptide that is expressed in the RIM and AVA (Cohen, et al., 2009). *In vitro* studies have shown that FLP-18 binds the neuropeptide receptors NPR-1, NPR-4, NPR-5 and NPR-10. NPR-5 is expressed in many head neurons and muscles. NPR-4 is expressed in a few neurons including the RIV and AVA (Li and Kim, 2008). Preliminary experiments suggest FLP-18 many play a role in body posture as well as omega turns in response to tap stimulation (Jeremy Florman personal communication). The *C. elegans* nervous system is a powerful tool in the field of neurobiology because of the known connectome. Being able to map complete neural circuits that govern behavior allows us to go deeper into the molecular foundations of behavior. Chapter III touches on the extrasynaptic connections that neurotransmitters make and this is compounded by the potential

modulatory effects of neuropeptide signaling. Having a completely mapped structural connectome allows us to study the molecular mechanisms that fine tune neuron communication.

The future of neural circuit imaging

In Chapter II, we imaged neural activity in live behaving animals. In order to measure the fluorescence of single neurons, the neurons had to be reliably identifiable in a moving animal. We used different promoters with limited expression patterns to label our cells of interest. Not only do promoters need to sparsely label the nervous system but the neurons have to be identifiable at potentially low magnifications because the behavior of the worm is being simultaneously recorded and tracked using a motorized stage. Some studies track worm movement by specifically tracking the fluorescent cells. This approach permits higher magnification of head neurons, but gross behavioral measurements are lost. In Chapter II, we used a dual objective system to image head neurons while tracking behavior. One imaging path recorded locomotion to be used for tracking purposes. A second imaging path recorded head neurons at high magnifications. In our hands, head neurons could be imaged and identified at 10-40x magnifications. Higher magnifications were more susceptible to small motion changes that resulted in losing the image of the neurons for a few frames. These motion changes were due to topographic imperfections in the agar substrate and subsequent changes in the vertical focal plane, and to rapid

locomotion changes that often occurred with high angle turns like the omega turn. Recent studies have recorded neural activity and behavior at relatively low magnifications (2.5-10x) (Larsch, et al., 2013; Shipley, et al., 2014); and the recent advent of the brighter and more sensitive GCaMP6 will only enhance the neuron fluorescence signals during behavior (Chen, et al., 2013). However, these systems still require sparse expression patterns for neuron identification. Because of this, we were limited to using promoters that labelled known neurons in the escape response neural circuit. The neurons that comprise this circuit are largely neurons that have pronounced behavioral impacts when ablated (Chalfie, et al., 1985; Wicks and Rankin, 1995; Gray, et al., 2005; Figures II-5, 6). Many more synaptic connections are not included in this circuit because other connected neurons have no discernable roles in the escape response when ablated. To know this for sure, neural activity of all neurons needs to be measured during behavior. Pan-neuronal imaging of the worm brain can be done in immobilized animals where neuron identification is largely dependent on using neurons with known activity patterns as anatomical reference points (Schrödel, et al., 2013). The technology is available; however, advances in cell identification techniques need to be developed to comprehensively measure whole brain activity

Optogenetics and calcium imaging can be combined to measure and manipulated the optical physiology of neurons in a behaving animal. Shipley et al. (2014) measured neural activity in locomotion interneurons following the

optogenetic stimulation of mechanosensory neurons. This is an optical correlate of using electrophysiology of stimulating one while recording from another to examine the functional connections between neurons. Optical physiology allows the activity dynamics of neurons not amenable to electrophysiology to be investigated during behavior.

New genetically encoded tools and improvements in optics are pushing the limits of measuring neural activity *in vivo.* Currently, fluorescent calcium indicators are the predominant tools used to measure neural activity. In terms of electrical signaling, calcium indicators do not compare with electrophysiology. When neurons communicate, electrical signals are propagated from one cell to another, and changes in membrane potential occur on the scale of milliseconds. Measuring this phenomenon via secondary changes in intracellular calcium concentrations is inherently imperfect. Compared to the timescales of measuring membrane potential changes using electrophysiology, the dynamics of calcium indicators are much slower (Looger and Griesbeck, 2012). When combined with the inherent noise of behavioral tracking, calcium dynamics are measured on the order of seconds (Figure II-3). This issue of signal speed can be addressed by optically measuring voltage. Rhodopsin based indicators, PROPS and VIP2, emit fluorescent signals in response to *in vitro* changes in membrane voltage (Kralj, et al., 2011; Kralj, et al., 2012). Voltage changes induce protonation of bound retinal within these rhodopsins, resulting in red fluorescent emission. We expressed the VIP2 indicator in *C. elegans,* but the resulting fluorescence was too dim to be

detected during behavior. Another voltage sensor, Arclight, has a much brighter fluorescent signal than the rhodopsin based indicators. Arclight is a mutated ecliptic pHluorin fused to the voltage sensing domain of the *Ciona intestinalis* voltage dependent phosphatase. Arclight expression in *C. elegans* muscles exhibits voltage dependent changes in fluorescence (Murata, et al., 2005; Jin, et al., 2012; Wooltorton, et al., 2013). Encouraged, we expressed Arclight in neurons; however, we could not detect any fluorescent changes when we during behavior. The most recent iteration of a fluorescent voltage sensor, QuasAr, is a variant of the VIP2 rhodopsin sensor with an increased voltage sensitivity and fluorescence. When compared with Arclight *in vitro*, QuasAr was still very dim but exhibited higher fold-fluorescent changes and faster responses to changes in membrane potential (Hochbaum, et al., 2014). We expressed QuasAr in worm neurons but the behavioral experimentation had not been conducted at the time of this thesis presentation.

In this dissertation, I demonstrate how a nervous system generates behavior. Studying neurobiology in the nematode *C. elegans* provides the opportunity to trace the path of a single stimulus as it is communicated from cell to cell and to its ultimate motor output. The sensorimotor circuit for the *C. elegans* escape response is a unique model to study circuit function in that the complete structural connectivity from sensory neurons to interneurons to motor neurons and muscle is known (White, et al., 1986). With this platform, I demonstrated how neural activity flows in a circuit during behavior, and identified

the behavioral contributions of those neurons to coordinating a compound behavior. This work, presented in Chapter II showed the activity dynamics of interneurons that integrate a sensory input to produce appropriate behavioral outputs. Coordination of the motor programs that make up the compound behavior is largely orchestrated by a single neurotransmitter. In Chapters II and III, I demonstrate how the neurotransmitter tyramine regulates two turning behaviors of the escape response. Tyramine plays a role in timing the initiation of the ventral turn that reorients forward locomotion, as shown in Chapter II. Chapter III explores the mechanism by which tyramine facilitates the deep ventral bend of the omega turn through G-protein modulation of GABA signaling in motor neurons. Chapter II demonstrates the strength of having a fully defined connectome by showing how a neural circuit transduces sensory information into behavior. Chapter III shows how neuromodulators tune neural circuit function to produce appropriate behaviors, and sheds light on the complex mechanisms of extrasynaptic signaling. As the connectomes and neural circuits of more systems are defined, the nature of neuron to neuron communication during behavior will have to be addressed. This dissertation defines principles of neural circuit organization function conserved from worms to vertebrates, and understanding these principles will aid in the functional characterization of higher organism connectomes as we continue to define the wiring of the brain.

PREFACE TO APPENDIX I

The work presented in this chapter highlights an evolutionary arms race between soil nematodes and nematophageous fungus. Nematophageous fungus has developed a variety of mechanisms to consume nematodes, including constricting rings that trap worms. We show that that a worm's ability to relax their neck and reverse out of a fungal trap increases the probability that they'll escape the encounter. Mutants unable to relax their head and coordinate a reversal when touched on the neck are caught more frequently than wild type animals. Therefore, we demonstrated a how genetic adaptations may have promoted the survival of soil nematodes from this specific predator prey interaction.

Sean Maguire performed the capture experiments for different fungus species and different *C. elegans* larval stages. Christopher Clark measured the trap locations along the worm's body. Sean Maguire and John Nunnari generated the electron micrograph images. Sean Maguire and Christopher Clark performed the experiments that measured the frequency of worms escaping from fungal encounters, the experiments measuring the interaction time of worms with the mesh that mimicked fungal nooses, and the survival competition experiments. Sean Maguire, Jennifer Pirri and Christopher Clark performed the measurements comparing wild type worms with *lgc-55* mutants. Sean Maguire and Mark Alkema designed the experiments. Sean Maguire and Mark Alkema co-wrote the

manuscript. All authors discussed the results and commented on the manuscript.

This work was published in the journal *Current Biology* in 2011.

APPENDIX I: THE *C. ELEGANS* TOUCH RESPONSE FACILITATES ESCAPE FROM PREADCIOUS FUNGI

Sean M Maguire, Christopher M Clark, John Nunnari, Jennifer K Pirri and Mark J Alkema

Department of Neurobiology, University of Massachusetts Medical School, 364 Plantation Street, Worcester, MA 01605, USA

Published in *Current Biology* (2011) 21: 1326-1330.

Highlights:

- Predacious fungi that use hyphal constricting rings catch *C. elegans* larvae
- *C. elegans* reverses and suppresses exploratory head movements in response to anterior touch
- Touch induced suppression of head movements facilitates escape from a hyphal noose
- Predacious fungi may have shaped the evolution of *C. elegans* escape behavior

Abstract

Predator-prey interactions are vital determinants in the natural selection of behavioral traits. However, we have few insights into both the neural mechanisms and the selective advantage of specific behavioral traits. Gentle touch to the anterior half of the body of *Caenorhabditis elegans* elicits an escape response in which the animal quickly reverses and suppresses exploratory head movements (Chalfie and Sulston, 1981). Even though the *C. elegans* touch response has provided one of the rare examples of how neural networks translate sensory input to a coordinated motor output (White, et al., 1986), the ecological significance of the escape response is unclear. We investigate predator-prey relationships between *C. elegans* and predacious fungi that catch nematodes using constricting rings as trapping devices. We show that the constricting rings of *Drechslerella doedycoides* catch early larval stages with a

diameter similar to the trap opening. There is a delay between the ring entry and ring closure, which allows the animal to withdraw from the trap before getting caught. Mutants that fail to suppress head movements in response to touch are caught more efficiently than the wild type in constricting fungal rings. Direct competition experiments show that the suppression of head movements in response to touch is an ecologically relevant behavior that allows the *C. elegans* to smoothly retract from a fungal noose and evade capture. These results suggest that selective pressures imposed by predacious fungi have shaped the evolution of *C. elegans* escape behavior.

Introduction

Escape behaviors increase the prey's odds of surviving an encounter with a predator and have been extensively studied from an ethological, neurophysiological and behavioral genetic perspective (Eaton, 1984; Barbosa and Castellanos, 2005; Allen, et al., 2006). However, the dichotomy between field and laboratory studies makes it difficult to unify investigations of both proximate and ultimate causes of behavior. Furthermore, since phenotypic selection is usually measured in natural populations, our current understanding of genotypic selection is largely correlative. Unraveling of causative relationships between phenotypic and genotypic selection requires the ability to experimentally manipulate behavioral traits. The ability to genetically manipulate behavioral traits and the defined neural architecture of the nematode *Caenorhabditis elegans*

provides a unique opportunity for a comprehensive neuroethological analysis of the behavior (Tinbergen, 1963).

C. elegans moves on its side by propagating a sinusoidal wave of body wall muscle contractions along the length of its body. Locomotion is accompanied by exploratory head movements, in which the tip of the nose moves rapidly from side to side (Figure AI-1A) (Croll, 1975). Gentle touch elicits an escape response in which *C. elegans* quickly moves away from the stimulus (Chalfie and Sulston, 1981). The animal backs up in response to light touch to the nose or anterior half of the body, while quickly moves forward when touched at the posterior half. Exploratory head movements continue in response to nose or tail touch but are suppressed during backing when the animal is touched on the anterior region of its body, between the pharyngeal bulb and the mid body (Figure AI-2) (Alkema, et al., 2005). The *C. elegans* touch response has provided one of the few examples for which the entire sensori-motor circuit has been defined (White, et al., 1986). However, the ecological significance of the touch response is unclear.

Why would *C. elegans* specifically suppress exploratory head movements in response to touch on the anterior region of its body, but not when it is touched on the nose or the tail end? In soil and decaying organic material, nematophagous fungi prey on nematodes as their main food source (Drechsler, 1937; Duddington, 1951; Thorn and Barron, 1984). Some of these fungi have developed distinctive trapping devices along their hyphae to catch nematodes.

Trapping structures include adhesive nets, knobs or branches, and constricting and non-constricting rings. Predatory fungi that use rings as a trapping mechanism have been found along with nematodes in 100-million-year-old amber (Schmidt, et al., 2007), indicating a long evolutionary predator-prey relationship. The constricting ring used by fungi such as *Drechslerella doedycoides*, are composed of three cells that form a closed ring at the end of a short hyphal branch (Figure AI-1F-H). When a nematode passes through the ring, gentle friction induces the cells of the ring to rapidly inflate inwards and catch the nematode (Movie AI-1). Once a nematode is captured, hyphae penetrate the cuticle and digest the worm.

Results

To determine if the nematode's touch response is important to avoid predation, we analyzed predator-prey relationships between fungi that use constricting rings and *C. elegans*. The average inner-diameter of constricting rings of the different fungi ranged from 10 µm to 25 µm (Figure AI-1B, G). The diameter of *C. elegans* increases throughout development from approximately 12 µm shortly after hatching to 50 µm in the young adult (Figure AI-1C). To determine which life stages were caught by fungal traps, we inoculated agar plates that contained the fungus *D. doedycoides* with different developmental stages of *C. elegans* (Figure AI-1D). L1 larvae were small enough to pass through constricting rings, often without setting off the trap. Since *C. elegans* is

tapered on either end, the slightly larger L2, and L3 larvae could enter a ring until the body diameter was too large to continue forward movement. L4 larvae and adult animals were too large to enter the ring during forward movement and usually swept the rings aside with foraging head movements. However, since the tail of *C. elegans* tapers more narrowly than the head region, larger animals could get caught while reversing into a ring. While adult animals were rarely caught, the majority of L2 larvae were caught within 4 hours of inoculation. Most animals were caught at the anterior half of the body (Figure AI-1E), indicating that animals with a diameter similar to or slightly larger than the trap aperture are caught most efficiently. Since both *C. elegans* (Felix and Braendle, 2010) and nematophagous fungi (Gray, 1987) have been found worldwide in decaying organic matter, it is likely that *C. elegans* will face fungal predation in its natural habitat.

Can *C. elegans* escape from a constricting hyphal ring? Although the inflation of the ring cells occurs very quickly once initiated (approximately 0.1 seconds) (Higgins and Pramer, 1967), there is a slight delay between an animal entering a trap and trap closure (Figure AI-3A). We found that on average the latency between initial contact of the worm with the inside of the ring until inflation occurred was 5 seconds, which is long enough to allow nematodes to enter and withdraw from the ring and escape without setting off the trap (Figure AI-3B). We monitored individual trap encounters and found that the large majority wild-type animals that entered a ring managed to exit the ring without getting caught (81 ±

4%). Occasionally, animals set off the fungal trap but still managed to withdraw and escape the constricting ring before it inflated (Figure AI-3C, Movie AI-2). Much like the anterior touch response elicited by a hair, the tightening noose around the worm's neck induced a quick reversal and the suppression of exploratory head movements. To determine if mechanosensory perception of the fungal hyphae increases the animal's chances to escape from constricting rings, we analyzed trap encounters of touch insensitive *mec-4* mutant animals. The MEC-4 DEG/ENaC channel is expressed in the touch sensory neurons and is required for mechanotransduction (Driscoll and Chalfie, 1991). Since *mec-4(u253)* complete loss-of-function animals are lethargic, we analyzed *mec-4(e1339)* partial loss-of-function mutants which have a strong reduction in the anterior touch withdrawal response (O'Hagan, et al., 2005). The fraction of *mec-4(e1339)* mutant animals that managed to escape from traps was drastically reduced (43 ± 8%) compared to the wild type (Figure AI-3B). *osm-9(n1603)* mutants are nose touch defective (Colbert, et al., 1997; Liedtke, et al., 2003), but did reverse and suppress head movements in response to anterior touch. Once *osm-9(n1603)* mutants animals entered a trap, they escaped as frequently (81 ± 6%) as the wild type. Thus, anterior touch but not nose touch sensation is crucial to *C. elegans'* ability to escape from constricting rings.

Does the suppression of head movements increase the animal's ability to escape from predacious fungi? We have previously shown that the biogenic amine, tyramine is required to coordinate head and body movements in the *C.*

elegans anterior touch response (Alkema, et al., 2005). The anterior touch sensory neurons activate backward locomotion command neurons, which are electrically coupled to the tyraminergic neurons. Tyramine release inhibits forward locomotion as well as exploratory head movements through the activation of the tyramine-gated chloride channel, LGC-55 (Pirri, et al., 2009; Ringstad, et al., 2009). Like the wild type, tyramine deficient *tdc-1(n3420)* and *lgc-55(tm2913)* mutants reverse normally in response to touch. However, *tdc-1* and *lgc-55* mutant animals back up slightly less far than the wild type and fail to suppress exploratory head movements during these reversals. We found that *tdc-1* and *lgc-55* mutants initiated reversals when wedged in a trap but escaped less frequently from constricting rings than the wild type (Figure AI-3B, *tdc-1*: 49 ± 10%; *lgc-55*: 60 ± 6%). *unc-4(e120)* mutants can move forward and suppress head movements in response to touch, but have severe defects in backward locomotion escape (White, et al., 1992). *unc-4(e120)* mutant animals escaped less frequently (59 ± 7%) than the wild type, indicating that the coordination of a reversal with the suppression head movements is required for an efficient escape.

To test whether increased captures of tyramine-signaling mutants are caused by increased attraction to fungi, or by a defect in the motor-program used to extricate from noose-like structures, we mimicked *C. elegans* trap encounters with a nylon mesh. We compared how young adult wild-type and *lgc-55* mutant animals crawl through a narrow opening of a nylon fence containing 37 μm

openings (Figure AI-4). Young adult animals can pass through these openings but this requires body contact with the threads of the mesh. *lgc-55* mutant animals are indistinguishable from the wild type with respect to developmental timing, size, locomotion rate, locomotion pattern, touch sensitivity and exploratory behavior (Figures AI-5 and AI-6). We found that once they entered the mesh, *lgc-55* mutants took more than twice as long to extricate themselves than wild-type animals (wt: 9 +/- 1 s; *lgc-55*: 23 +/- 4 s). A transgenic *lgc-55* rescuing construct restored the behavior of *lgc-55* mutants back to that of the wild type (P*lgc-55*::LGC-55: 10 +/- 1 s). Thus, our findings indicate that the tyraminergic coordination of backward locomotion with the suppression of the head movements facilitates retraction from a narrow ring.

To directly test if the suppression of head movements provides a selective advantage, we performed a competition experiment. We inoculated *D. doedycoides* cultures with a mix of wild-type and *lgc-55* mutant L2 larvae (Figure AI-7). We used a transcriptional *lgc-55::*GFP reporter to label one of the strains in the selection experiments. The GFP marker did not affect capture. A mix of equal amounts of staged L2 larvae of each genotype were transferred onto the hyphal mats of *D. doedycoides*. After 90 minutes, animals that were not caught were washed off the plate and the number of captured GFP positive and GFP negative animals were counted. The capture index was calculated by subtracting the fraction of the caught tested genotype from the fraction of the caught control animals. A positive capture index indicates a selective disadvantage compared to

the wild-type strain (Figure AI-8). In these competition experiments a larger fraction of *lgc-55* mutants were caught than the wild type (Capture index 0.36 +/- 0.02). Expression of wild-type copies of *lgc-55* under its endogenous promoter completely rescued the selective disadvantage of the *lgc-55* mutants (Capture index 0.02 +/- 0.02). Our previous studies have shown that *lgc-55* is expressed in neck muscles and neurons that receive presynaptic inputs form the tyraminergic RIM neurons (Figure AI-2) (Pirri, et al., 2009). *lgc-55* expression in neck muscles is required to suppress head movements, while expression in the AVB forward locomotion command neurons is required to suppress forward locomotion, which leads to longer reversals in response to touch. While the suppression of head movements may allow a smooth retraction, long reversals may also facilitate escapes once the animal moved far into the ring. To determine if the suppression of head movements alone aids in the escape, we performed competition assays with *lgc-55* mutant animals in which wild-type copies of *lgc-55* were expressed in muscles using a *myo-3*::LGC-55 transgene. *lgc-55; myo-3*::LGC-55 animals are not rescued for reversal defects but do suppress their head movements in response to anterior touch (Pirri, et al., 2009). We found that the capture index of *lgc-55* mutants in which only the defect in the suppression of head movements was rescued, is significantly lower than those of the original mutant strain (Capture index 0.12 +/- 0.02). This demonstrates that the suppression of head movements in response to anterior touch increases the animal's chances to smoothly reverse without getting caught in the deadly noose (Figure AI-8B).

Therefore, the coordination of motor programs that control head movements with locomotion is of vital importance for *C. elegans* to evade predation in the wild.

Discussion

The suppression of head movements in response to anterior touch is conserved in related *Caenorhabditis* species (data not shown). Moreover, phylogenetic analyses of predacious fungi and morphology of fungal trapping devices suggests that constricting rings might have evolved from non-constricting rings (Li, et al., 2005). This raises the intriguing possibility that the touch-induced suppression of head movements may be the consequence of an evolutionary arms race between predacious fungi and nematodes. Further characterization of the habitat of soil nematodes *and* predacious fungi will be key to our understanding of the selection pressures that shape behavioral adaptation. Since we know the molecular and neural underpinnings of the *C. elegans* escape response in exquisite detail, comparative studies of soil nematodes provides a powerful model to study the mechanisms that underlie the evolution of escape behaviors.

Experimental Procedures

Strains

The following nematophageous fungi strains were used: *Drechslerella dactyloides* ATCC 2041022, *Drechslerella doedycoides* ATCC 96678, *Drechslerella brochopaga* ATCC 96710, *Drechslerella bembicodes* CBS 106.38. Nematophagous fungi were maintained on agar supplemented with 1x malt extract, at room temperature. To induce trap formation for predation assays, fungi from malt extract plates were subcultured on 2% water agar plates and grown until hyphal mats completely covered the agar surface.

C. elegans strains were grown under standard conditions (Brenner, 1974). The *C. elegans* strains used include: wild type: N2, QW89: *lgc-55(tm2913),* QW284: *tdc-1(n3420),* CB1339: *mec-4(e1339),* TU253: *mec-4(u253)*, MT3642: *osm-9(n1603)*, CB120: unc-4(e120), SS104: *glp-4 (bn2ts)*, QW124: *lgc-55::*GFP *(zfIs6)*, QW191: *lgc-55(tm2913); lin-15(n765ts); zfEx2[*P*lgc-55::LGC-55; lin-15(+)]*, QW420: *lgc-55(tm2913); lin-15(n765ts); zfEx53[*P*myo-3::LGC-55; ceh-22::*GFP*; lin-15(+)]*. Transgenic strains were generated by microinjection of plasmid DNA into the germline. *lgc-55* rescuing lines were made by co-injecting a *lgc-55* genomic rescuing plasmid at 20 ng/µl along with the *lin-15* rescuing construct pL15EK at 80 ng/ul into *lgc-55(tm2913)*; *lin-15(n765ts)* animals. Muscle specific rescuing lines were generated by co-injecting a *myo-3*::LGC-55 plasmid at 20 ng/µl along with *ceh-22::*GFP (coelomocyte GFP) and the *lin-15* rescuing plasmid at 80 ng/µl into *lgc-55(tm2913);lin-15(n765ts)* animals.

Behavioral assays

Behavioral and capture assays were performed with young adult animals (24 hours post L4) at room temperature (22ºC) unless otherwise noted. Different genotypes were scored in parallel. Statistical analyses were conducted using the Student's t-test. Velocity, amplitude, wavelength assays were conducted on NGM plates without food using worm tracking software (Feng, et al., 2004). For exploration assays, animals were transferred to NGM plates without food for 30 minutes prior to assay. Animals were then mouth-pipetted to a new NGM plate without food and video recorded for ten minutes. Movement and distance travelled of individual animals was manually tracked from pixel coordinates of the recording. Nose touch, anterior touch (behind the posterior pharyngeal bulb), posterior touch (tail) and touch sensitivity assays were conducted using a fine hair attached to a glass pipet. The presence or absence of head movements were scored during the escape response. Brood size was determined by counting the total progeny yielded from individual animals

The body diameter of the different developmental stages and genotype comparisons was measured directly behind the posterior pharyngeal bulb. Body length was measured from the tip of the nose to the tip of the tail. Relative trap positions along the anterior-posterior axis of L2 larvae were determined by measuring the distance from the tip of the nose to the center of the constricting ring divided by the total length of the animal. To compare the capture rates of different developmental stages animals were transferred to fungal plates. After 4

hours at room temperature, the plates were placed at 4°C to stop the movement of the animals.

To analyze how animals crawl through a small opening a small strip of nylon mesh with 37 μm openings was inserted perpendicular into an NGM plate seeded with a thin lawn of OP50. The size of the nylon mesh strip contained approximately 4 x 200 openings. Approximately 100 animals were transferred to the nylon mesh plate and video recorded for 2 hours. The time spent in mesh was measured as the time between the first insertion of the animal's nose to the time when the animal completely extricated itself from the mesh. Animals that did not enter the mesh at a perpendicular angle, or that the entered the mesh but crawled into the agar were not scored.

Fungal Assays

Constricting-ring fungi form traps on low nutrient plates in the presence of nematodes. For predation assays *D. doedycoides* fungi from malt extract plates were sub-cultured on 2% water agar plates and grown for approximately 2 weeks until hyphal mats completely covered the agar surface. Fungal plates were inoculated with 10 to 20 sterile adult *glp-4(bn2)* mutant animals to induce trap formation. *glp-4(bn2)* mutants were removed from the plates after two days when the trap density on the plates was approximately 40 constricting rings per mm^2. To compare the capture rates of different developmental stages, staged animals were transferred to fungal plates with constricting rings. After 4 hours the number

of caught and uncaught animals was counted. The diameter of uninflated rings, nematode diameter, and relative trap position were measured from still images. using ImageJ from images taken through a dissection microscope. Trap diameter of constricting rings was measured from the inner diameter of non-inflated ring cells.

To score the outcome of individual trap encounters for different genotypes, animals were transferred to fungal plates and video recorded for 3 hours. An encounter with a trap was defined as any time a worm entered a trap with the anterior portion of its body. Each encounter was scored as either a capture or an escape. In encounters that resulted in a capture, the latency from the time from trap entry until trap closure was measured. An exit from a constricting ring by reversing qualified as an escape.

For competition assays L1 arrested animals were incubated on NGM plates with OP50 at room temperature. After 16 hours L2 larvae were then collected in M9 buffer and washed twice to remove residual bacteria. Genotypes were mixed in a 1:1 volume ratio. Approximately 200-600 animals of the mixed population were transferred to three control NGM plates with OP50 and the fraction of GFP positive and GFP negative animals was determined. Approximately 1000-2000 animals of the mixed L2 population were transferred in 50 µl M9 buffer onto *D. doedycoides* plates at room temperature. After 90 minutes, the fungal plates were gently washed twice with M9 buffer to remove all non-captured animals. In general, 200 to 800 animals were caught in the traps.

GFP positive and GFP negative animals were then counted under a fluorescence-dissecting microscope. *lgc-55::*GFP and *ceh-22::*GFP transgenes were used as fluorescence markers. The number of captured animals of each genotype was corrected for the fraction of each genotype on the control NGM plates without fungi (# caught genotype X) / (0.5 / control fraction of genotype X). The capture index is the weighted caught fraction of the test genotype minus the weighted caught fraction of the GFP marked wild-type strain. A capture index of zero indicated that both genotypes were captures at an equal rate. A positive capture index indicated that the test genotype was captured more than the wild type.

Scanning Electron Microscopy

Agar plates with *D. doedycoides* were inoculated for 2 hours with L2 larvae until a large number of animals were caught. Plates were gently rinsed with water to remove uncaught larvae. Plates with freshly caught larvae were fixed in 2.5% glutaraldehyde, 2% paraformaldehyde, 0.1 M sucrose overnight at 4˚C. Plates were rinsed with PBS and post fixed with 2% osmium tetroxide in 0.15 M cacodylate buffer at 4˚C for 1 hour. Fixed agar plugs of 1.5 cm in diameter were super-glued to circular round cover slips and dehydrated in a graded ethanol series (15%, 30%, 75% and 95%) for 15 minutes in each and then two changes of 100% ethanol for one hour each. Samples were submerged at 30˚C in a 50:50 ethanol/PelDri II (PELCO INTERNATIONAL) mixture for 1

hour and then transferred to 100% PelDri II for an additional hour. Samples were then flipped right-side up and removed from the hot plate. The samples were left at room temperature until the PelDri II had solidified. Samples were placed in a vacuum dessicator overnight to sublimate the PelDri II. Samples were sputter coated with a gold/palladium mixture and viewed with a FEI Quanta 200 FEG-MKII field-emission scanning electron microscope.

Acknowledgements

We thank the *Caenorhabditis* Genetic Center for nematode strains, the Agricultural Research Service collection of Entomopathogenic Fungi and the ATCC for fungal strains, Matthew Smith for advice, Claire Bénard , Vivian Budnik and Hans A. Hofmann for critically reading the manuscript. This work was supported by NIH grant GM084491.

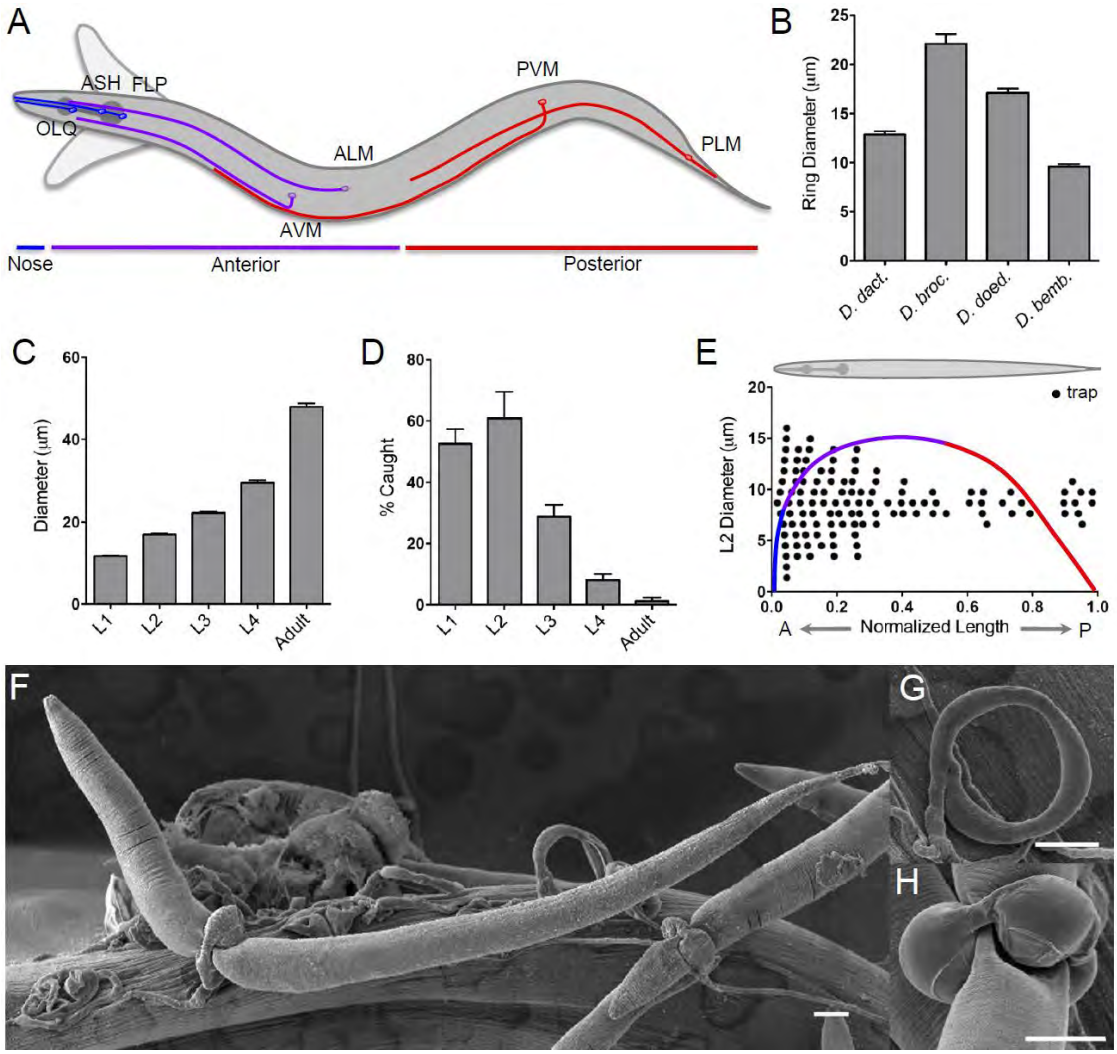

Figure AI-1. Constricting fungal rings entrap *C. elegans* larvae.

(A) *C. elegans* makes exploratory head movements during locomotion (Croll, 1975; Alkema, et al., 2005). Extent of head movements is outlined. In response to light anterior touch, the animal reverses and suppresses head movements (Figure AI-2). Nose touch induces a reversal but head movements are suppressed less efficiently. Posterior touch leads to the acceleration of forward locomotion but not the suppression of head movements. Cell bodies and

neuronal processes of neurons involved in nose touch (blue: ASH, FLP and OLQ) (Kaplan and Horvitz, 1993), anterior touch (purple: ALM and AVM) and posterior touch (red: PLM and PVM) (Chalfie and Sulston, 1981). (B) Inner diameter of uninflated constricting rings. *D. dactyloides*, 12.9 +/- 0.3 μm (n=51); *D. brochopaga*, 22.1 +/- 1.0 μm (n=25); *D. doedycoides*, 17.1 +/- 0.4 μm (n=27); *D. bembicoides*, 9.6 +/- 0.3 μm (n=20). (C) Average diameter of L1: 11.7 +/- 0.2 μm (n=55); L2: 17.0 +/- 0.2 μm (n=49); L3: 22.2 +/- 0.3 μm (n=92); L4: 29.6 +/- 0.6 μm (n=16); Adult: 47.9 +/- 0.8 μm (n=33). (D) Average percentage of worms caught after four hours: L1: 53 +/- 5 % (n=165); L2: 61 +/- 9% (n=1533); L3: 29 +/- 4% (n=1893); L4: 8 +/- 2% (n=499); Adult, 1 +/- 1% (n=461). Error bars represent standard error of the mean (SEM). (E) *C. elegans* is tapered on both ends. Colored line represents the diameter of an L2 larvae along the anterior-posterior (A-P) axis. Color of the line corresponds to nose (blue), anterior (purple) and posterior (red) regions of the body. Dots represent distance along the A-P axis where the animal is caught by a constricting ring (n=117). L2 larvae are mostly caught at the anterior end (See Movie AI-1). (F-H) Scanning Electron micrographs: (F) L2 larvae caught in constricting rings of *D. doedycoides*. (G) A constricting ring prior to inflation. (H) Expanded ring cells of the trap impinging on the cuticle of the worm. Scale bar is 10 μm.

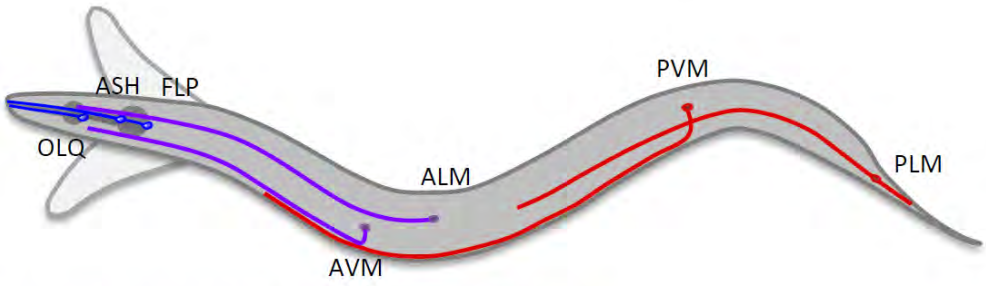

% suppressing head oscillations in response to touch

	Nose	Anterior	Posterior
L2 larvae	48 ± 3%	97 ± 1%	1 ± 1%
Adult	37 ± 1%	91 ± 3%	1 ± 1%

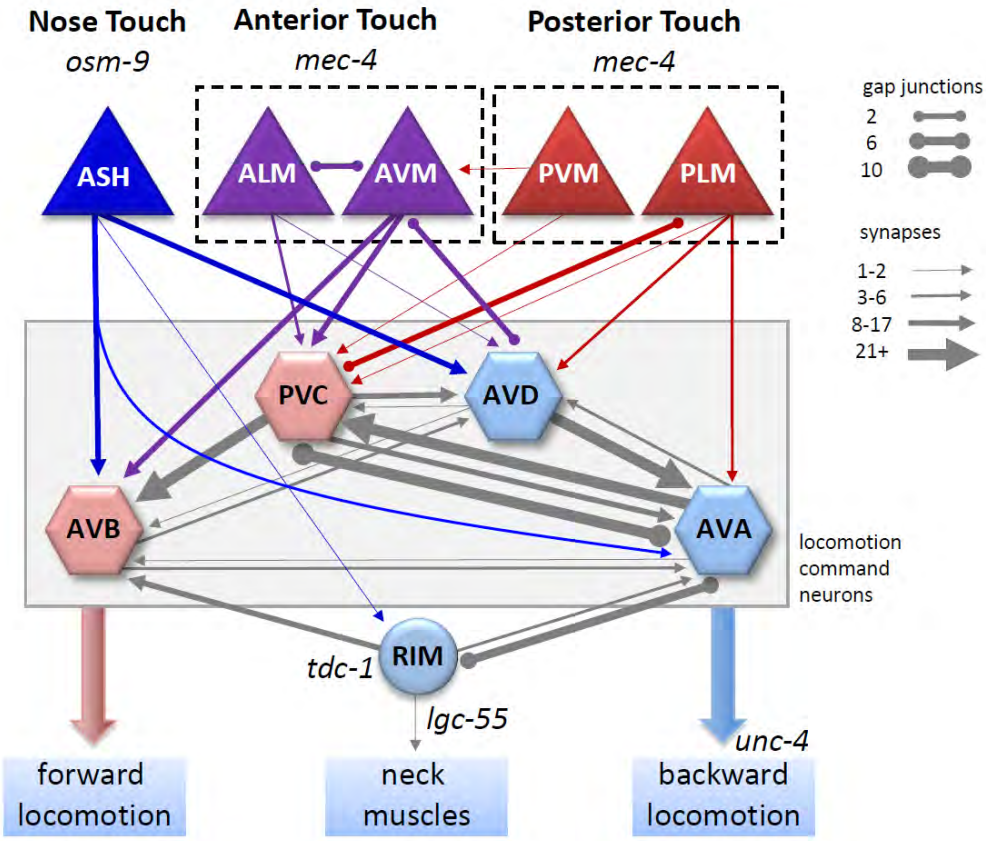

Figure AI-2. Touch induces an escape response where *C. elegans* moves away from the stimulus.

(A) Cell bodies and neuronal processes of neurons involved in nose touch (blue: ASH, FLP and OLQ), anterior touch (purple: ALM and AVM) and posterior touch (red: PLM and PVM) are indicated. Animals were gently touched on the nose, the anterior portion of the body or the posterior portion of the body. Adults and L2 larvae were scored and the percentage ± SEM of animals that suppressed head movements in response to touch is indicated. The suppression of head movements was scored during the escape response. In response to light anterior touch, the *C. elegans* reverses and suppresses head movements (adult: 97 +/- 1%, n=120; L2: 91 +/- 3%, n=120). Nose touch induces a reversal but head movements are suppressed less efficiently (adult: 37 +/- 1%, n=120; L2: 48 +/- 3%, n=120). Posterior touch leads to the acceleration of forward locomotion but not the suppression of head movements (adult: 1 +/- 1%, n=120; L2: 1 +/- 1%, n=120). (B) Diagram of the *C.elegans* mechanosensory circuits that control locomotion. Synaptic connections (arrows) and gap junctions (circles) are weighed according to the number of connections made to each neuron as described by White, et al (1986). Sensory neurons are shown as triangles, locomotion command neurons, are shown as hexagons and motor neurons are depicted as circles. FLP and OLQ were omitted for clarity. Backward locomotion is correlated with the activation of the AVA backward command neuron (Chronis, et al., 2007; Ben Arous, et al., 2010). The AVA activates the RIM through gap

junctions, which triggers tyramine release (Guo, et al., 2009). In general nose touch induces shorter reversals and head movements are less efficiently suppressed than in response anterior touch. This suggests that the RIM is not sufficiently activated to trigger tyramine release in response to nose touch. *mec-4* encodes a DEG/ENaC channel required for mechanosensation in the ALM, AVM, PLM and PVM touch sensory neurons; *osm-9* encodes a TRP-like channel required for nose touch sensation in the ASH; *unc-4* encodes a homeo-domain protein required for specifying the A motorneurons and thus required for backward locomotion; *tdc-1* encodes a tyrosine decarboxylase required for tyramine synthesis in the RIM motorneurons; *lgc-55* encodes a tyramine gated chloride channel that acts in the AVB neurons to inhibit forward locomotion and the neck muscles (and RMD and SMD neurons) to inhibit exploratory head movements.

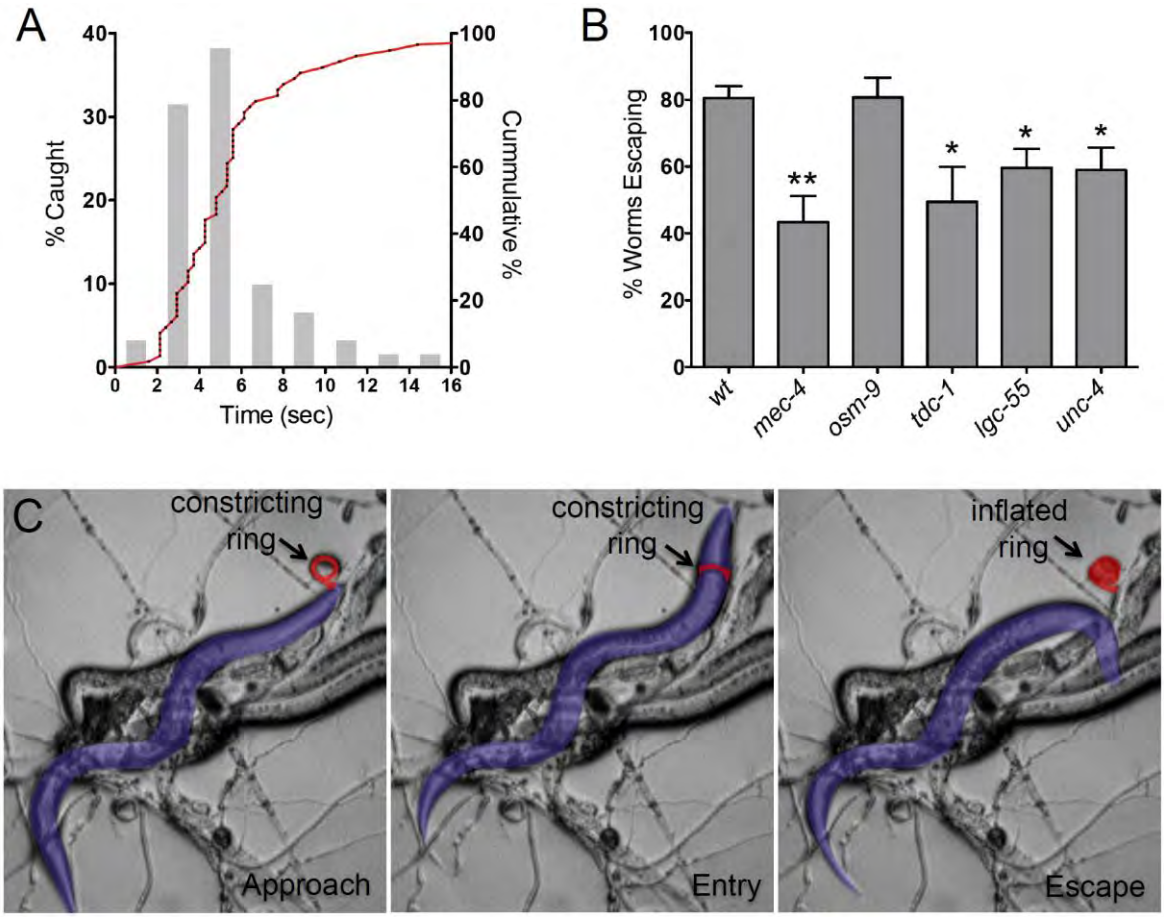

Figure AI-3. *C. elegans* can escape from constricting rings.

(A) Lag time between an animal entering a ring and ring closure of *D. doedycoides*. The average latency time of trap closure in successful capture events was 5.8 ± 0.5 s (n=59). Left: Bar diagram shows the percentage of trap closure events in 2 seconds binned intervals. Right: red line shows the cumulative percentage of ring closures. (B) The percentage of L2 larvae that entered and escaped the trap by reversing. Wild type (N2): 81 ± 4% (n=170); *mec-4(e1339)*: 43 ± 8% (n=87), p= 0.0050; *osm-9(n1603)*: 81 +/- 6 %, (n=112) n.s. p= 0.9804; *tdc-1(n3420):* 49 ± 10% (n=94), p=0.0482; *lgc-55(tm2913)*: 60 ±

6% (n=125), p=0.0213; *unc-4(e120)*: 59 +/- 7% (n=126) p=0.0289. Error bars represent SEM. Statistical difference from wild type; ** p-value < 0.005; * p-value < 0.05, two-tailed Student's t-test. (C) Still images of an L2 animal entering and escaping from a constricting ring (See Movie AI-2). After the animal wedged itself in the ring (entry) the animal reversed and suppressed head movements allowing it to exit the ring just before the ring cells inflate (escape).

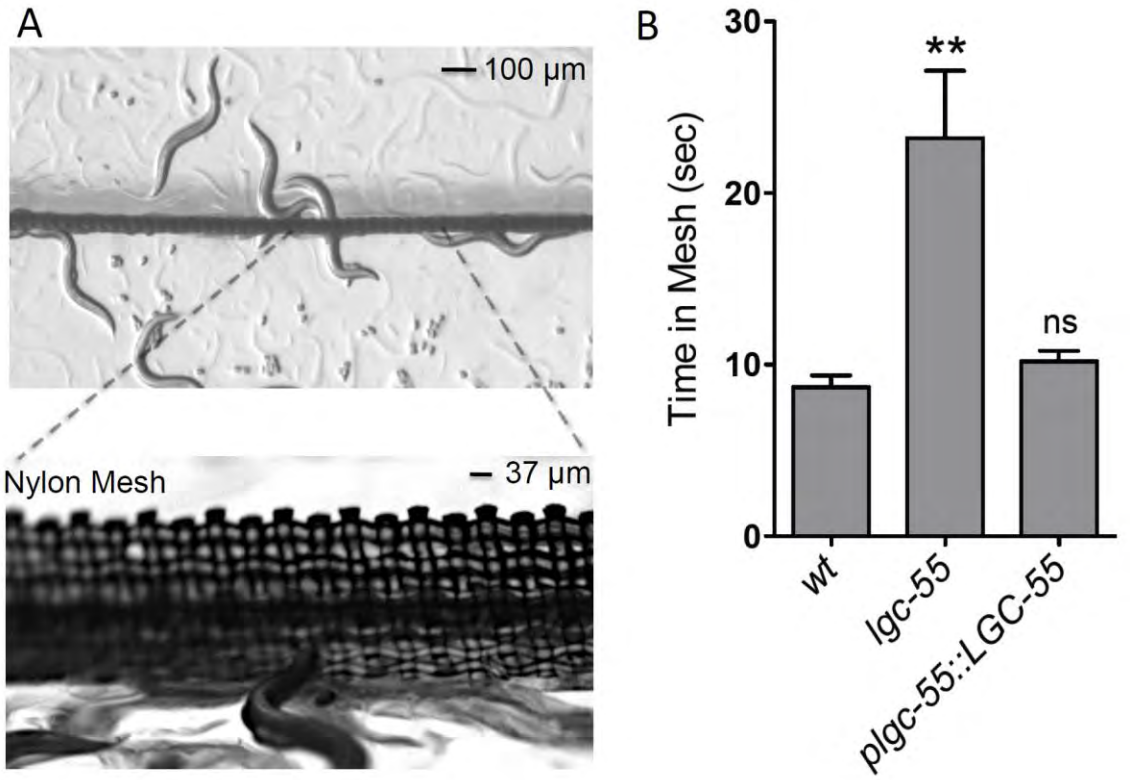

Figure AI-4. Tyramine signaling facilitates extraction from a noose.

(A) Young adult animals moving through a nylon mesh. Animals make contact with the threads of the mesh when they pass through the 37 µm openings. (B) The time animals spent in a 37 µm opening of a nylon mesh before exiting: Wild type (N2): 9 +/- 1 s (n=156), *lgc-55(tm2913)*: 23 +/- 4 s (n=274), p=0.0059; P*lgc-55*::LGC-55: 10 +/- 1 s (n=418), p=0.1675. Error bars represent SEM. Statistical difference from wild type; ** p-value < 0.005; * p-value < 0.05, two-tailed Student's t-test.

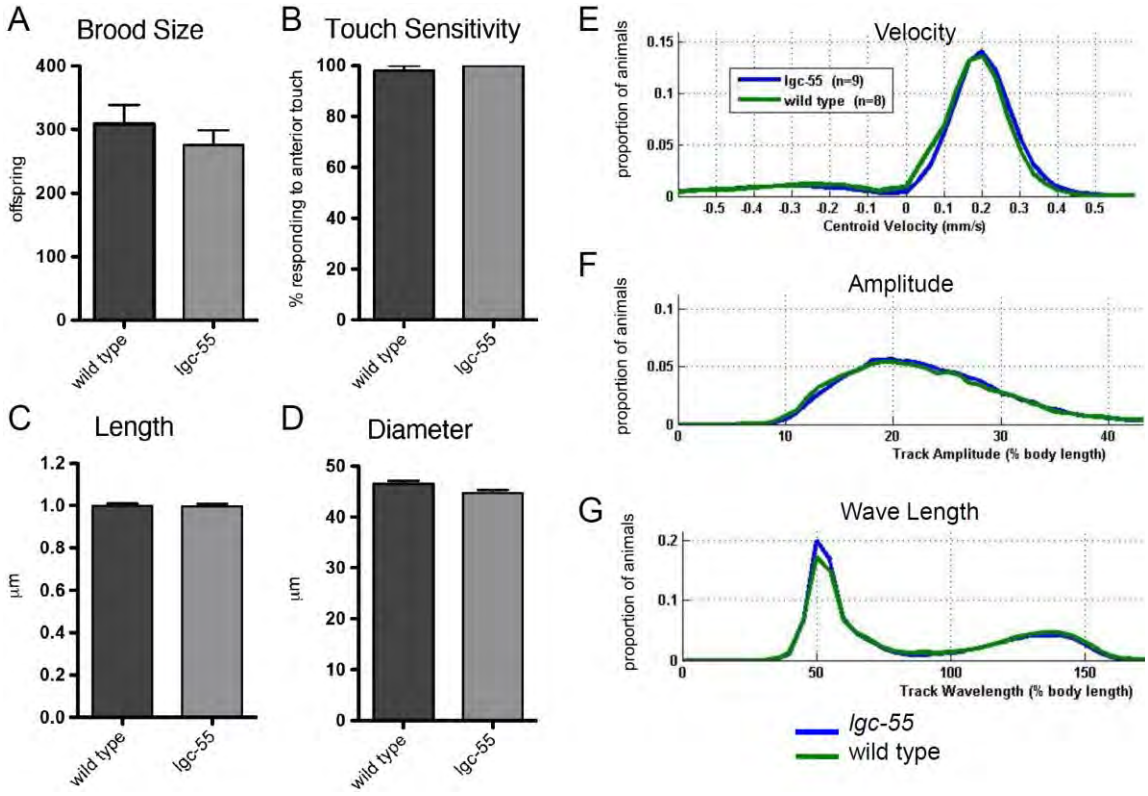

Figure AI-5. *lgc-55* mutants are indistinguishable from wild type with respect to developmental timing, overall health, size, locomotion and touch sensitivity.

Wild-type (N2) and *lgc-55(tm2913)* mutant animals are not different in the body parameters that may influence their susceptibility to capture: (A) brood size N2 309 ± 30 offspring (n=50); *lgc-55(tm2913)* 276 ± 23 offspring (n=50), (B) touch sensitivity to anterior touch N2, 98 ± 2% responding (n=100); *lgc-55(tm2913)*, 100 ± 0% responding (n=100). (C) length of young adults N2, 0.998 ± 0.01 mm (n=42); *lgc-55(tm2913)*, 0.997 ± 0.01 mm (n=43) and (D) diameter N2, 46.5 ± 0.6 mm (n=19); *lgc-55(tm2913)*, 44.7 ± 0.6 mm (n=19). Error bars represent SEM. Wild-type (N2) (n=8) and *lgc-55(tm2913)* (n=9) mutant animals do not have

different locomotion patterns in the following parameters: (E) velocity off of food, (F) amplitude of sinusoidal waves during locomotion, and (G) wavelength of sinusoidal locomotion. Locomotion parameters were quantified using worm tracking software (Feng, et al., 2004).

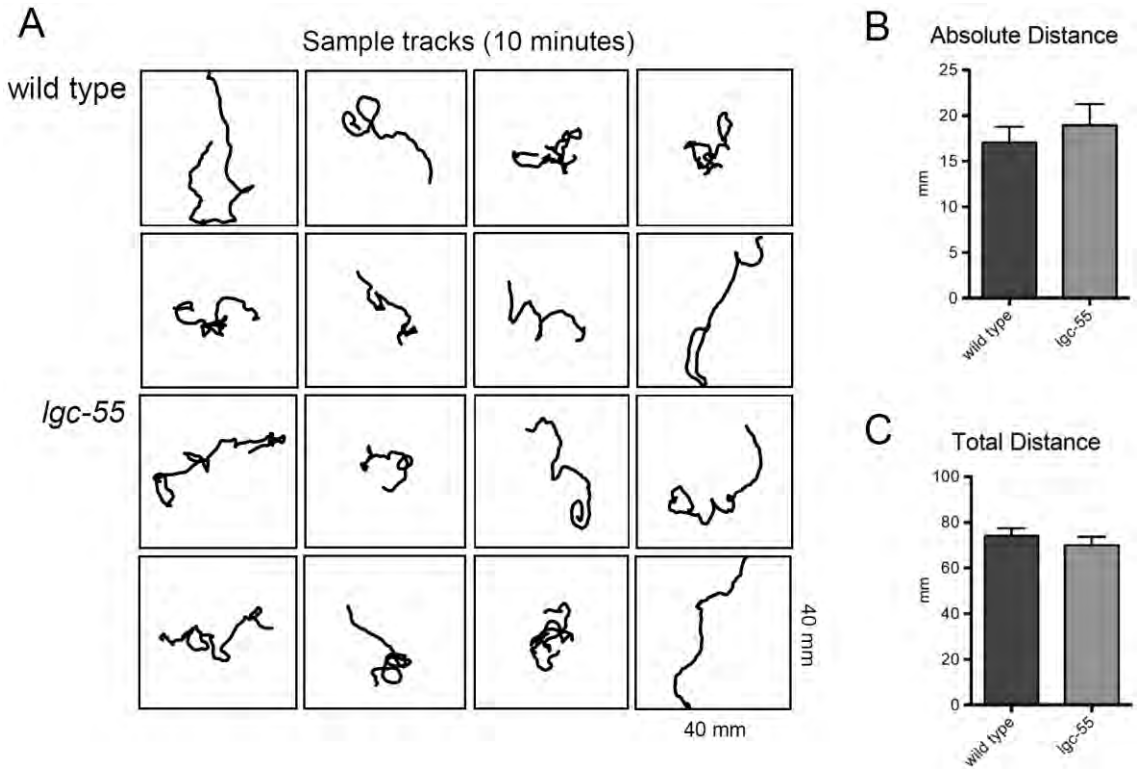

Figure AI-6. *lgc-55* mutants have no defects in exploratory behavior.

(A) Eight representative ten minute tracks of wild type (N2) and *lgc-55* mutant animals (no food). (B) Absolute distance traveled away from starting position. N2 traveled 17 ± 2 mm (n=21) and *lgc-55(tm2913)* traveled 19 ± 2 mm (n=20) away from their origin. (C) N2 traveled a total of 74 ± 3 mm (n=21) and *lgc-55(tm2913)* traveled 70 ± 4 mm (n=20) in ten minutes. Error bars represent SEM.

A

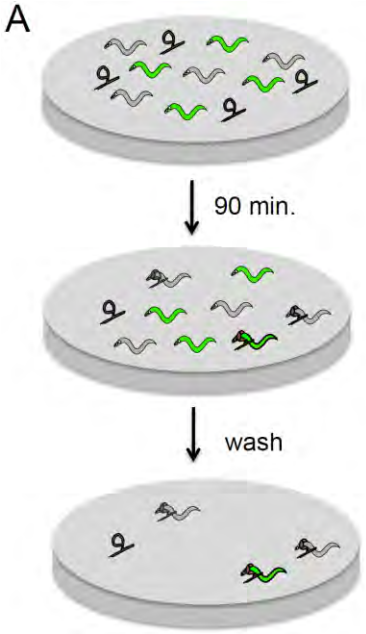

B

Genotypes	% Captured	Total # captured	n (assays)
N2 vs *lgc-55*::GFP	50.4/49.6 ± 0.9 % n.s. p=0.538	5110	14
lgc-55(tm2913); *lgc-55*::GFP vs N2	56.5/43.5 ± 0.9% p<0.0001	13655	16
lgc-55(tm2913) vs *lgc-55*::GFP	68.1/31.9 ± 1.0% p<0.0001	10528	17
lgc-55; lgc-55::LGC-55 rescue vs *lgc-55*::GFP	51.1/48.9 ± 1.2% n.s. p=0.204	8003	12
lgc-55; myo-3::LGC-55 rescue vs *lgc-55*::GFP	55.9/44.1 ± 1.2 p<0.0001	12617	17

Figure AI-7. Fungal competition assay.

(A) Two populations of L2 larvae animals were mixed in an approximate 1:1 ratio by volume. The two mixed genotypes consisted of wild type animals with mutant or transgenic animals, one of which expressed a GFP reporter. The L2 larvae were placed on a fungal lawn with a large number of traps and allowed to explore the plate for 90 minutes. The plates were then gently washed with M9 buffer to remove all non-captured animals. The captured animals that remained on the plate were counted and the two genotypes were discriminated by GFP. The captured animals for each genotype were compared to the total captured to calculate a capture index. (B) Percentage of animals captured in the competition assay was corrected for the fraction of genotypes on control plates with no fungus.. Error represents SEM. p-values were calculated by two tailed Student's t-test.

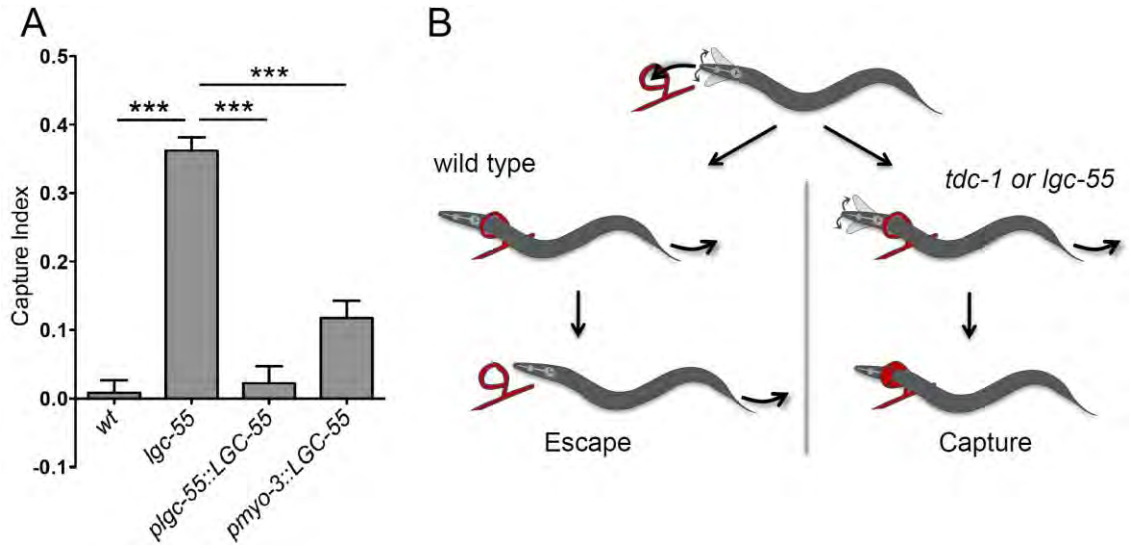

Figure AI-8. Touch induced suppression of head movements facilitates escape form fungal constricting rings.

(A) Animals that fail to suppress head movements are caught more often than the wild type in competition experiments. Genotypes were mixed in a 1:1 ratio and the caught fraction of each genotype was determined. Fluorescent reporters were used to mark the different genotypes. The capture index was calculated by subtracting the weighted fractions of the caught testing genotype from that of the control. A capture index of 0 represents an equal distribution of animals caught between the testing genotype and the wild type. A positive capture index indicates a selective disadvantage compared to the wild type. Wild type (N2): -0.01+/-0.02 (n=14); *lgc-55(tm2913)*: 0.36 +/- 0.02 (n=17); *lgc-55;* P*lgc-55*::LGC-55 rescue: 0.02 +/- 0.02 (n=12); *lgc-55;* P*myo-3*::LGC-55 rescue: 0.12 +/- 0.02 (n=17). Error bars represent SEM. Statistical difference as noted; *** p-value < 0.0001, two-tailed Student's t-test. (See also Figure AI-6) (B) *C. elegans*

locomotion is accompanied by exploratory head movements. When an animal wedges itself into a constricting ring activation of the anterior touch sensory neurons induces an escape response. Wild-type animals reverse and suppress exploratory head movements allowing a smooth exit from the constricting ring. Tyramine-signaling mutants *tdc-1(n3420)* and *lgc-55(tm2913)* reverse but fail to suppress head movements during an escape making it more likely for the animal to activate the ring cells and get caught.

Movie AI-1.

C. elegans L2 larvae getting caught by a constricting ring of *D. doedycoides.* There is a delay between the initial entry of the worm and the time the constricting ring inflates.

Movie AI-2.

C. elegans L2 larvae entering and escaping from a constricting ring of *D. doedycoides* (Figure AI-3C). The animal moves into the ring; reverses and suppresses head movements allowing it to back out of the ring before the ring cells inflate (escape)

APPENDIX II: ADDITIONAL PUBLICATIONS

While building the body of work that comprises this dissertation, I made contributions to the following published works:

Bhattacharya R, Touroutine D, Climer J, Barbagallo B, Lambert CM, **Clark CM**, Alkema MJ, Francis MM (2014) A conserved dopamine-cholecystokinin signaling pathway shapes context-dependent *C. elegans* behavior. PLoS Genetics 10: e1004584.

- I performed *C. elegans* laser ablation surgeries for this study

Das G, Vrontou E, Perisse E, **Clark CM**, Burke CJ, Waddell S (2014) Learning with discrete aversive signals uses common reinforcing dopaminergic neurons in *Drosophila.* Current Biology 24: 1723-1730.

- I performed preliminary *Drosophila* behavior experiments for this study.

Shipley FB, **Clark CM**, Alkema MJ, Leifer AM (2014) Simultaneous optogenetic manipulation and calcium imaging in freely moving *C. elegans*. Frontiers in Neural Circuits 8(28).

- I generated optogenetic reagents used in this study. I also helped design and perform preliminary experiments for this study.

Sun L, Shay J, McLeod M, Roodhouse K, Chung S, **Clark C**, Pirri J, Alkema M, Gabel (2014) C. Neuronal regeneration in *C. elegans* requires sub-cellular calcium release by ryanodine receptor channels and can be enhanced by optogenetic stimulation. J Neurosci (*in press*).

- I generated optogenetic reagents used in this study.

APPENDIX III: GLOSSARY OF C. ELEGANS GENES

acr-2	Nicotinic ACh receptor alpha subunit
acr-16	Nicotinic ACh receptor non-alpha subunit
avr-14	Glutamate-gated chloride channel subunit
cex-1	Calcium binding GTPase
ceh-22	Homeodomain factor
dgk-1	Diacylglycerol kinase theta
eat-16	RGS protein
egl-30	G-protein $G_q\alpha$ subunit
flp-13	FMRF-amide-like neuropeptide
flp-18	FMRF-amide-like neuropeptide
glp-4	Germ-line proliferation factor
goa-1	G-protein $G_o\alpha$ subunit
glr-1	AMPA glutamate receptor subunit
inx-1	Gap junction innexin
lgc-55	Tyramine-gated chloride channel
lite-1	Gustatory-family light receptor
lim-4	LIM homeodomain protein
lin-15	Developmental factor with zinc finger-like motif
mec-4	Mechanotransduction sodium channel subunit
myo-3	Myosin heavy chain A
nmr-1	NMDA glutamate receptor subunit
npr-9	Neuropeptide receptor
osm-9	TRPV channel
rig-3	Immunoglobulin super family protein
ser-2	Tyramine GPCR
tdc-1	Tyramine biosynthetic enzyme, tyrosine decarboxylase
tbh-1	Octopamine biosynthetic enzyme, tyramine beta-hydroxylase

tyra-2	Tyramine GPCR
tyra-3	Tyramine GPCR
unc-3	Transcription factor containing immunoglobulin domain
unc-4	Homeodomain protein
unc-17	ACh vesicle transporter
unc-25	GABA biosynthetic enzyme, glutamic acid decarboxylase
unc-29	Nicotinic ACh receptor non-alpha subunit
unc-47	GABA vesicle transporter
unc-122	Collagen-like extracellular protein

BIBLIOGRAPHY

Adamo SA, Linn CE, Hoy RR (1995) The role of neurohormonal octopamine during 'fight or flight' behaviour in the field cricket *Gryllus bimaculatus*. J Exp Biol 198: 1691-1700.

Alfonso A, Grundahl K, Duerr JS, Han HP, Rand JB (1993) The *Caenorhabditis elegans unc-17* gene: a putative vesicular acetylcholine transporter. Science 261: 617-619.

Alkema MJ, Hunter-Ensor M, Ringstad N, Horvitz HR (2005) Tyramine functions independently of octopamine in the *Caenorhabditis elegans* nervous system. Neuron 46: 247-260.

Allen MJ, Godenschwege TA, Tanouye MA, Phelan P (2006) Making an escape: development and function of the *Drosophila* giant fibre system. Semin Cell Dev Biol 17: 31-41.

Altun ZF, Chen B, Wang ZW, Hall DH (2009) High resolution map of *Caenorhabditis elegans* gap junction proteins. Dev Dyn 238: 1936-1950.

Baier A, Wittek B, Brembs B (2002) *Drosophila* as a new model organism for the neurobiology of aggression? J Exp Biol 205: 1233-1240.

Barbosa P and Castellanos I (2005) Ecology of Predator-Prey Interactions, (Oxford, NY: Oxford University Press).

Bargmann CI and Avery L (1995) Laser killing of cells in *Caenorhabditis elegans.* Meth Cell Biol 48: 225–250.

Bargmann CI (2012) Beyond the connectome: How neuromodulators shape neural circuits. Bioessays 34(6): 458-465.

Ben Arous J, Tanizawa Y, Rabinowitch I, Chatenay D, Schafer WR (2010) Automated imaging of neuronal activity in freely behaving *Caenorhabditis elegans*. J Neurosci Meth 187: 229-234.

Bendesky A, Tsunozaki M, Rockman MV, Kruglyak L, Bargmann CI (2011) Catecholamine receptor polymorphisms affect decision-making in *C. elegans*. Nature 472: 313-318.

Bhattacharya R, Touroutine D, Climer J, Barbagallo B, Lambert CM, Clark CM, Alkema MJ, Francis MM (2014) A conserved dopamine-cholecystokinin signaling

pathway shapes context-dependent *C. elegans* behavior. PLoS Genet 10: e1004584.

Bicker G, Menzel R (1989) Chemical codes for the control of behaviour in arthropods. Nature 337: 33-39.

Bieszke JA, Braun EL, Bean LE, Kang S, Natvig DO, Borkovich KA (1996) The *nop-1* gene of *Neurospora crassa* encodes a seven transmembrane helix retinal-binding protein homologous to archaeal rhodopsins. Proc Natl Acad Sci USA 96: 8034-8039.

Brede M, Philipp M, Knaus A, Muthig V, Hein L (2004) alpha2-adrenergic receptor subtypes - novel functions uncovered in gene-targeted mouse models. Biol Cell 96: 343-348.

Brenner S (1974) The genetics of *Caenorhabditis elegans*. Genetics 77: 71-94.

Brundage L, Avery L, Katz A, Kim UJ, Mendel JE, Sternberg PW, Simon MI (1996) Mutations in a *C. elegans* Gqalpha gene disrupt movement, egg laying, and viability. Neuron 16: 999-1009.

Burrell BD, Smith BH (1995) Modulation of the honey bee (*Apis mellifera*) sting response by octopamine. J Insect Phys 41: 671-680.

Card D and Dickinson M (2008) Performance trade-offs in the flight initiation of *Drosophila*. J Exp Biol 211: 341-353.

Camhi JM (1984) Neuroethology: Nerve Cells and the Natural Behavior of Animals. (Sunderland, MA: Sinauer Associates Inc. Publishers).

Certel SJ, Savella MG, Schlegel DC, Kravitz EA (2007) Modulation of *Drosophila* male behavioral choice. Proc Natl Acad Sci USA 104: 4706-4711.

Chalasani SH, Chronis N, Tsunozaki M, Gray JM, Ramot D, Goodman MB, Bargmann CI (2007) Dissecting a circuit for olfactory behaviour in *Caenorhabditis elegans*. Nature 450: 63-70.

Chalfie M and Sulston J (1981) Developmental genetics of the mechanosensory neurons of *Caenorhabditis elegans*. Dev Biol 82: 358-370.

Chalfie M, Sulston JE, White JG, Southgate E, Thomson JN, Brenner S (1985) The neural circuit for touch sensitivity in *Caenorhabditis elegans*. J Neurosci 5: 956-964.

Chase DL, Pepper JS, Koelle MR (2004) Mechanism of extrasynaptic dopamine signaling in *Caenorhabditis elegans*. Nat Neurosci 7: 1096-1103.

Chen BL, Hall DH, Chklovskii DB (2006) Wiring optimization can relate neuronal structure and function. Proc Natl Acad Sci USA 103: 4723–4728.

Chen TW, Wardill TJ, Sun Y, Pulver SR, Renninger SL, Baohan A, Schreiter ER, Kerr RA, Orger MB, Jayaraman V, Looger LL, Svoboda K, Kim DS (2013) Ultrasensitive fluorescent proteins for imaging neuronal activity. Nature 499: 295-300.

Chronis N, Zimmer M, Bargmann CI (2007) Microfluidics for *in vivo* imaging of neuronal and behavioral activity in *Caenorhabditis elegans*. Nat Meth 4: 727-731.

Colbert HA, Smith TL, Bargmann CI (1997) OSM-9, a novel protein with structural similarity to channels, is required for olfaction, mechanosensation, and olfactory adaptation in *Caenorhabditis elegans*. J Neurosci 17: 8259-8269.

Croll NA (1975) Components and patterns in the behaviour of the nematode *Caenorhabditis elegans*. J Zoology 176: 159-176.

Das G, Vrontou E, Perisse E, Clark CM, Burke CJ, Waddell S (2014) Learning with discrete aversive signals uses common reinforcing dopaminergic neurons in *Drosophila.* Curr Biol 24: 1723-1730.

Davis MW, Morton JJ, Carroll D, Jorgensen EM (2008) Gene activation using FLP recombinase in *C. elegans*. PLoS Genet 4: e1000028.

Donnelly JL, Clark CM, Leifer AM, Pirri JK, Haburcak M, Francis MM, Samuel AD, Alkema MJ (2013) Monoaminergic orchestration of motor programs in a complex *C. elegans* behavior. PLoS Biol 11: e1001529.

Douglass AD, Kraves S, Deisseroth K, Schier AF, Engert F (2008) Escape behavior elicited by single, channelrhodopsin-2-evoked spikes in zebrafish somatosensory neurons. Curr Biol 18: 1133-1137.

Drechsler C (1937) Some hyphomycetes that prey on free-living terricolous nematodes. Mycologia 29: 447-552.

Driscoll M and Chalfie M (1991) The *mec-4* gene is a member of a family of *Caenorhabditis elegans* genes that can mutate to induce neuronal degeneration. Nature 349: 588-593.

Duddington CL (1951) The ecology of predacious fungi: I. Preliminary survey. Trans British Mycol Soc 34: 322-331.

Eastman C, Horvitz HR, Jin Y (1999) Coordinated transcriptional regulation of the *unc-25* glutamic acid decarboxylase and the *unc-47* GABA vesicular transporter by the *Caenorhabditis elegans* UNC-30 homeodomain protein. J Neurosci 19: 6225-6234.

Eaton RC (1984) Neural Mechanisms of Startle Behavior. (New York: Plenum Press).

Edwards SL, Charlie NK, Milfort MC, Brown BS, Gravlin CN, Knecht JE, Miller KG. (2008) A novel molecular solution for ultraviolet light detection in *Caenorhabditis elegans*. PLoS Biol 6: e198.

Felix MA and Braendle C (2010) The natural history of *Caenorhabditis elegans*. Curr Biol 20: R965-R969.

Feng Z, Cronin CJ, Wittig JHJ, Sternberg PW, Schafer WR (2004) An imaging system for standardized quantitative analysis of *C. elegans* behavior. BMC Bioinformatics 5: 115.

Francis MM, Evans SP, Jensen M, Madsen DM, Mancuso J, Norman KR, Maricq AV (2005) The Ror receptor tyrosine kinase CAM-1 is required for ACR-16-mediated synaptic transmission at the *C. elegans* neuromuscular junction. Neuron 46: 581-594.

Friesen WO, Poon M, Stent GS (1978) Neuronal control of swimming in the medicinal leech. IV. Identification of a network of oscillatory interneurones. J Exp Biol 75: 25-43.

Furshpan EJ and Furukawa T (1962) Intracellular and extracellular responses of several regions of the Mauthner cell of the goldfish. J. Neurophysiol 25: 732–771.

Giles AC and Rankin CH (2009) Behavioral and genetic characterization of habituation using *Caenorhabditis elegans*. Neurobiol Learning Memory 92: 139-146.

Gray NF (1987) Nematophagous fungi with particular reference to their ecology. Biol Rev 62: 245-304.

Gray JM, Hill JJ, Bargmann CI (2005) A circuit for navigation in *Caenorhabditis elegans*. Proc Natl Acad Sci USA 102: 3184-3191.

Grillner S, Jessell TM (2009) Measured motion: searching for simplicity in spinal locomotor networks. Curr Opin Neurobiol 19: 572-586.

Guo ZV, Hart AC, Ramanathan S (2009) Optical interrogation of neural circuits in *Caenorhabditis elegans*. Nat Meth 6: 891-896.

Hajdu-Cronin YM, Chen WJ, Patikoglou G, Koelle MR, Sternberg PW (1999) Antagonism between G(o)alpha and G(q)alpha in *Caenorhabditis elegans*: the RGS protein EAT-16 is necessary for G(o)alpha signaling and regulates G(q)alpha activity. Genes Dev 13: 1780-1793.

Hallam S, Singer E, Waring D, Jin Y (2000) The *C. elegans* NeuroD homolog *cnd-1* functions in multiple aspects of motor neuron fate specification. Development 127: 4239-4252.

Han X, Boyden ES (2007) Multiple-color optical activation, silencing, and desynchronization of neural activity, with single-spike temporal resolution. PLoS One 2: e299.

Hapiak V, Summers P, Ortega A, Law WJ, Stein A, Komuniecki R (2013) Neuropeptides amplify and focus the monoaminergic inhibition of nociception in *Caenorhabditis elegans*. J Neurosci 33: 14107-14116.

Harris GP, Hapiak VM, Wragg RT, Miller SB, Hughes LJ, Hobson RJ, Steven R, Bamber B, Komuniecki (2009) Three distinct amine receptors operating at different levels within the locomotory circuit are each essential for the serotonergic modulation of chemosensation in *Caenorhabditis elegans*. J Neurosci 29: 1446-1456.

Harris-Warrick RM (2011) Neuromodulation and flexibility in Central Pattern Generator networks. Curr Opin Neurobiol 21: 685-692.

Hegemann P, Fuhrmann M, Kateriya S (2001) Algal sensory photoreceptors. J. Phycol 37: 668-676.

Hendricks M, Ha H, Maffey N, Zhang Y (2012) Compartmentalized calcium dynamics in a *C. elegans* interneuron encode head movement. Nature 487: 99-103.

Higgins ML and Pramer D (1967) Fungal Morphogenesis: Ring Formation and Closure by *Arthrobotrys dactyloides*. Science 155: 345-346.

Hille B (1992) G protein-coupled mechanisms and nervous signaling. Neuron 9: 187-195.

Hochbaum DR, Zhao Y, Farhi SL, Klapoetke N, Werley CA, Kapoor V, Zou P, Kralj JM, Maclaurin D, Smedemark-Margulies N, Saulnier JL, Boulting GL, Straub C, Cho YK, Melkonian M, Wong GK, Harrison DJ, Murthy VN, Sabatini BL, Boyden ES, Campbell RE, Cohen AE (2014) All-optical electrophysiology in mammalian neurons using engineered microbial rhodopsins. Nat Meth 11: 825-833.

Horvitz HR, Chalfie M, Trent C, Sulston JE, Evans PD (1982) Serotonin and octopamine in the nematode *Caenorhabditis elegans*. Science 216: 1012-1014.

Hoyle G (1985) Generation of Behaviour: The Orchestration Hypothesis. Feedback and Motor Control in Invertebrates and Vertebrates (ed by Barnes WJP and Gladden MH, Croom Helm: London 57-75).

Huang KM, Cosman P, Schafer WR (2006) Machine vision based detection of omega bends and reversals in *C. elegans*. J Neurosci Meth 158: 323-336.

Husson SJ, Wagner SC, Schmitt C, Gottschalk A (2012) Keeping track of worm trackers. ed. The *C. elegans* Research Community, (Wormbook: http://www.wormbook.org).

Husson SJ, Gottschalk A, Leifer AM (2013) Optogenetic manipulation of neural activity in *C. elegans*: From synapse to circuits and behavior. Biol Cell 105: 235-250.

Iino Y and Yoshida K (2009) Parallel use of two behavioral mechanisms for chemotaxis in *Caenorhabditis elegans*. J Neurosci 29: 5370-5380.

Iwasaki T, Chen J, Friesen WO (2014) Biological clockwork underlying adaptive rhythmic movements. Proc Natl Acad Sci USA 111: 978-983.

Jiang G, Zhuang L, Miyauchi S, Miyake K, Fei YJ, Ganapathy V (2005) A Na+/Cl--coupled GABA transporter, GAT-1, from *Caenorhabditis elegans*: structural and functional features, specific expression in GABA-ergic neurons, and involvement in muscle function. J Biol Chem 280: 2065-2077.

Jin L, Han Z, Platisa J, Wooltorton JRA, Cohen LB, Pieribone VA (2012) Single action potentials and subthreshold electrical events imaged in neurons with a fluorescent protein voltage probe. Neuron 75: 779-785.

Jin Y, Jorgensen E, Hartwieg E, Horvitz HR (1999) The *Caenorhabditis elegans* gene *unc-25* encodes glutamic acid decarboxylase and is required for synaptic transmission but not synaptic development. J Neurosci 19: 539-548.

Jose AM, Koelle MR (2005) Domains, amino acid residues, and new isoforms of *Caenorhabditis elegans* diacylglycerol kinase 1 (DGK-1) important for terminating diacylglycerol signaling *in vivo*. J Biol Chem 280: 2730-2736.

Kaplan JM and Horvitz HR (1993) A dual mechanosensory and chemosensory neuron in *Caenorhabditis elegans*. Proc Natl Acad Sci USA 90: 2227-2231.

Katz PS (1998) Neuromodulation intrinsic to the central pattern generator for escape swimming in *Tritonia*. Ann NY Acad Sci 860: 181-188.

Kawano T, Po MD, Gao S, Leung G, Ryu WS, Zhen M (2011) An imbalancing act: gap junctions reduce the backward motor circuit activity to bias *C. elegans* for forward locomotion. Neuron 72: 572-586.

Kim K, Li C (2004) Expression and regulation of an FMRFamide-related neuropeptide gene family in *Caenorhabditis elegans*. J Comp Neurol 475: 540-550.

Kocabas A, Shen CH, Guo ZV, Ramanathan S (2012) Controlling interneuron activity in *Caenorhabditis elegans* to evoke chemotactic behavior. Nature 490: 273-277.

Korn H, Faber DS (2005) The Mauthner cell half a century later: a neurobiological model for decision-making? Neuron 47: 13-28.

Kralj JM, Hochbaum DR, Douglass AD, Cohen AE (2011) Electrical spiking in *Escherichia coli* probed with a fluorescent voltage-indicating protein. Science 333: 345-348.

Kralj JM, Douglass AD, Hochbaum DR, Maclaurin D, Cohen AE (2012) Optical recording of action potentials in mammalian neurons using a microbial rhodopsin. Nat Meth 9: 90-95.

Kravitz EA (1988) Hormonal control of behavior: amines and the biasing of behavioral output in lobsters. Science 241: 1775-1781.

Kravitz AV, Freeze BS, Parker PR, Kay K, Thwin MT, Deisseroth K, Kreitzer AC (2010) Regulation of parkinsonian motor behaviours by optogenetic control of basal ganglia circuitry. Nature 466: 622-626.

Lackner MR, Nurrish SJ, Kaplan JM (1999) Facilitation of synaptic transmission by EGL-30 Gqalpha and EGL-8 PLCbeta: DAG binding to UNC-13 is required to stimulate acetylcholine release. Neuron 24: 335-346.

Larsch J, Ventimiglia D, Bargmann CI, Albrecht DR (2013) High-throughput imaging of neuronal activity in *Caenorhabditis elegans*. Proc Natl Acad Sci USA 110: E4266-4273.

Lashley KS (1951) The problem of serial order in behavior. ed. Jeffress LA. Cerebral mechanisms in behavior: 112-146. (New York: Wiley).

Lau HL, Timbers TA, Mahmoud R, Rankin CH (2013) Genetic dissection of memory for associative and non-associative learning in *Caenorhabditis elegans*. Genes Brain Behav 12: 210-223.

Leifer AM, Fang-Yen C, Gershow M, Alkema MJ, Samuel AD (2011) Optogenetic manipulation of neural activity in freely moving *Caenorhabditis elegans*. Nat Meth 8: 147-152.

Lev-Ram V and Grindvald A (1987) Activity-dependent calcium transients in central nervous system myelinated axons revealed by the calcium indicator Fura-2. Biophys J 52: 571-576.

Li Y, Hyde KD, Jeewon R, Cai L, Vijaykrishna D, Zhang K (2005) Phylogenetics and evolution of nematode-trapping fungi (*Orbiliales*) estimated from nuclear and protein coding genes. Mycologia 97: 1034-1046.

Li C, Kim K (2008) Neuropeptides. ed. The *C. elegans* Research Community, (Wormbook: http://www.wormbook.org).

Liedtke W, Tobin DM, Bargmann CI, Friedman JM (2003) Mammalian TRPV4 (VR-OAC) directs behavioral responses to osmotic and mechanical stimuli in *Caenorhabditis elegans*. Proc Natl Acad Sci USA 100 (Suppl 2): 14531–14536.

Lima SQ, Miesenbock G (2005) Remote control of behavior through genetically targeted photostimulation of neurons. Cell 121: 141-152.

Liu P, Chen B, Altun ZF, Gross MJ, Shan A, Schuman B, Hall DH, Wang ZW (2013) Six innexins contribute to electrical coupling of *C. elegans* body-wall muscle. PLoS One 8: e76877.

Lockery SR (2011) The computational worm: spatial orientation and its neuronal basis in *C. elegans*. Curr Opin Neurobiol 21: 782-790.

Long MA, Jin DZ, Fee MS (2010) Support for a synaptic chain model of neuronal sequence generation. Nature 468: 394-399.

Looger LL, Griesbeck O (2012) Genetically encoded neural activity indicators. Curr Opin Neurobiol 22:18-23.

Lorenz K and Tinbergen N (1938) Taxis und instinkthandlung in der eirollbewegung der Graugans [Taxis and instinctive action in the egg-retrieving behavior of the Greylag goose]. Zeitschrift für Tierpsychologie 2: 1-29.

Loria PM, Duke A, Rand JB, Hobert O (2003) Two neuronal, nuclear-localized RNA binding proteins involved in synaptic transmission. Curr Biol 13: 1317-1323.

Maguire SM, Clark CM, Nunnari J, Pirri JK, Alkema MJ (2011) The *C. elegans* touch response facilitates escape from predacious fungi. Curr Biol 21: 1326-1330.

Macosko EZ, Pokala N, Feinberg EH, Chalasani SH, Butcher RA, Clardy J, Bargmann CI (2009) A hub-and-spoke circuit drives pheromone attraction and social behaviour in *C. elegans*. Nature 458:1171-1175.

Mank M, Santos AF, Direnberger S, Mrsic-Flogel TD, Hofer SB, Stein V, Hendel T, Reiff DF, Levelt C, Borst A, Bonhoeffer T, Hübener M, Griesbeck O (2008) A genetically encoded calcium indicator for chronic in vivo two-photon imaging. Nat Methods 5: 805-811.

Marder E, Bucher D (2001) Central pattern generators and the control of rhythmic movements. Curr Biol 11: R986-96.

McIntire SL, Jorgensen E, Kaplan J, Horvitz HR (1993) The GABAergic nervous system of *Caenorhabditis elegans*. Nature 364: 337-341.

Mendel JE, Korswagen HC, Liu KS, Hajdu-Cronin YM, Simon MI, Plasterk RH, Sternberg PW (1995) Participation of the protein Go in multiple aspects of behavior in *C. elegans*. Science 267: 1652-1655.

Miller KG, Emerson MD, Rand JB (1999) Goalpha and diacylglycerol kinase negatively regulate the Gqalpha pathway in *C. elegans*. Neuron 24: 323-333.

Miyawaki A, Llopis J, Heim R, McCaffery JM, Adams JA, Ikura M, Tsien RY (1997) Fluorescent indicators for Ca2+ based on green fluorescent proteins and calmodulin. Nature 388: 882-887.

Murata Y, Iwasaki H, Sasaki M, Inaba K, Okamura Y (2005) Phosphoinositide phosphatase activity coupled to an intrinsic voltage sensor. Nature 435: 1239-1243.

Nagel G, Szellas T, Huhn W, Kateriya S, Adeishvili N, Berthold P, Ollig D, Hegemann P, Bamberg E (2003) Channelrhodopsin-2, a directly light-gated cation-selective membrane channel. Proc Natl Acad Sci USA 100: 13940-13945.

Nagel G, Brauner M, Liewald JF, Adeishvili N, Bamberg E, Gottschalk A (2005) Light activation of channelrhodopsin-2 in excitable cells of *Caenorhabditis elegans* triggers rapid behavioral responses. Curr Biol 15: 2279-2284.

Nakai J, Ohkura M, Imoto K (2001) A high signal-to-noise Ca(2+) probe composed of a single green fluorescent protein. Nat Biotechnol 19: 137-141.

Nonet ML, Grundahl K, Meyer BJ, Rand JB (1993) Synaptic function is impaired but not eliminated in *C. elegans* mutants lacking synaptotagmin. Cell 73: 1291-1305.

Nurrish S, Segalat L, Kaplan JM (1999) Serotonin inhibition of synaptic transmission: Galpha(0) decreases the abundance of UNC-13 at release sites. Neuron 24: 231-242.

O'Hagan R, Chalfie M, Goodman MB (2005) The MEC-4 DEG/ENaC channel of *Caenorhabditis elegans* touch receptor neurons transduces mechanical signals. Nat Neurosci 8: 43-50.

Oheim M, van 't Hoff M, Feltz A, Zamaleeva A, Mallet JM, Collot M (2014) New red-fluorescent calcium indicators for optogenetics, photoactivation and multi-color imaging. Biochim Biophys Acta. 1843: 2284-306.

Okazaki A, Sudo Y, Takagi S (2012) Optical silencing of *C. elegans* cells with arch proton pump. PLoS One 7: e35370.

Palmer AE, Giacomello M, Kortemme T, Hires SA, Lev-Ram V, Baker D, Tsien RY (2006) Ca2+ indicators based on computationally redesigned calmodulin-peptide pairs. Chem Biol 13: 521-530.

Pfluger HJ (1999) Neuromodulation during motor development and behavior. Curr Opin Neurobiol 9: 683-689.

Pierce-Shimomura JT, Morse TM, Lockery SR (1999) The fundamental role of pirouettes in *Caenorhabditis elegans* chemotaxis. J Neurosci 19: 9557-9569.

Piggott BJ, Liu J, Feng Z, Wescott SA, Xu XZ (2011) The neural circuits and synaptic mechanisms underlying motor initiation in *C. elegans*. Cell 147: 922-933.

Pirri JK, McPherson AD, Donnelly JL, Francis MM, Alkema MJ (2009) A tyramine-gated chloride channel coordinates distinct motor programs of a *Caenorhabditis elegans* escape response. Neuron 62: 526-538.

Pirri JK, Alkema MJ (2012) The neuroethology of *C. elegans* escape. Curr Opin Neurobiol 22: 187-193.

Pirri J, Rayes D, Alkema MJ (submitted 2014) A change in the ion selectivity of ligand gated ion channels provides a mechanism to switch behavior.

Prasad BC, Ye B, Zackhary R, Schrader K, Seydoux G, Reed RR (1998) *unc-3*, a gene required for axonal guidance in *Caenorhabditis elegans*, encodes a member of the O/E family of transcription factors. Development 125: 1561-1568.

Proctor J, Holmes P (2010) Reflexes and preflexes: on the role of sensory feedback on rhythmic patterns in insect locomotion. Biol Cybern 102: 513-531.

Ramot D, Johnson BE, Berry TLJ, Carnell L, Goodman MB (2008) The Parallel Worm Tracker: a platform for measuring average speed and drug-induced paralysis in nematodes. PLoS One 3: e2208.

Rex E, Komuniecki RW (2002) Characterization of a tyramine receptor from *Caenorhabditis elegans*. J Neurochem 82: 1352-1359.

Rex E, Molitor SC, Hapiak V, Xiao H, Henderson M, Komuniecki R (2004) Tyramine receptor (SER-2) isoforms are involved in the regulation of pharyngeal pumping and foraging behavior in *Caenorhabditis elegans*. J Neurochem 91: 1104-1115.

Rex E, Hapiak V, Hobson R, Smith K, Xiao H, Komuniecki R (2005) TYRA-2 (F01E11.5): a *Caenorhabditis elegans* tyramine receptor expressed in the MC and NSM pharyngeal neurons. J Neurochem 94: 181-191.

Richmond JE, Jorgensen EM (1999) One GABA and two acetylcholine receptors function at the *C. elegans* neuromuscular junction. Nat Neurosci 2: 791-797.

Ringstad N, Abe N, Horvitz HR (2009) Ligand-gated chloride channels are receptors for biogenic amines in *C. elegans*. Science 325: 96-100.

Roeder T (2005) Tyramine and octopamine: ruling behavior and metabolism. Ann Rev Entomol 50: 447-477.

Sagasti A, Hobert O, Troemel ER, Ruvkun G, Bargmann CI (1999) Alternative olfactory neuron fates are specified by the LIM homeobox gene *lim-4*. Genes Dev 13: 1794-1806.

Schafer WR, Kenyon CJ (1995) A calcium-channel homologue required for adaptation to dopamine and serotonin in *Caenorhabditis elegans*. Nature 375: 73-78.

Schmidt AR, Dorfelt H, Perrichot V (2007) Carnivorous fungi from Cretaceous amber. Science 318: 1743.

Schoène H (1984) Spatial Orientation: The Spatial Control of Behavior in Animals and Man. (Princeton, NJ: Princeton University Press xviii, 347 p).

Schrödel T, Prevedel R, Aumayr K, Zimmer M, Vaziri A (2013) Brain-wide 3D imaging of neuronal activity in *Caenorhabditis elegans* with sculpted light. Nat Meth 10: 1013-1020.

Segalat L, Elkes DA, Kaplan JM (1995) Modulation of serotonin-controlled behaviors by Go in *Caenorhabditis elegans*. Science 267: 1648-1651.

Shipley FB, Clark CM, Alkema MJ, Leifer AM (2014) Simultaneous optogenetic manipulation and calcium imaging in freely moving *C. elegans*. Front Neur Circuits 8(28).

Stevenson PA, Dyakonova V, Rillich J, Schildberger K (2005) Octopamine and experience-dependent modulation of aggression in crickets. J Neurosci 25: 1431-1441.

Stirman JN, Crane MM, Husson SJ, Wabnig S, Schultheis C, Gottschalk A, Lu H (2011) Real-time multimodal optical control of neurons and muscles in freely behaving *Caenorhabditis elegans*. Nat Meth 8: 153-158.

Sun L, Shay J, McLeod M, Roodhouse K, Chung S, Clark C, Pirri J, Alkema M, Gabel C (2014) Neuronal regeneration in *C. elegans* requires sub-cellular calcium release by ryanodine receptor channels and can be enhanced by optogenetic stimulation. J Neurosci (*n press*).

Swierczek NA, Giles AC, Rankin CH, Kerr RA (2011) High-throughput behavioral analysis in *C. elegans*. Nat Meth 8: 592-598.

Thorn RG, Barron GL (1984) Carnivorous mushrooms. Science 224: 76-78.

Tian L, Hires SA, Mao T, Huber D, Chiappe ME, Chalasani SH, Petreanu L, Akerboom J, McKinney SA, Schreiter ER, Bargmann CI, Jayaraman V, Svoboda K, Looger LL (2009) Imaging neural activity in worms, flies and mice with improved GCaMP calcium indicators. Nat Meth 6: 875-881.

Tinbergen N (1948) Physiologische instinktforschung [Physiological research on instinct]. Experientia 4: 121-133.

Tinbergen N (1963) On aims and methods of ethology. Zeitschrift für Tierpsychologie 20: 410-433.

Touroutine D, Fox RM, Von Stetina SE, Burdina A, Miller DM III, Richmond JE (2005) *acr-16* encodes an essential subunit of the levamisole-resistant nicotinic receptor at the *Caenorhabditis elegans* neuromuscular junction. J Biol Chem 280: 27013-27021.

Tsalik EL, Niacaris T, Wenick AS, Pau K, Avery L, Hobert O (2003) LIM homeobox gene-dependent expression of biogenic amine receptors in restricted regions of the *C. elegans* nervous system. Dev Biol 263: 81-102.

von Uexküll J (1934) A Stroll Through the Worlds of Animals and Men. trans. Schiller CH. (1957) Instinctive Behavior: 5-80. (New York, NY: International Universities Press).

Varshney LR, Chen BL, Paniagua E, Hall DH, Chklovskii DB (2011) Structural properties of the *Caenorhabditis elegans* neuronal network. PLoS Comput Biol 7: e1001066.

Vashlishan AB, Madison JM, Dybbs M, Bai J, Sieburth D, Ch'ng Q, Tavazoie M, Kaplan JM (2008) An RNAi screen identifies genes that regulate GABA synapses. Neuron 58: 346-361.

Wei X, Potter CJ, Luo L, Shen K (2012) Controlling gene expression with the Q repressible binary expression system in *Caenorhabditis elegans*. Nat Methods 9: 391-395.

White JG, Southgate E, Thomson JN, Brenner S (1986) The structure of the of the nervous system of the nematode *Caenorhabditis elegans*. Philos Trans R Soc Lond B Biol Sci 314: 1-340.

White JG, Southgate E, Thomson JN (1992) Mutations in the *Caenorhabditis elegans unc-4* gene alter the synaptic input to ventral cord motor neurons. Nature 355: 838-841.

Wooltorton JR, He L, Salzberg BM, Fang-Yen C (abstract 2013) *In vivo* optical recording of action potentials in *C. elegans* muscles using Arclight, a genetically expressed voltage sensitive fluorescent protein. Biophys Soc Jour 104: 340a.

Wicks SR, Rankin CH (1995) Integration of mechanosensory stimuli in *Caenorhabditis elegans*. J Neurosci 15: 2434-2444.

Willows AO, Dorsett DA, Hoyle G (1973) The neuronal basis of behavior in *Tritonia*. III Neuronal mechanism of a fixed action pattern. J Neurobiol 4: 255-285.

Wragg RT, Hapiak V, Miller SB, Harris GP, Gray J, Komuniecki PR, Komuniecki RW (2007) Tyramine and octopamine independently inhibit serotonin-stimulated aversive behaviors in *Caenorhabditis elegans* through two novel amine receptors. J Neurosci 27: 13402-13412.

Xu M, Jarrell TA, Wang Y, Cook SJ, Hall DH, Emmons SW (2013) Computer assisted assembly of connectomes from electron micrographs: application to *Caenorhabditis elegans*. PLoS One 8: e54050.

Zhang F, Wang LP, Brauner M, Liewald JF, Kay K, Watzke N, Wood PG, Bamberg E, Nagel G, Gottschalk A, Deisseroth K (2007) Multimodal fast optical interrogation of neural circuitry. Nature 446: 633-639.

Zhao B, Khare P, Feldman L, Dent JA (2003) Reversal frequency in *Caenorhabditis elegans* represents an integrated response to the state of the animal and its environment. J Neurosci 23: 5319-5328.

Zhou C, Rao Y, Rao Y (2008) A subset of octopaminergic neurons are important for *Drosophila* aggression. Nat Neurosci 11: 1059-1067.